Isoprene Photooxidation via the Hydroperoxyl Pathway

Isoprene Photooxidation via the Hydroperoxyl Pathway

A dissertation presented

by

Yingjun Liu

to

The School of Engineering and Applied Sciences

in partial fulfillment of the requirements

for the degree of

Doctor of Philosophy

in the subject of

Engineering Sciences

Harvard University

Cambridge, Massachusetts

December, 2014

Isoprene Photooxidation via the Hydroperoxyl Pathway

Abstract

Photooxidation of isoprene has a large influence on the oxidation capacity of the atmosphere and is a significant source of secondary organic material (SOM) of atmospheric particles. A quantitative understanding of isoprene photooxidation mechanism, in particular in the clean atmosphere, is important but challenging. This thesis presents laboratory and field studies of isoprene photooxidation via the hydroperoxyl (HO_2) pathway, believed to be the most important reaction pathway of isoprene-derived peroxy radicals under clean conditions, by using a switchable-reagent-ion (NO^+; H_3O^+) time-of-flight mass spectrometer (SRI-TOF-MS).

Isoprene photooxidation via the HO_2 pathway was investigated in a continuous-flow chamber. Production yields of methyl vinyl ketone (MVK) and methacrolein (MACR) pathway were determined as (3.8 ± 1.3)% and (2.5 ± 0.9)%, respectively, at <2% RH at 25 ^oC. Production of MVK and MACR via the HO_2 pathway implies concomitant production of hydroxyl ((6.3± 2.1)%) and hydroperoxyl ((6.3± 2.1)%) radicals.

The experiments also revealed an unexpected instrument bias that isoprene-derived hydroperoxides (ISOPOOH), the major isoprene oxidation products via the HO_2 pathway, were detected as the same product ions as the MVK and MACR. This finding implies that scientific conclusions based on previous ambient measurements of MVK and MACR under clean conditions using similar techniques need to be revisited. As a follow-up study, preliminary analysis of the ambient measurements in the Amazon Basin

showed that ISOPOOH isomers contributed to (36±15)% of the total concentration of MVK, MACR, and ISOPOOH isomers under clean conditions. The value is useful for re-evaluation of previous measurements and also defines range of possible anthropogenic influence on isoprene chemistry in the region.

SOM production from isoprene photooxidation via the HO_2 pathway was also investigated. Isoprene photooxidation was separated from SOM production by using two continuous-flow reactors connected in series and operated at steady state. Relative importance of various intermediates was directly compared from the drop of their gas-phase signals. Isoprene epoxydiols (IEPOX) had a much larger contribution to SOM production than other previously suggested isoprene SOM precursor, ISOPOOH isomers and isoprene, for a wide range of acidity.

The IEPOX contribution to isoprene SOM production was further quantified. IEPOX isomers lost from the gas phase accounted for (46 ±11)% of the produced SOM mass concentration. The IEPOX isomers comprised (59±21)% (molecular count) of the loss of monitored gas-phase species. The implication is that for the investigated reaction conditions IEPOX pathway accounted for half of the SOM mass concentration.

Table of Contents

List of Tables

List of Figures

Previously Published Work

Results in Chapter 2 and Appendix A were published as

Liu, Y. J., I. Herdlinger-Blatt, K. A. McKinney, and S. T. Martin (2013), Production of methyl vinyl ketone and methacrolein via the hydroperoxyl pathway of isoprene oxidation, Atmos. Chem. Phys., 13(11), 5715-5730. Reproduced under the Creative Commons Attribution 3.0 License together with an author copyright.

Results in Chapter 4, Appendix B, and Appendix C were published as

Liu, Y. J., M. Kuwata, B. F. Strick, F. M. Geiger, R. J. Thomson, K. A. McKinney, and S. T. Martin (2014), Uptake of Epoxydiol Isomers Accounts for Half of the Particle-Phase Material Produced from Isoprene Photooxidation via the HO_2 Pathway, Environ. Sci. Technol., 49(1), 250-258. Reproduced with permission from Environmental Science & Technology.

Acknowledgements

I would first like to express my deepest gratitude to my advisor, Professor Scot T. Martin, for providing me incredible scientific guidance throughout the years. His mentoring was not limited to deliver the result, but to educate me as an independent scientist. He taught me how to formulate scientific questions from literature reading in my first-semester 299r course, how to design an experiment on my own, and how to structure a paper and write a topic sentence for each paragraph. He gave me tremendous supports and freedom to try my own ideas and insightful suggestions for data analysis and interpretation. Professor Martin was also truly supportive and understanding outside of work, especially during my tough time periods of foot injury and family issue.

I have been extremely fortunate to pursue my Ph.D. at Harvard University, with exposure to so many great scientists: professors who have taught me, researchers and students with whom I have worked, and scientists who have visited Harvard. I would like to thank especially the past and present members of Martin group for all their helps on my research: Alberto Algarra, Adam Bateman, Luca Capppellin, Zhaoheng Gong, Irina Herdlinger-Blatt, Mikinori Kuwata, Ben Langford, Seung-bok Lee, Yongjie Li, Pengfei Liu, Ying Liu, Karena McKinney, Suzane de Sa, Madeleine Sanchez, Mackenzie Smith, Yuanzhi Tang, Yue Zhang, and Soeren Zorn. In particular, Karena McKinney introduced me the world of PTR-MS and mentored me throughout my degree. Mikinori Kuwata gave me tremendous help and shared with me many frustrating or exciting moments throughout our half-year experiments and even longer periods of data analysis and paper writing. Qi Chen, Ying Liu, and Irina Herdlinger-Blatt were lovely office mates, close friends, and constant sources of valuable advice for science and life.

I would also like to extent my acknowledgement to my talented collaborators Benjamin Strick, Franz Geiger, Regan Thomson (Northwestern University), Matthew Dorris, Jean Rivera-Rios, and Frank Keutsch (University of Wisconsin-Madison) who synthesized the invaluable organic standards for my research. I thank the members of my thesis committee and qualifying exam committee: Steven Wofsy, Daniel Jacob, Chad Vecitis, and Elsie Sunderland for their insightful comments and supports and the NASA Earth and Space Science Fellowship for funding my research. I also thank Professor Tong Zhu, my former advisor for Master's Degree at Peking University, China. He is the person who told me that I should apply for Harvard and has given me a lot of encouragement along the way.

Conducing field work in the Amazon basin would have been impossible without the team of dedicated scientists and technicians whom I have been fortunate enough to work with. I thank all the team members of GoAmazon 2014/5, in particular Stephen Springston, Thomas Watson, Arthur Sedlacek, Allison Aiken, Heath Powers, David Anderson (ARM), Juarez Viegas, Bruno Takeshi, Antonio Manzi (INPA), and Rodrigo de Souza (UEA) for collaboration, help and assistance. I also thank all the T3'ers who made the forth-month field work full of fun.

Lastly, I would like to acknowledge all the supports I have received from my family and friends, near and far. The unconditioned love from my parents and my sister is the source of my courage to go through all the difficulties. My dear roommates Jingyi Yu and Lihua Jin have accompanied me through the wonderful five years at Harvard.

Abbreviations

BVOC	Biogenic volatile organic compound
CIMS	Chemical ionization mass spectrometry
CPC	Condensation particle counter
DMA	Differential mobility analyzer
GC	Gas chromatography
IE	Ionization energy
IOP	Intensive observation period
IEPOX	Isoprene-derived epoxydiol
ISOP	Isoprene
ISOPOO	Isoprene-derived peroxy radical
ISOPOOH	Isoprene-derived hydroperoxide
HEC	Harvard environmental chamber
HR-TOF-AMS	High-resolution time-of-flight aerosol mass spectrometer
MACR	Methacrolein
MEGAN	Model of Emissions of Gases and Aerosols from Nature
MCM	Master Chemical Mechanism
MVK	Methyl Vinyl Ketone
PFA	Polyfluoroalkoxy
PMF	Ppositive-matrix factorization
PTR-TOF-MS	Proton-transfer-reaction time-of-flight mass spectrometer
PTR-MS	Proton-transfer-reaction mass spectrometer
SMPS	Scanning mobility particle sizer

SOM	Secondary organic material
SRI-NO^+-TOF-MS	Switchable-reagent-ionization time-of-flight mass spectrometer using NO^+ as reagent ions
SRI-TOF-MS	Switchable-reagent-ionization time-of-flight mass spectrometer
VOC	Volatile organic compound

1. Introduction

By emissions, isoprene is the dominant nonmethane hydrocarbon emitted from the Earth to the atmosphere. The atmospheric oxidation of isoprene, primarily by the hydroxyl radicals (OH), affects the oxidation capacity of the atmosphere, contributes significantly to the production of a range of important gas-phase species and also the formation of particulate secondary organic material (SOM). A solid understanding of the mechanism of isoprene oxidation and SOM production is critical to an accurate representation of atmospheric chemistry in global chemical transport models, and crucial to a more confident prediction of ongoing and future climate change.

The introduction is organized as follows: Sections 1.1-1.3 review the current understanding of isoprene emission, gas-phase chemistry, and SOM formation, respectively. Section 1.4 presents a brief introduction of the instrument used to advance the above topics in this thesis. Section 1.5 specifies the scientific questions investigated in this thesis and their logic connections.

1.1 Emission of isoprene

Emission of isoprene from plant species was first discovered in the 1950s by scientists in the former Soviet Union and in the US [Rasmussen and Went, 1965; Sanadze, 2004], leading to a considerable interest to this compound. In the following decades, emissions of isoprene have been studies for hundreds of plant species using enclosure techniques [as reviewed in Kesselmeier and Staudt, 1999] and more recently above canopies from tower, aircraft and tethered balloon sampling platforms [e.g., Jacob and Wofsy, 1988; Kuhn et al., 2007; Karl et al., 2013]. These different techniques can characterize isoprene

emissions at a variety of scales, from leaf and branch scale using enclosure method, to canopy scale of a few km^2 using tower-based methods, to spatial scales of tens to hundreds of km^2 using aircraft and tethered-balloon based methods.

These laboratory and field studies have advanced the understanding of isoprene emission substantially, as reviewed earlier [Guenther et al., 1995; Kesselmeier and Staudt, 1999; Sanadze, 2004; Guenther et al., 2006]. In brief, isoprene is produced by the plants as a by-product of photosynthesis [Sanadze, 2004]. It is never stored in plants after its production and instead rapidly lost by volatilization [Kesselmeier and Staudt, 1999]. A number of physical and biological factors regulate the capacity of a leaf to emit isoprene [Guenther et al., 2006]. Incident solar radiation and leaf temperature are two key factors, which control emissions on short (seconds to minutes) time scales and also have an influence for a longer (hours to weeks) time scales. A leaf's ability to emit isoprene is also influenced by leaf phenology. Generally speaking, very young leaves of isoprene-emitting species emit no isoprene, mature leaves emit maximally, and as leaves senesce, emission capacity gradually declines. Moreover, soil moisture and changes in the composition of the atmosphere also affect isoprene emission capacity. Isoprene-emitting species occur in many plant taxa throughout many functional types, but they are more often found in woody plant species than in herbs and crops [Kesselmeier and Staudt, 1999]. Very high and very low emitters often occur within a given plant family and even within some globally important plant genera [Guenther et al., 2006].

Efforts have been made to develop emission inventories of isoprene based on the emission rates measured for various species and landscapes. The most widely-used global emission inventory of iosprene is the Model of Emissions of Gases and Aerosols from

Nature (MEGAN), developed by Guenther et al. [1995; 2006; 2012]. MEGAN estimates the net emission rate of isoprene from terrestrial ecosystem into the above-canopy atmosphere at a specific location and time as

$$\text{Emission} = [\varepsilon][\gamma][\rho] \quad (1\text{-}1)$$

where ε (mg m^{-2} h^{-1}) is an emission factor which represents the emission into the canopy at standard conditions, γ (normalized ratio) is an emission activity factor that accounts for emission changes due to deviations from standard conditions driven by environmental and biological factors, and ρ (normalized ratio) is a factor that accounts for production and loss within plant canopies.

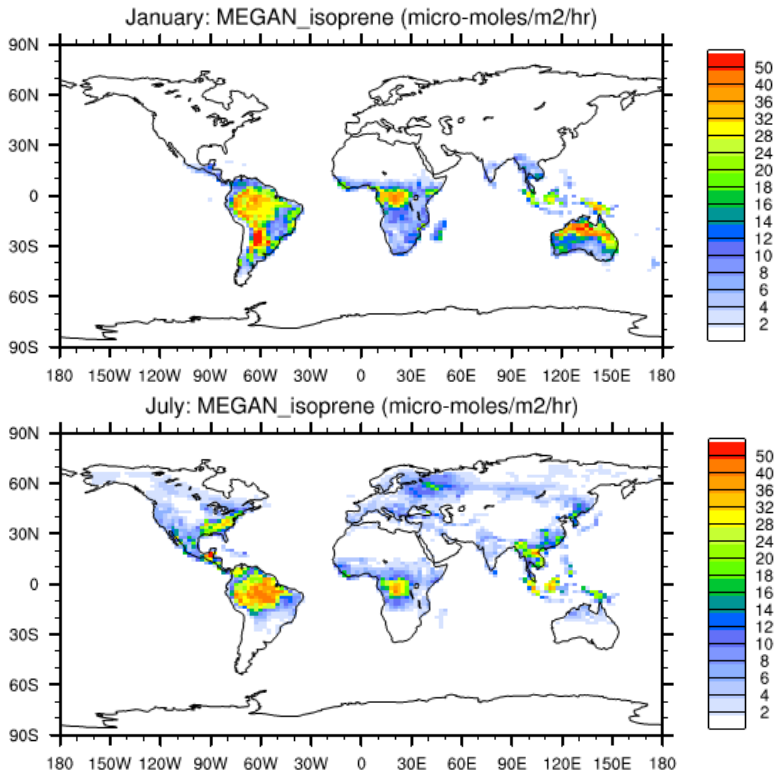

Figure 1-1 January and July 2000 global emission of isoprene simulated with MEGAN 2.1. Adopted from Guenther et al. [2012].

The estimated annual global isoprene emission is ~600 Tg yr^{-1} with MEGAN using the standard driving variables [Guenther et al., 2006] and ranges from 412 to 682

Tg yr^{-1} with other models [as summrized in Sindelarova et al., 2014]. It comprises half of the total global biogenic volatile organic compound (BVOC) emission [Guenther et al., 2012]. Tropical broadleaf trees contribute almost half of the estimated global flux of isoprene and the remaining flux is primarily from shrubs which have a widespread distribution. Figure 1-1 shows the global distribution of isoprene emission. 40% of isoprene emission is from South America due in large part to the year-round growing season and high biomass of the Amazon tropical forests.

1.2 Isoprene Photooxidation

Isoprene (C_5H_8) contains two double C-C double bonds and can hence be readily oxidized in the atmosphere. The lifetime of isoprene with respective to the reaction with OH (2×10^6 molecule cm^{-3}), O_3 (30 ppb), and NO_3 radicals (5×10^8 molecule cm^{-3}) is 1.4 hr, 1.3 day, and 48 min, respectively [Ziemann and Atkinson, 2012]. Oxidation by OH is the dominant fate of isoprene in the atmosphere since isoprene is emitted during daytime.

Isoprene oxidation by OH is initiated by addition of a OH radical across a double bond followed by rapid reaction of the alkyl radical with molecular oxygen (O_2), leading to the initial formation of hydroxyl-substituted peroxy radicals (ISOPOO). Theoretical studies suggested that OH addition to terminal carbon atoms (>90%) dominates over addition to inner carbon atoms and ISOPAOO, ISOPBOO, ISOPCOO, and ISOPDOO (shown in Figure 1-2) are the major products [Jenkin et al., 1998; Francisco-Marquez et al., 2003]. The subsequent ISOPOO chemistry is determined by several competing pathways, which correspondingly lead to different dominant products. Consistent with a wealth of laboratory studies of the reactivity of peroxy radicals [Atkinson and Arey, 2003], the competing pathways of ISOPOO include reactions with NO [e.g., Tuazon and

Atkinson, 1990], HO_2 [Paulot et al., 2009b] and self- and cross- reactions with other peroxy (RO_2) radicals [Jenkin et al., 1998]. More recently, Peeters et al. [2009] and Silva et al.[2009] also identified some unimolecular hydrogen-shift reactions of ISOPOO through quantum chemistry methods. The reaction with NO dominates in polluted, urban regions of the planet. Many isoprene source regions, particularly remote tropical forests, have sufficiently low NO_x concentrations that the other three pathways could become important.

Table 1-1 Estimated lifetime of ISOPOO with respect to its four reaction pathways in isoprene source regions

Pathway	k_{RO2}[1] (cm^3 $molec^{-1}$ s^{-1})	Borneo[2]		Amazon[3]	
		Mixing Ratio (ppt)	RO_2 lifetime (min)	Mixing Ratio (ppt)	RO_2 lifetime (min)
NO	8.8×10^{-12}	40±20	2 (1.3-3.9)	20±20	3.9 (>2.9)
HO_2	1.74×10^{-11}	14.7±3.5	2.6 (2-3.5)	43±11	0.9 (0.7-1.2)
RO_2	7×10^{-14}-6×10^{-12}	19.8±4.9	10-110	-	-
Isomerization	0.002±0.001 (s^{-1})		5-13		5-13

[1]The reaction rate coefficients k_{RO2} of isoprene-derived RO_2 are from IUAPC recommendation[Atkinson et al., 2006] for reactions with NO and HO_2, from MCM recommendation based on measurements by Jenkin et al.[1998] for reaction with RO_2, and from the measurement by Crounse et al.[2011] for isomerization reaction.

[2]The mixing ratios over tropical forests in Borneo are from publications of OP3 project [Hewitt et al., 2010; Stone et al., 2011]. Note that RO_2 mixing ratio was not directly measured, it was estimated by subtracting HO_2 mixting ratio measured by FAGE (Fluorescence Assay by Gas Expansion) from HO_2+RO_2 mix ratio measured by PERCA (Peroxy radical chemical amplifier).

[3]The mixing ratios over rain forests are from the aircraft measurements by Lelieveld et al. [2008]

Table 1-1 shows the concentrations of NO, HO_2, and RO_2 observed in two tropical rainforest regions and the estimated lifetime of ISOPOO with respect to each pathway. As shown in Table 1-1, HO_2 pathway is a key contributor in both locations, but the presence of trace-amounts of NO (>40 ppt) could make the NO pathway equally important. The contributions from the isomerization pathway and the RO_2 pathway are

relatively smaller but they are not negligible. To summarize, a good understanding of the photochemistry of isoprene in the atmosphere requires a careful laboratory investigation of all four pathways, especially the NO and HO_2 pathways.

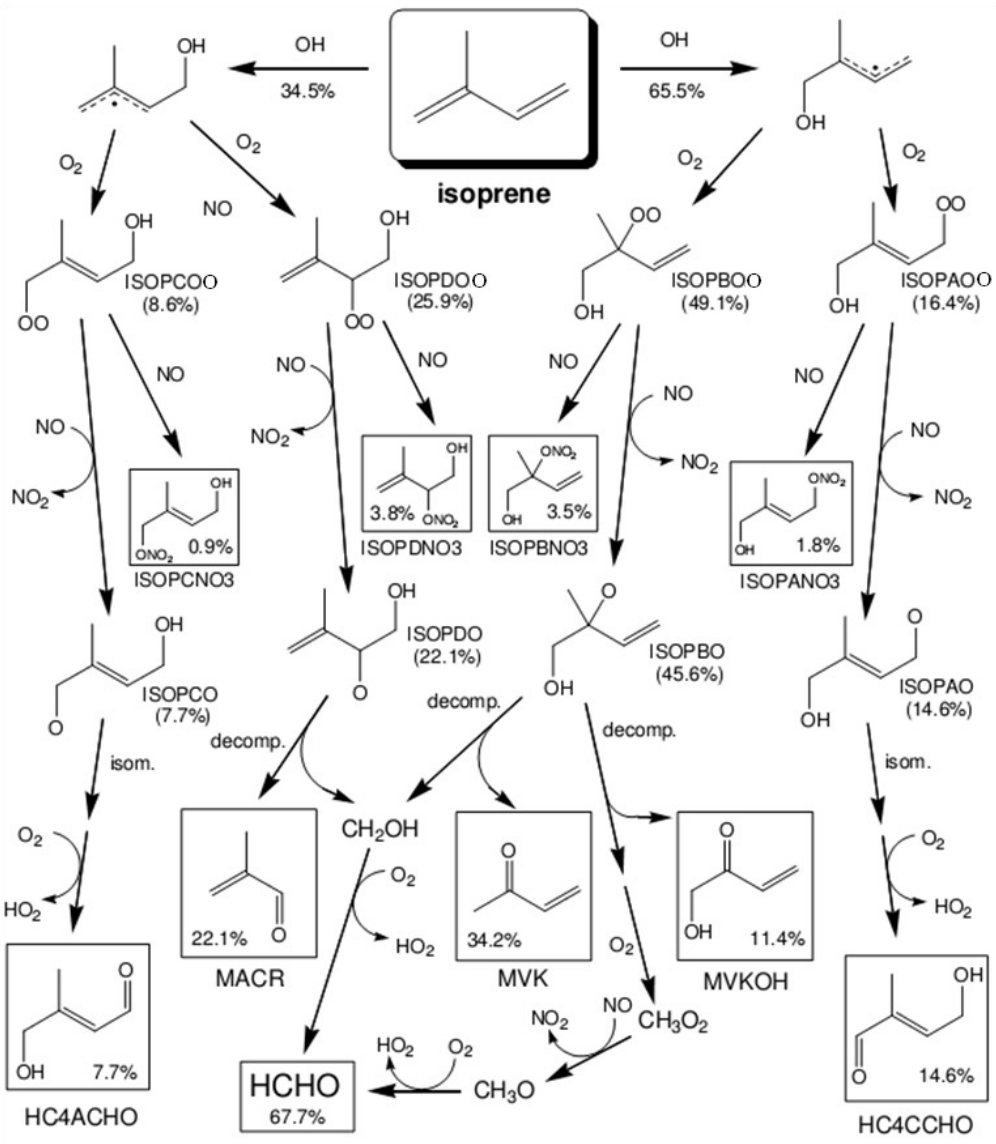

Figure 1-2 Isoprene photooxidation via the NO pathway as represented in MCM v3.1. Adopted from Archibald et al. [2010].

Most previous chamber studies of isoprene photooxidation were conducted under NO-dominant conditions by using very high concentration of NO (ppm level) [Tuazon and Atkinson, 1990; Paulson et al., 1992; Miyoshi et al., 1994; Yu et al., 1995; Chen et

al., 1998; Ruppert and Becker, 2000; Sprengnether et al., 2002; Zhao et al., 2004; Baker et al., 2005; Karl et al., 2006; Paulot et al., 2009a; Galloway et al., 2011]. The NO pathway is now relatively well understood [Archibald et al., 2010]. Methyl vinyl ketone (MVK), methacrolein (MACR), and formaldehyde (HCHO) have been consistently observed as the major first-generation products, and other reported products include organic nitrates [Miyoshi et al., 1994; Sprengnether et al., 2002; Paulot et al., 2009a], C_5-hydroxyl aldehydes [Zhao et al., 2004; Baker et al., 2005], hydroxyl methyl vinyl ketone [Yu et al., 1995; Ruppert and Becker, 2000; Zhao et al., 2004], methyl furan [Tuazon and Atkinson, 1990; Paulson et al., 1992; Ruppert and Becker, 2000], and some C_2-C_3 carbonyls [Galloway et al., 2011]. Figure 1-2 shows the products along the NO pathway represented in Master Chemical Mechanism (MCM) version 3.1.

For the other three pathways, there have been a limited number of laboratory studies [Miyoshi et al., 1994; Benkelberg et al., 2000; Ruppert and Becker, 2000; Lee et al., 2005; Paulot et al., 2009b; Crounse et al., 2011; Navarro et al., 2011]. In comparison with the high-NO_x experiments discussed above, these experiments are usually categorized as "low-NO_x" since NO was not added intentionally. Table 1-2 summarizes the experimental conditions, identified products and yields of these studies.

In these "low-NO_x" experiments, the reaction of ISOPOO radicals often had more than one significant contributing pathway, complicating the product identification of individual pathways. As shown in Table 1-2, most studies used H_2O_2 as OH precursor and ppm-level initial concentrations of isoprene [Miyoshi et al., 1994; Benkelberg et al., 2000; Ruppert and Becker, 2000; Lee et al., 2005; Navarro et al., 2011], under which conditions the HO_2 and RO_2 pathways could be both important and it is difficult to

distinguish their individual contributions. In addition, the background mixing ratios of NO in most of the experiments were not directly measured due to instrument limitations, although these experiments were generally assumed to be NO_x-free. As suggested by Karl et al. [2006], the background concentrations of NO in the laboratory reaction systems, especially in Teflon chambers (<1 up to 10 ppb), were likely high enough to make the NO pathway quantitatively important.

Table 1-2 Summary of experimental conditions and observations of previous "low-NO_x" experiments.

		Miyoshi et al. 1994	Ruppert and Becker 2000	Benkelberg et al. 2000	Lee et al. 2005	Paulot et al. 2009	Navarro et al. 2010	Crounse et al. 2011
Experimental Condition	Reactor	Teflon chamber	Quartz reactor	Glass bulb	Quartz reactor	Teflon chamber	Quartz reactor	Teflon chamber
	C_5H_8	1-2 ppm	2-8 ppm	1000 ppm	200 ppm	20-70 ppb	30 ppm	20 ppb
	NO_x	NA	<20 ppb	NA	NA	0.1-1.3 ppb	NA	NA
	OH source	H_2O_2	H_2O_2	H_2O_2	H_2O_2	H_2O_2	H_2O_2	CH_3ONO
Products and Yields (%)	HCHO	ca. 34	33±3		> 23.4			
	MVK	ca. 17	15.3±1.2	19.1	14.4±0.1	<30	8.9-15.5	
	MACR	ca. 22	17.8±1.4	20.5	19±0.2		10.9-13.0	
	3-methyl furan		ca. 1	2.8	2.9±0.2			
	C_5 hydroperoxides	yes				>70		yes
	C_5 diols		8.2±2					
	C_5 carbonyls		17	3.7				
	HPALDs							yes
	Epoxide (2nd generation)					yes		

In recent years, Wennberg group in Caltech made several breakthroughs in the laboratory studies of isoprene photooxidation under "low-NO_x" conditions. The study by Paulot et al. [2009b] had a focus of the HO_2 pathway. By using ppb level of isoprene and ppm level of H_2O_2, the HO_2 pathway dominated over the RO_2 pathway. Isoprene-derived hydroperoxides (ISOPOOH; $C_5H_{10}O_3$) were unambiguously detected for the first time by using chemical ionization mass spectrometry (CIMS) with CF_3O^- as the reagent ion.

More importantly, isoprene epoxydiols (IEPOX; $C_5H_{10}O_3$) were discovered as second-generation products (i.e., further reaction of ISOPOOH isomers with OH) unexpectedly. The IEPOX isomers have been shown to provide a missing link tying the gas-phase degradation of isoprene to the observed formation of SOM in the follow-up studies (cf. Section 1.3). Figure 1-3 shows the chemical structures of the expected ISOPOOH and IEPOX isomers. More recently, they also provided first laboratory evidence of the theoretically proposed isomerization pathway by detecting the predicted hydroperoxyl aldehyde (HPALD) products [Crounse et al., 2011]. Despite of their importance, these two studies alone are not enough to reveal the whole picture of the HO_2 and isomerization pathways and more targeted studies are needed.

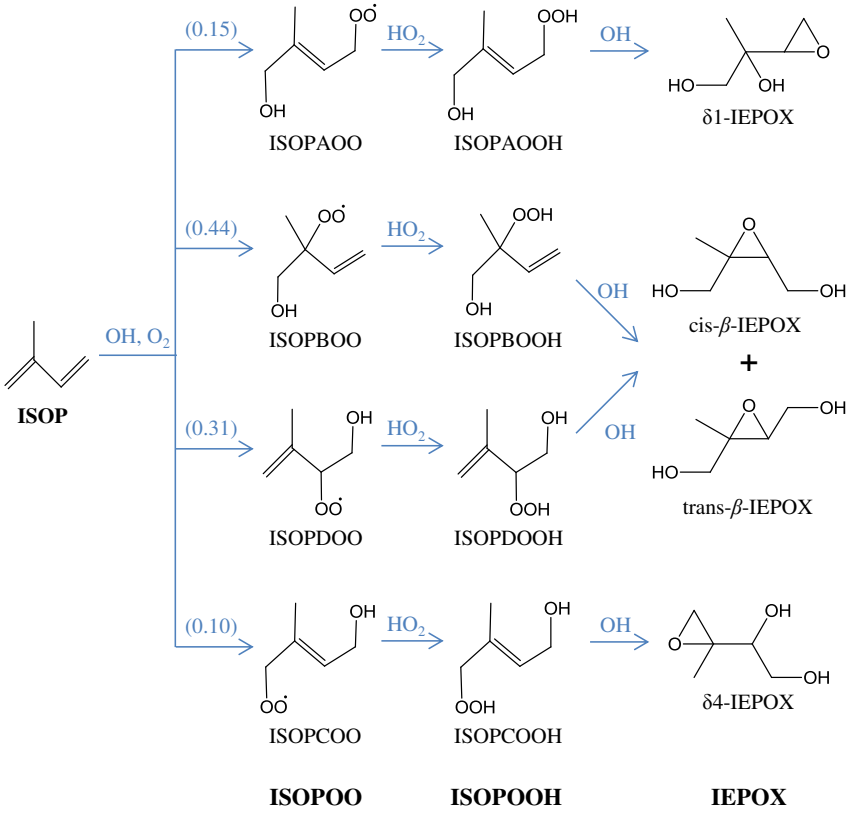

Figure 1-3 Isoprene photooxidation via the HO_2 pathway as represented in MCM v3.2. Branching ratios to specific products are shown in parentheses.

1.3 Formation of Particulate Organic Material from Isoprene Photooxidation

The understanding of SOM production from isoprene photooxidation has changed significantly over time. For a long time, atmospheric oxidation of isoprene was considered as an unimportant source of SOM since known products (cf. Figure 1-2) were too volatile to partition appreciably into the particle phase. Early laboratory studies showed that isoprene photooxidation can form SOM only at isoprene concentrations (hundreds of ppb) much higher than those in the ambient environment (a few ppb) [Pandis et al., 1991; Miyoshi et al., 1994]. In 2004, this conventional understanding was challenged by a field study, which found some previously unidentified compounds, 2-methyltetrols, present in the particle samples collected over the Amazonian rainforests [Claeys et al., 2004]. 2-methyltetrols have the same carbon skeleton as isoprene (Figure 1-4) and exhibited similar diurnal and seasonal trend to isoprene emission [Plewka et al., 2006; Kleindienst et al., 2007]. Follow-up studies also found the presence of 2-methyltetrols in the particles of many other biogenic-influenced environments [as summarized in Carlton et al., 2009]. In addition, a few other compounds having the same carbon skeleton as isoprene or methacrolein (Figure 1-4) have also been identified in ambient particles [Ion et al., 2005; Wang et al., 2005; Surratt et al., 2006; 2007b; 2008]. These observational results strongly suggested that oxidation of isoprene could be an important source of SOM in the atmosphere.

Intrigued by these field observations, SOM production from isoprene photooxidation has been reexamined in many laboratory studies [Edney et al., 2005; Kroll et al., 2005; Dommen et al., 2006; Kleindienst et al., 2006; Kroll et al., 2006; Ng et al., 2006; Surratt et al., 2006; Surratt et al., 2010]. It was confirmed that isoprene

photooxidation indeed formed SOM under a variety of experimental conditions, spanning wide ranges in particle acidity, NO_x concentration, relative humidity, and initiating oxidant. The measured particle yields were usually a few percent, although with a large variation within studies [as summarized in Carlton et al., 2009]. 2-methyltetrols and other isoprene-related particle-phase tracers have also been detected in isoprene SOM produced in some of these laboratory studies [Edney et al., 2005; Surratt et al., 2006; 2010].

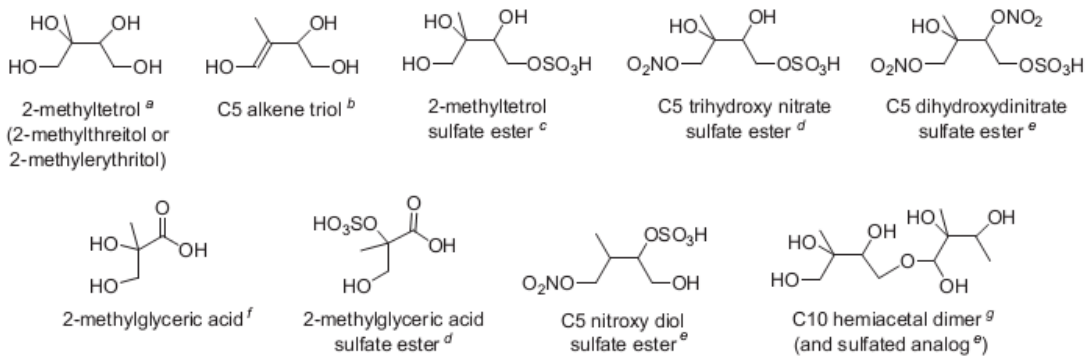

Figure 1-4 Compounds found in ambient particles sharing the carbon skeleton of isoprene or methacrolein. All the compounds have multiple isomers. Adopted from Carlton et al.[2009]

There are two major findings in terms of how the experimental conditions affect SOM yields from isoprene photooxidation. First of all, SOM yield depends on RO_2 chemistry. SOM production is more favorable via the HO_2 pathway than via the NO pathway. Kroll et al. [2006] found that the SOM yield decreased with the increase of NO_x concentration using H_2O_2 as the OH source (HO_2 can be formed from the reaction of H_2O_2 and OH). In addition, the SOM yields of the studies using H_2O_2 as the OH source [Kroll et al., 2005; 2006] were in general higher than the reported yields using NO_x alone. Secondly, SOM production is promoted in the presence of acidic particles. Higher yield has been observed at higher particle acidity for photooxidation [Edney et al., 2005; Kleindienst et

al., 2006; Surratt et al., 2007a] and ozonolysis [Jang et al., 2002; Czoschke et al., 2003] of isoprene. The important role of particle acidity suggested that some oxidation products could possibly undergo reactive uptake into the particle phase and form lower-volatility oligomers.

The laboratory studies have also revealed some possible direct carbon sources of isoprene SOM. SOM production was observed when high concentrations of isoprene were exposed to acidic sulfate particles in the absence of oxidations [Limbeck et al., 2003; Liggio et al., 2007], suggesting that isoprene itself might contribute to SOM production through particle-phase reactions under acidic conditions. Organic peroxides were found to constitute a large portion of the SOM produced under "low-NO_x" conditions [Surratt et al., 2006] and ISOPOOH isomers were hence suspected to contribute to SOM production through particle-phase reactions [Kroll et al., 2006; Surratt et al., 2006]. More recently, converging evidence indicates that IEPOX isomers are important intermediates for isoprene SOM production via the HO_2 pathway [e.g., Surratt et al., 2010; Budisulistiorini et al., 2013; Gaston et al., 2014]. Under "high-NO_x" conditions, further-step oxidation products of MACR, methacrylic acid epoxide, was recently proposed to play a crucial role for SOM formation [Lin et al., 2013]. In addition, glyoxal and methyl glyoxal, which are major second-generation products via the NO pathway, have also been shown to contribute to SOM production through multiphase reactions [Ervens et al., 2008].

Among all of the possible intermediates for isoprene SOM production, the importance IEPOX isomers have been highlighted by recent studies. Reactive uptake of IEPOX isomers has been reported for both acidic and nonacidic conditions and with a

faster uptake rate at higher acidity [Eddingsaas et al., 2010; Gaston et al., 2014; Nguyen et al., 2014a]. Particle-phase ring-opening reactions of IEPOX isomers, catalyzed by H^+ and NH_4^+, have been shown to produce many molecular tracers of isoprene SOM identified in the field studies, including 2-methyltetrols, C_5 alkene triols, and C_5 sulfate esters [Surratt et al., 2010; Lin et al., 2011; Nguyen et al., 2014a]. In addition, analysis of IEPOX-derived SOM by aerosol mass spectrometry [Budisulistiorini et al., 2013] suggests that reactive uptake of IEPOX possibly contribute to a unique factor resolved from positive-matrix factorization of the SOM mass spectra collected in several isoprene-influence regions [Robinson et al., 2011; Slowik et al., 2011; Budisulistiorini et al., 2013; Chen et al., 2014].

1.4 Switchable-Reagent-Ionization Time-of-Flight Mass Spectrometer

Switchable-reagent-ionization time-of-flight mass spectrometer (SRI-TOF-MS) is a new instrument developed by Ionicon Analytik GmbH very recently [Jordan et al., 2009b; 2009a]. This instrument serves as an upgraded version of proton-transfer-reaction mass spectrometer (PTR-MS), which has been widely used for the measurements of gaseous organic compounds in the ambient air [de Gouw and Warneke, 2007; Blake et al., 2009].

PTR-MS is one type of chemical ionization mass spectrometers, using hydronium ion as the reagent ion (H_3O^+). The instrument consists of three parts: ion source, drift tube, and mass detector, as shown in Figure 1-5. Hydronium ions are continuously produced in the ion source through hollow cathode discharge of water vapor and ionize organic molecules of the sample air in the drift tube. At the end drift tube, the reagent and product ions are measured by a quadrupole mass spectrometer. Ionization of organic molecules by H_3O^+ processes via proton transfer reaction:

$$H_3O^+ + R \rightarrow RH^+ + H_2O \quad \text{(R1-1)}$$

Proton transfer is a relatively soft ionization technique and usually yields a spectrum with less fragmentation so that the molecular species is possibly recognized. The reaction is thermodynamically spontaneous for organic molecules having proton affinity greater than water, allowing numerous VOCs of atmospheric interested to be monitored. In addition, PTR-MS also has low detection limit (< 10 pptv) and fast time response (< 1s) [Lindinger et al., 1998]. A major disadvantage of PTR-MS is that it only determines the mass (unit resolution) of product ion, which makes it impossible to distinguish isomeric and isobaric compounds. Moreover, the interpretation of mass spectra could be further complicated by the formation of cluster ions and the fragmentation of product ions.

Compared with its predecessor PTR-MS, SRI-TOF-MS has two major improvements: (1) the use of TOF mass detector and (2) the availability of another two alternative reagent ions NO^+ and O_2^+. The TOF detector has much higher mass resolution ($m/\Delta m > 4000$) than the quadrupole-based instrument (unit mass), enabling molecules with the same nominal mass but containing different elements to be resolved. It is hence possible to determine the molecular formula of any measured ions. Another advantage of the TOF detector is high time resolution. A full spectrum could be obtained in less than 0.1 ms. The availability of NO^+ and O_2^+ as reagent ions expand the list of molecules detectable and distinguishable. NO^+ is like H_3O^+ a soft ionizer, but unlike H_3O^+ the ionization reaction by NO^+ varies for different types of organic compounds, enabling separation of some isomeric molecules [Blake et al., 2006]. O_2^+ is a less soft chemical ionization agent and can be used where proton transfer does not work [Jordan et al., 2009b]. These two features allow the new SRI-TOF-MS to be a more powerful

instrument to quantitatively measure a wider range of organic compounds and to identify unknown compounds.

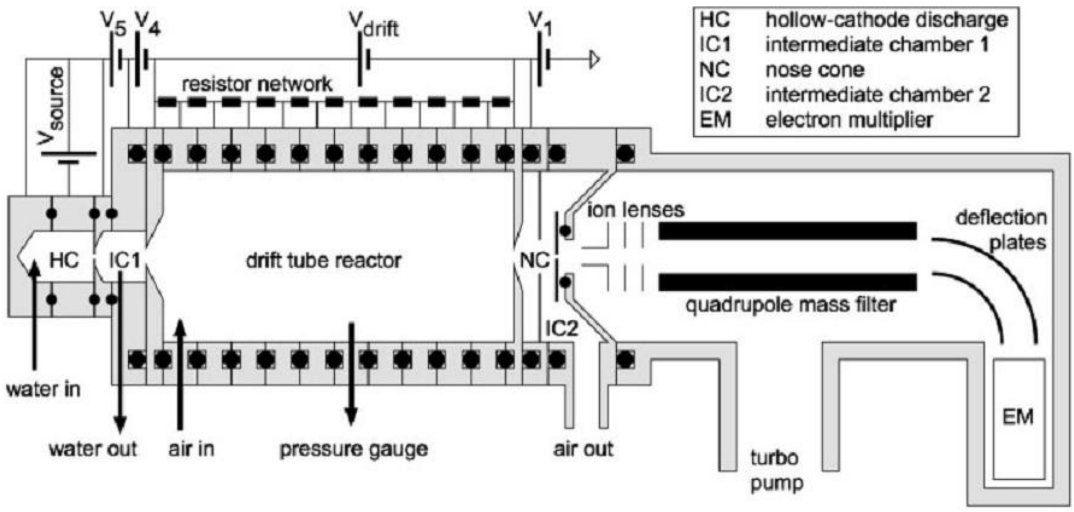

Figure 1-5 Schematic drawing of PTR-MS instrument. Adopted from de Gouw and Warneke [2007].

There have been two laboratory studies of isoprene photooxidation using PTR-MS [Zhao et al., 2004; Lee et al., 2005]. In both studies, the total concentration of MVK and MACR were measured, since PTR-MS could not separate isomeric molecules. Zhao et al. [2004] detected a few C_4 and C_5 hydroxylcarbonyls as products via the NO pathway, and demonstrated that these hydroxycarbonyl compounds accounted for most of the previously unquantified carbon, enabling isoprene carbon closure, i.e., full apportionment of carbon product yields. Lee et al. [2006] found a list of unidentified product ions under low-NO_x conditions, but the unit mass resolution of the quadrupole-based PTR-MS instrument prevented them from determining the chemical formulas of these ions.

In many field studies, PTR-MS has been used to measure isoprene and its oxidation products, especially the total concentration of MVK and MACR

(MVK+MACR). Fast time response of PTR-MS makes it possible to measure isoprene flux over canopies using eddy covariance method [e.g., Rinne et al., 2002], which is the most direct and accurate way of flux measurements. The concentration ratio of MVK+MACR to isoprene has been used as an indicator of the extent of oxidation and to infer the ambient concentration of OH radicals [e.g., Kuhn et al., 2007]. The measured concentration levels of isoprene, MVK+MACR, and further oxidation products, have been used to evaluate the validity of the current reaction mechanism [Karl et al., 2009; Stone et al., 2011].

The use of SRI-TOF-MS instrument in both laboratory and field studies of isoprene photooxidation is expected to lead to separate measurements of some isomeric products, such as MVK and MACR, and also help to better identify unknown products. The latter is extremely important for improving the isoprene reaction mechanism and searching possible SOM intermediates.

1.5 Motivation and Organization of Thesis

Although laboratory and field studies in the past few years greatly advanced our understanding of isoprene photooxidation and SOM formation, there are still some important open questions and uncertainties. As discussed in Section 1.2, an incomplete representation of the HO_2, RO_2, and isomerization pathways of isoprene photooxidation is a major limitation of the current reaction mechanism of isoprene. This limitation is supported by field evidence that the state-of-art models underestimated the OH concentrations in the Amazon rain forests [Lelieveld et al., 2008], tropical forests in southeast Asia [Stone et al., 2011], and other isoprene source regions with low NO_x concentrations. Systematic experimental studies of isoprene photooxidation under distinct

chemical regimes, with good control and characterization of NO, HO_2, and RO_2, are necessary. For SOM production from isoprene photooxidation, several possible key intermediates have been identified as discussed in Section 1.3, but their relative importance is less well-understood and it is not clear whether there are still other important intermediates unidentified yet. For example, the known particle-phase products of IEPOX isomers could only account for 20% of the mass concentration of isoprene-derived SOM in a laboratory study [Surratt et al., 2010]. Further studies are needed to evaluate the relative contributions of different possible intermediates to isoprene SOM production and to further look for other unidentified intermediates.

The works presented in the thesis aim to further advance the knowledge of isoprene photooxidation and SOM production via the HO_2 pathway using SRI-TOF-MS and other instruments. HO_2 pathway is estimated to account for a large fraction of ISOPOO reactions globally, particularly in the low-NO_x atmosphere [Crounse et al., 2011], and also has a large particle yield (cf. Section 1.3).

The thesis is organized as follows. Chapter 2 presents a set of photooxidation experiments of isoprene conducted in Harvard Environmental Chamber (HEC). Efforts were made to make sure that the ISOPOO reaction was dominant by the HO_2 pathway. The goal was to quantify the separate yields of MVK and MACR as first-generation products via the HO_2 pathway and the concomitant OH recycling. Chapter 3 evaluates the relative importance of previously proposed intermediates for SOM production via the HO_2 pathway for a wide range of particle acidity. The strategy is to mix isoprene oxidation products produced from a first reactor with sulfate particles in a second reactor and monitor the change in gas-phase mass spectrum due to particle injection. As a further

analysis of the data sets presented in Chapter 3, Chapter 4 quantitatively determines the contribution of IEPOX pathway alone to isoprene SOM production via the HO_2 pathway under the experimental conditions. Chapter 5 provides preliminary results from a field study in Amazonia in 2014, which was designed based on the findings in the laboratory studies of previous chapters and aimed to evaluate anthropogenic influence to isoprene photochemistry over Amazonia. Finally, Chapter 6 summaries the main findings in the thesis.

2. Production of Methyl Vinyl Ketone (MVK) and Methacrolein (MACR) via the Hydroperoxyl (HO_2) Pathway of Isoprene Photooxidation

2.1 Introduction

By abundance, isoprene (ISOP; C_5H_8) is the dominant non-methane biogenic volatile organic compound (VOC) in the atmosphere, and its reactive chemistry plays an important role in the oxidative cycles of the atmosphere (Poisson et al., 2000). Isoprene oxidation is typically initiated by the addition of a hydroxyl radical (OH) across a double bond followed by rapid reaction of the alkyl radical with molecular oxygen (O_2), resulting in the production of a series of isomeric hydroxyl-substituted alkyl peroxyl radicals (ISOPOO; $HOC_5H_8OO\cdot$) (Figure 1). The subsequent chemistry of the ISOPOO radicals proceeds along several competing pathways: (i) reactions with nitric oxide (NO) [e.g., Tuazon and Atkinson, 1990], (ii) reactions with hydroperoxyl radicals (HO_2) [e.g., Paulot et al., 2009b], (iii) self- and cross-reactions with other organic peroxyl radicals (RO_2) [Jenkin et al., 1998], and (iv) possible unimolecular isomerization reactions [Peeters et al., 2009; da Silva et al., 2010; Crounse et al., 2011]. For atmospheric conditions, the NO and HO_2 pathways are the major competing reaction pathways affecting the fate of ISOPOO [Crounse et al., 2011]. The reaction with NO dominates in polluted, urban regions of the planet. Many isoprene source regions, particularly remote tropical forests, have sufficiently low NO_x concentrations [e.g., Lelieveld et al., 2008; Hewitt et al., 2010] that the HO_2 pathway dominates. The HO_2 pathway is estimated to account globally for one half of the reactive fate of ISOPOO [Crounse et al., 2011].

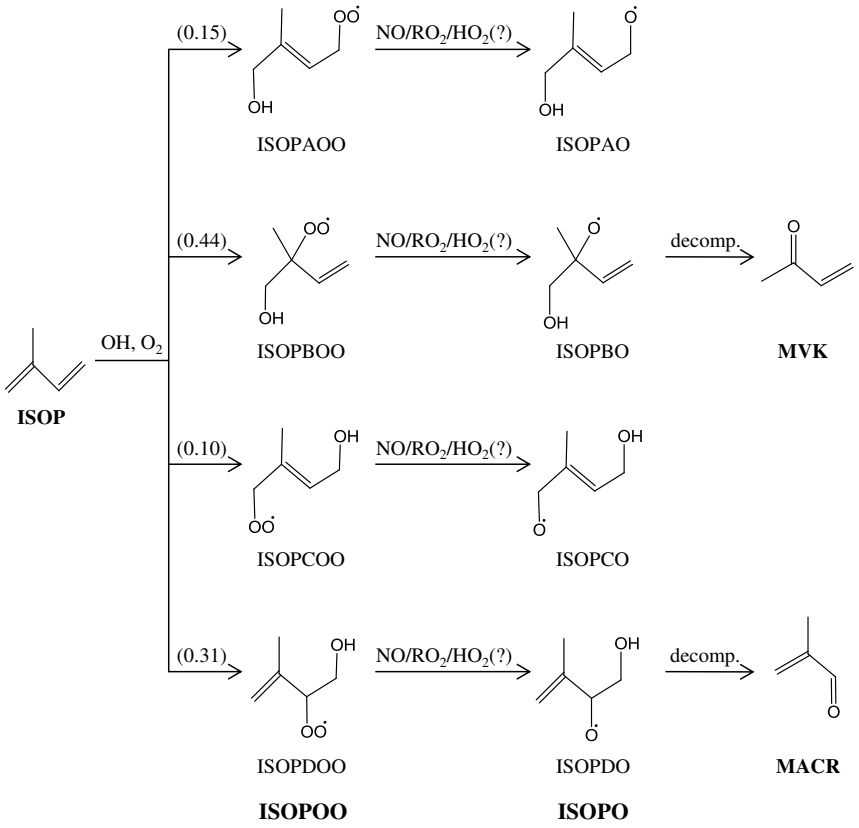

Figure 2-1 Mechanism of isoprene oxidation to produce MVK and MACR as first-generation products. Results are shown for NO and RO_2 pathways, as represented in MCM v3.2. Branching ratios to specific products are shown in parentheses. The present study evaluates the extent, represented by the question mark, to which ISOPOO alkyl peroxy radicals might react with HO_2 to produce ISOPO alkoxy radicals (Reaction (R2-2)) and thereby MVK and MACR (Reaction (R2-3) and (R2-4)).

There remain significant uncertainties in the branching ratios and principal products of isoprene photo-oxidation for the HO_2 reaction pathway. Mechanisms employed in many regional and global models, including the near-explicit Master Chemical Mechanism (MCM v3.2) [Jenkin et al., 1997; Saunders et al., 2003], treat the reaction of HO_2 with ISOPOO as a radical-termination reaction, as follows:

$$\text{ISOPOO} + HO_2 \rightarrow \text{ISOPOOH} + O_2 \qquad \text{(R2-1)}$$

in which organic hydroperoxides (ISOPOOH; HOC_5H_8OOH) are formed with 100% yield (cf. Figure 1-3). A competing, less investigated pathway, however, might also be important [Dillon and Crowley, 2008]:

$$ISOPOO + HO_2 \rightarrow ISOPO + OH + O_2 \quad \text{(R2-2)}$$

This pathway produces alkoxy radicals (ISOPO, $HOC_5H_8O\cdot$) and an OH radical. Given that the oxidation pathway was initiated by OH attack on isoprene, the production of the OH radical implies a recycling of the reactant. This type of reaction has been demonstrated in the laboratory for some RO_2 radicals [Sulbaek Andersen et al., 2003; Hasson et al., 2004; Jenkin et al., 2007; Dillon and Crowley, 2008; Jenkin et al., 2008]. Theoretical studies suggest that this reaction is favored for peroxyl radicals having the forms RCHXOO and $RCHXCH_2OO$ that can pass through a hydrotetroxide intermediate, where X is an electronegative atom [Hasson et al., 2005]. The internal hydrogen bonding between the hydrotetroxide and atom X lowers the transition state energy. Two ISOPOO isomers, namely ISOPBOO and ISOPDOO, accounting together for 75% of ISOPOO based on the MCM, have this chemical form (Figure 2-1).

Methyl vinyl ketone (MVK, C_4H_6O) and methacrolein (MACR, C_4H_6O) can be produced by the decomposition of the ISOPBOO and ISOPDOO isomers, as follows (cf. Figure 2-1):

$$ISOPBO \xrightarrow{O_2} MVK + HCHO + HO_2 \quad \text{(R2-3)}$$

$$ISOPDO \xrightarrow{O_2} MACR + HCHO + HO_2 \quad \text{(R2-4)}$$

Radical termination by Reaction (R2-1) does not produce MVK or MACR. Hence, the yields of MVK and MACR can serve as tracers for the occurrence of Reaction (R2-2). The experimental strategy of the present study is to take advantage of MVK and MACR as indicators of Reaction (R2-2), compared to Reaction (R2-1), to assess the importance of the former as a reaction channel of ISOPOO with HO_2. Furthermore, HO_2 is also a

product of Reaction (R2-2) followed by Reactions (R2-3) and (R2-4), implying a recycling of this reactant. Taken together, Reactions(R2-2), (R2-3), and (R2-4) indicate possible significant recycling of the HO_x family in this reaction sequence.

The isoprene photo-oxidation experiments described herein were conducted in a continuous-flow chamber. Efforts were made to ensure and to verify that the HO_2 pathway was the dominant fate of the ISOPOO species, as opposed to the competing NO, RO_2, and isomerization pathways. The concentrations of MVK and MACR were measured using a switchable-reagent-ionization time-of-flight mass spectrometer (SRI-TOF-MS) with switchable reagent ion capability (H_3O^+, NO^+), for which the NO^+ mode was used to distinguish between MVK and MACR.

2.2 Experimental

The reaction conditions for seven different isoprene photooxidation experiments are listed in Table 2-1. Experiments #1 to #6 correspond to HO_2-dominant conditions and Experiment #7 to NO-dominant conditions. For Experiments #1 to #6, the reaction of H_2O_2 with OH radicals was used to produce HO_2 radicals: $OH + H_2O_2 \rightarrow HO_2 + H_2O$. For Experiment #7, a flow of NO into the chamber in the absence of H_2O_2 was used, so that the HO_2 pathway was not important under these conditions. Experiment #1 was the main experiment. For Experiments #2 through #6, the value of one chamber parameter was halved or doubled relative to Experiment #1 as an approach to validate experimentally (i) that MVK and MACR were first-generation products (cf. Section 2.3.3) and (ii) that the HO_2 pathway was dominant (cf. Section 2.3.4). Experiment #7 for NO-dominant conditions facilitated comparison of the present study's results to those

reported previously in the literature for the yields of MVK and MACR under high-NO_x conditions.

Table 2-1 Summary of experimental conditions and results.

	Chamber condition [1]	Mixing ratio at steady state (ppb) [4]					Yield (%) [4]	
		NO^+ mode			H_3O^+ mode		MVK	MACR
		ISOP	MVK	MACR	ISOP	MVK+ MACR		
#1	Main experiment [2]	16.0±0.6	1.3±0.1	0.8±0.1	15.8±1.4	2.1±0.2	4.6±0.7	3.2±0.6
#2	0.5 τ_{ref}	25.4±1.1	1.1±0.1	0.8±0.1	25.2±2.2	2.0±0.2	4.3±0.7	3.4±0.6
#3	2 τ_{ref}	9.5±0.4	1.6±0.2	0.8±0.1	9.3±0.9	2.4±0.2	6.6±1.2	4.3±0.9
#4	0.5 $[H_2O_2]_{in,ref}$	16.9±0.7	1.7±0.2	1.1±0.2	17.3±1.4	2.7±0.3	6.1±0.9	4.4±0.8
#5	2 $[H_2O_2]_{in,ref}$	15.8±0.7	1.3±0.2	0.7±0.1	16.2±1.4	2.0±0.2	4.5±0.9	2.8±0.6
#6	2 $[ISOP]_{in,ref}$	34.5±1.4	2.1±0.2	1.6±0.2	34.1±3.0	3.6±0.4	3.7±0.5	3.2±0.5
#7	NO-dominant [3]	18.3±0.7	10.3±0.8	7.9±0.4	18.4±1.7	18.1±1.8	41.4±5.5	29.6±4.2

[1] Experiment #1 is the main experiment. For the other experiments, chamber conditions varied with respect to Experiment #1 are listed. $[M]_{in,ref}$ represents the inflow mixing ratio of species M for the the main experiment. τ_{ref} is the mean residence time in the chamber for the main experiment. For example, 0.5 $[H_2O_2]_{in,ref}$ in Experiment #4 indicates that the inflow H_2O_2 mixing ratio for Experiment #4 was half that of the main experiment. Other experimental conditions remain unchanged.

[2] Condition for main experiment: $[ISOP]_{in,ref}$ = 59 ppb; $[H_2O_2]_{in,ref}$ = 16 ppm; no injection of NO_x and measured NO less than minimum detection limit (70 ppt); τ = 3.7 hr; 25 °C; < 2% relative humidity.

[3] Chamber condition for NO-dominant experiment: no injection of H_2O_2; $[NO]_{in}$ = 28 ppb; other conditions same as those of the main experiment.

[4] (mean value) ± (2 × standard deviation) for mixing ratios and yields. The uncertainties were estimated by Monte Carlo methods.

2.2.1 Harvard Environmental Chamber

The experiments were carried out in the Harvard Environmental Chamber (HEC; Figure S1). Detailed descriptions of the chamber were published previously [King et al., 2009; Shilling et al., 2009; 2010]. The chamber was operated as a continuously mixed flow reactor, with balanced inflows and outflows. A new polyfluoroalkoxy (PFA) Teflon bag with a volume of 5.3 m^3 was installed for these experiments. The mean reactor residence

time was varied from 1.8 to 7.4 hr. Temperature and relative humidity were held at 25 ± 1 °C and < 2%, respectively. Ultraviolet irradiation was provided by forty-six Sylvania 350BL blacklights (40 W) affixed to the walls [King et al., 2009]. They had negligible emission for wavelengths below 310 nm.

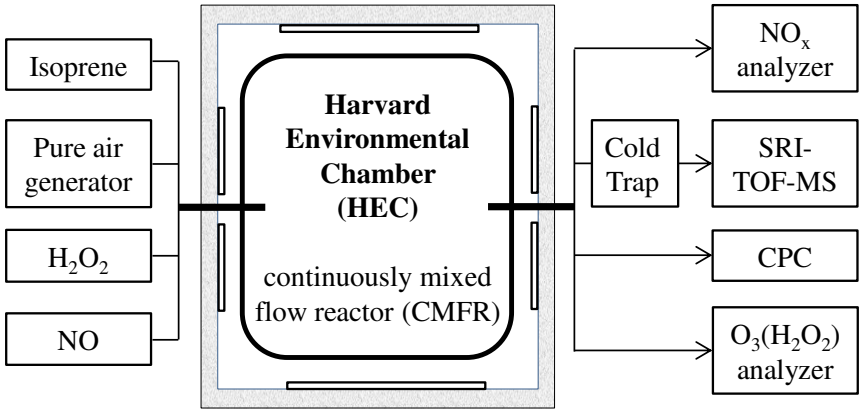

Figure 2-2 Schematic diagram of experimental set-up.

For the HO_2-dominant experiments (#1 to #6), isoprene (50 ppm in nitrogen, Scott Specialty Gases), hydrogen peroxide, and dry air (pure air generator, Aadco 737) were continuously injected. Depending on reaction conditions, isoprene concentrations were 59 to 118 ppb in the inflow to the chamber bag and 10 to 35 ppb in the outflow (Table 2-1). A commercially available ultrapure H_2O_2 solution (31.50 wt%, TraceSELECT$^{@}$ Ultra, Fluka) was used to avoid nitrogen-containing impurities that are present, often as EDTA ligands to stabilize trace metal impurities that enhance the decomposition rate of H_2O_2, in typical commercial H_2O_2 solutions. In earlier experiments, the observations showed that nitrogen impurities in the typical H_2O_2 solutions ultimately contributed to elevated NO_x in the bag. Compared to earlier experiments using the HEC [King et al., 2010], H_2O_2 injection system was updated to improve stability. An H_2O_2 solution was continuously introduced by a syringe pump into a warmed glass bulb. The syringe pump was housed in a refrigerator at 4 °C to avoid

H_2O_2 decomposition. Dry air at a flow rate of 1-4 sLpm was blown through the bulb to evaporate the injected H_2O_2 solution and carry it into the chamber bag. Within the HEC, photolysis of H_2O_2 by ultraviolet light produced OH radicals, initiating isoprene oxidation. For the NO-dominant experiment (#7), NO (1.02 ppm NO in nitrogen with 0.01 ppm NO_2 impurity; Scott Specialty Gases) was injected in place of H_2O_2 to produce an inflow concentration of 28.2 ppb NO and 0.03 ppb NO_2. Coupled NO_x and HO_x photochemical cycles were initiated by photolysis of NO_2. The injected NO contributed to increasing the OH concentration by promoting the conversion of HO_2 to OH according to the reaction: $HO_2 + NO \rightarrow OH + NO_2$.

The outflow from the HEC was sampled by a SRI-TOF-MS, a condensation particle counter (CPC, TSI 3022A), an ozone monitor (Teledyne 400E), and a high-sensitivity NO_x analyzer (Eco Physics CLD 899 Y). The CPC instrument was used to measure the background number concentration of particles in the HEC, which was below 0.5 cm^{-3} during the experiments. This low particle number concentration indicated insignificant new particle production. The NO concentration was below the instrument detection limit (3σ) of 70 ppt for Experiments #1 to #6. The ozone monitor was used to estimate the H_2O_2 concentration in Experiments #1 to #6 by using the ratio of the absorption cross-section of H_2O_2 to that of O_3 (254 nm) under the assumption that absorption was dominated by H_2O_2. The H_2O_2 concentration measured by this method was 6.7 to 26 ppm for Experiments #1 to #6. The expected concentration based on in-flow concentrations but not accounting for physical and reactive losses inside the chamber bag was 8.0 to 32 ppm.

2.2.2 Mass spectrometry

A switchable-reagent-ionization time-of-flight mass spectrometry (SRI-TOF-MS, Ionicon Analytik GmbH, Austria) was used to measure the concentrations of gaseous organic species in the chamber. For sampling, chamber air was pulled through a PFA sampling line at 1.25 sLpm. The SRI-TOF-MS subsampled from this flow at a rate of 0.25 sLpm, resulting in a transit time of 4 s between the chamber and the instrument.

The SRI-TOF-MS was described by Jordan et al. [2009b; 2009a] and Graus et al. [2010]. In the present study, either H_3O^+ or NO^+ reagent ions were generated in the ion source and used to selectively ionize organic molecules in the sample air. The use of NO^+ reagent ions allowed separation of isomeric aldehydes and ketones [Blake et al., 2006], specifically MVK and MACR. The chemical ionization reaction by NO^+ or H_3O^+ is soft, typically resulting in little fragmentation, although relatively weakly bound species still have the possibility for some fragmentation in the drift tube [Smith and Spanel, 2005]. The high-resolution TOF detector (Tofwerk AG, Switzerland) was used to analyze the reagent and product ions and allowed for exact identification of the ion molecular formula (mass resolution > 4000).

A calibration system was used to establish the instrument sensitivities to ISOP, MVK, and MACR. Gas standards (5.12 ppm ISOP and 5.26 ppm MVK in N_2, and 5.27 ppm MACR in N_2; Scott Specialty Gases) were added into the sample flow at controlled flow rates. In each experiment, the inlet flow was switched to dry air from the pure air generator to establish background intensities.

Settings of the drift tube were optimized to measure MVK and MACR at high sensitivity. The instrument was operated with a drift tube temperature of 60 °C and a drift

tube pressure of 2.2 mbar. In H_3O^+ mode, the drift tube voltage was set to 520 V, resulting in an E/N = 118 Td (E, electric field strength; N, number density of air in the drift tube; unit, Townsend, Td; 1 Td = 10^{-17} V cm^2). In NO^+ mode, a drift tube voltage of 300 V was used, resulting in E/N = 68 Td. At this reduced E/N ratio, ionization of MVK and MACR led to distinct product ions while retaining a highly sensitive instrument response.

SRI-TOF-MS spectra were collected at a time resolution of 1 min. A custom data processing package was developed in Mathematica (ver 8.0, Wolfram Research, USA) to analyze the recorded mass spectra. Using this package, the relative mass deviation was less than 10 ppm over the spectrum. The package consisted of several sub-routines: peak shape fitting, mass calibration, peak assignment, and signal analysis. Compared with the analysis method reported in Muller et al. [2010], the main difference was in fitting of the asymmetric peak shape. Muller et al. approximated the peak shape using the superposition of four Gaussian peaks, but this method did not work well for the peaks of the present study, possibly because of different instrument tuning. Instead, several strong single-ion peaks (e.g., the peak for $H_3{}^{18}O^+$ ion for H_3O^+ mode) were used to produce an empirically derived reference peak shape, which was then used globally in the peak fitting routine.

2.2.3 Low-temperature trap

The reactions of ISOPOO with HO_2 can produce C_5 products that have multiple functional groups, including organic hydroperoxides ISOPOOH and its further oxidation products dihydroxyl epoxides (IEPOX; cf. Figure 1-3) [Paulot et al., 2009b]. These products possibly fragment after collision with H_3O^+ or NO^+ in the SRI-TOF-MS [Smith

and Spanel, 2005], and the resultant fragment ions may have the same m/z values as the product ions of MVK and MACR because they all inherit the carbon skeleton from isoprene. As an approach to separate possible ISOPOOH and IEPOX products from MVK and MACR, prior to injection into the PTR-TOF-MS the outflow from the HEC was passed through a 1-m PFA coil (3/16 inch inner diameter) that was immersed in a low temperature liquid bath. As the temperature of the bath was decreased in discrete steps from +25 to -40 °C, molecules of progressively lower vapor pressures sequentially condensed in the coil and were thereby removed from the gas flow. This approach is particularly suited to separating low-volatility compounds such as ISOPOOH and IEPOX from high-volatility species like MVK and MACR. The quantification of MVK and MACR was based on SRI-TOF-MS measurements downstream of the trap at -40 °C (cf. Sections 2.3.2 and 2.3.3 for further discussion).

2.2.4 Modeling with Master Chemical Mechanism

The contribution by different reaction pathways was estimated for each experiment using a kinetic box model [Chen et al., 2011]. The kinetic scheme for isoprene chemistry was extracted from the Master Chemical Mechanism (MCM) v3.2 via website: http://mcm.leeds.ac.uk/MCM [Jenkin et al., 1997; Saunders et al., 2003]. Model runs were initialized using the conditions of each experiment (Table 2-1), with the exception of the H_2O_2 concentration. Instead of using the H_2O_2 injection rates as shown in Table 2-1, the spectroscopically measured steady-state H_2O_2 concentrations of each experiment were used as a constraint in the model. The one-sun photolysis rates of the MCM model were scaled by 0.3 to match the lower light intensity of the HEC.

2.3 Results and Discussion

The results and discussion section is organized as follows. Section 2.3.1 presents the separate measurement of MVK and MACR using the NO^+ reagent ion and the quantification of the concentrations of ISOP, MVK, and MACR. Section 2.3.2 presents evidence of chemical interferences for MVK and MACR that without precaution can confound the analytic method (cf. Section 2.3.1) and that these species are organic hydroperoxides. Section 2.3.3 explains how the yields of MVK and MACR (Y_{MVK} and Y_{MACR}) were obtained from the concentration measurements. The quantitative uncertainties of Y_{MVK} and Y_{MACR} were also established. Section 2.3.4 presents the qualitative evidence that these yields were recorded under conditions of HO_2-dominant reactions for the ISOPOO species (Reactions (R2-1) and (R2-2)). Section 2.3.5 explains how to constrain the minor contribution of the NO pathway to Y_{MVK} and Y_{MACR} using the yields measured under varying experimental conditions, yielding a best estimate for the yields of MVK and MACR via the HO_2 pathway (Y_{MVK,HO_2} and Y_{MACR,HO_2}). Section 2.3.6 provides a comparison of the results of the present study to those reported previously in the literature.

2.3.1 Quantification of isoprene, MVK and MACR

The NO^+ mass spectra recorded for zero air, ISOP, MVK, and MACR standards are shown in Figure 2-3. The dominant product ion of the reaction of ISOP (C_5H_8) with NO^+ was the charge-transfer ion $C_5H_8^+$ (m/z 68.0621), in agreement with Karl et al. [2012]. NO^+ reacted with the aldehyde MACR (C_4H_6O) to yield mainly the dehydride ion $C_4H_5O^+$ (m/z 69.0335) and a small amount of the $C_4H_6O{\cdot}NO^+$ cluster ion (m/z 100.0393). NO^+ reacted with the ketone MVK (C_4H_6O) to produce mainly the $C_4H_6O{\cdot}NO^+$ cluster

ion. Ion-molecule clustering reactions are favorable when no other exothermic channel is available, as is especially the case for the reaction of NO^+ with ketones [*Španěl et al.*, 1997]. The hydride ion (H^-) transfer reaction is favorable for aldehydes because extraction of the H^- ion from a -CHO moiety requires less energy than from a hydrocarbon chain. These ionization patterns have been observed for ketones and aldehydes using NO^+ in selective-ion flow-tube studies (E/N = 0 Td) [*Španěl* et al., 2002]. In comparison, the proton transfer reaction of MVK and MACR with H_3O^+ gave rise dominantly to $C_4H_7O^+$ (m/z 71.0492).

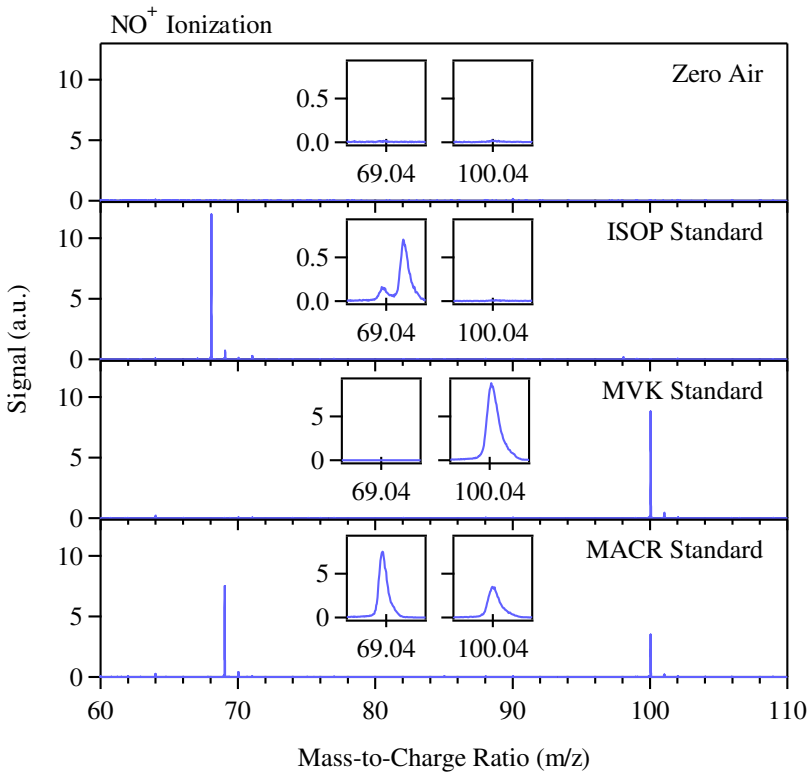

Figure 2-3 Mass spectra of zero air, ISOP, MVK, and MACR measured using SRI-TOF-MS with NO^+ reagent ion. Insets show expansions near m/z 69 and m/z 100, corresponding at m/z 69.0335 to $C_4H_5O^+$ contributed by MACR and ISOP, at m/z 69.0654 to $C_4{}^{13}CH_8^+$ contributed by ISOP, and at m/z 100.0393 to $C_4H_6O{\cdot}NO^+$ contributed by MVK and MACR.

In an iterative process, the E/N value was optimized to isolate the product ions of MACR from those of MVK while retaining high instrument sensitivity. Compared with

an earlier drift tube study using NO^+ [Blake et al., 2006], less fragmentation was observed in the present study, both for MVK and MACR, possibly because of the lower drift tube energies used here (i.e., E/N = 68 Td compared to E/N = 165 Td). The good separation achieved with NO^+ enabled separate quantification of MVK and MACR in the mixed composition present in the chamber outflow. The small contribution of MACR to the $C_4H_6O{\cdot}NO^+$ cluster ion was corrected for algebraically.

Table 2-2 Sensitivities of the SRI-TOF-MS to ISOP, MVK, and MACR

Species	Chemical Formula	NO^+ mode			H_3O^+ mode		
		Product Ion	Sensitivity (ncps ppb^{-1}) [1]		Product Ion	Sensitivity (ncps ppb^{-1})	
			+25 °C	-40 °C [2]		+25 °C	-40 °C
ISOP	C_5H_8	$C_5H_8^+$	15.7±0.4[3]	15.9±0.6	$C_5H_9^+$	16.8±1.4	16.2±1.1
MVK	C_4H_6O	$C_4H_6O{\cdot}NO^+$	23.1±1.8	23.7±1.2	$C_4H_7O^+$	30.6±2.9	29.2±1.5
MACR	C_4H_6O	$C_4H_5O^+$	15.0±0.8	15.0±0.4	$C_4H_7O^+$	30.0±2.8	28.7±2.2
		$C_4H_6O{\cdot}NO^+$	8.8±0.8	8.9±0.5			

[1] The unit ncps is the measured counts per second (cps) normalized to a primary ion signal of 10^6 cps.

[2] Sensitivities were determined for trap temperatures of +25 and -40 °C.

[3] Measurements are represented as (mean value) ± (2 × standard deviation) based on sensitivities determined across Experiments #1 through #7.

The sensitivities of the SRI-TOF-MS to ISOP, MVK, and MACR determined for trap temperatures of +25 and -40 °C are listed in Table 2-2. To account for possible matrix effects, calibrations for both H_3O^+ and NO^+ were carried out for each experiment by standard addition to the outflow air from the chamber (i.e., prior to the low-temperature trap). For both the H_3O^+ and NO^+ modes, the sensitivities did not depend on trap temperature. This temperature independence indicates that ISOP, MVK, and MACR did not condense at a trap temperature of -40 °C. Hence, MVK and MACR were effectively separated from other oxidation products of lower volatility by use of the trap

at -40 °C (vide infra). The ISOP, MVK, and MACR concentrations reported herein were based on NO^+ ionization and using the -40 °C trap prior to the SRI-TOF-MS.

As a comparison point, the sensitivity of ISOP in NO^+ mode measured in this study agreed with the value reported by Karl et al. [2012] for similar E/N ratios. With respect to the H_3O^+ mode, the sensitivities of ISOP, MVK, and MACR differed from the theoretically expected values by less than 10% [Zhao and Zhang, 2004; de Gouw and Warneke, 2007]. The signal for $C_3H_5^+$ (m/z 41.039), an isoprene fragment in H_3O^+ mode, was 6% of the main isoprene signal and lay within the range of 3% to 16% reported in the literature [e.g., Ammann et al., 2004; McKinney et al., 2011].

Table 2-1 presents the steady-state concentrations of ISOP, MVK, and MACR measured in NO^+ mode as well as the steady-state concentrations of ISOP and MVK + MACR measured in H_3O^+ mode determined from the data at -40 °C. The combined concentration of MVK and MACR measured using H_3O^+ ionization agreed with the sum of the speciated measurements using NO^+ ionization for all experiments.

2.3.2 Unexpected Interference of MVK and MACR measurements

Changes in the signal intensities of $C_5H_8^+$, $C_4H_5O^+$, and $C_4H_6NO_2^+$ ions produced using the NO^+ reagent ion are shown in Figure 2-4 for stepwise decreases in trap temperature from +25 to -40 °C. Results are shown for Experiments #1 and #7, representing HO_2-dominant and NO-dominant conditions, respectively. The ion intensities plotted in Figure 2-4 nominally represent ISOP, MACR, and MVK: the data show that in the HO_2-dominant experiments additional species contributed to these ions for trap temperatures warmer than -30 °C. The more general formula $C_4H_6NO_2^+$ is therefore used in place of $C_4H_6O{\cdot}NO^+$ because specific formulas of the additional species are not known.

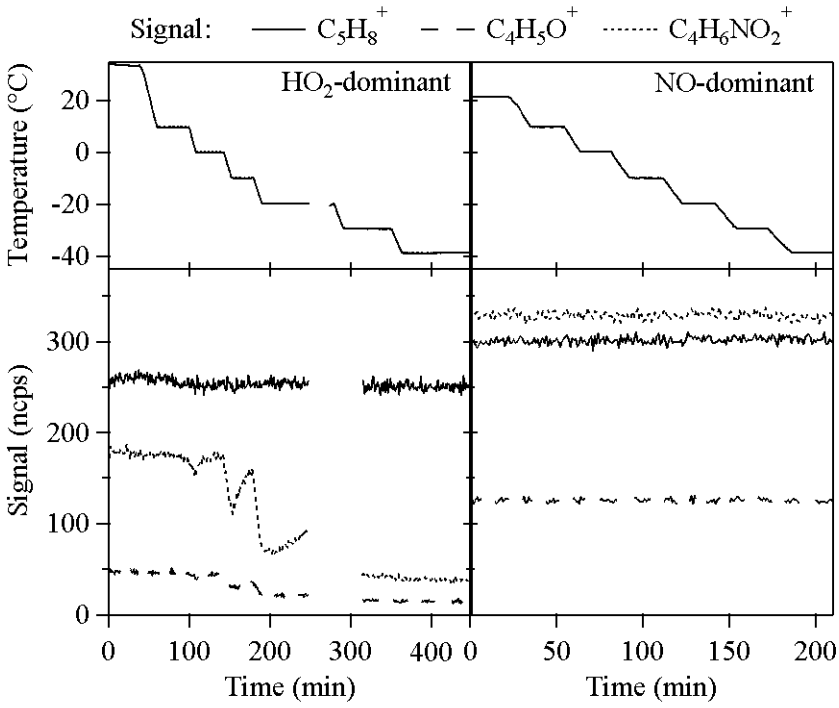

Figure 2-4 Time series of (top) trap temperature and (bottom) signal intensities of $C_5H_8^+$, $C_4H_5O^+$, and $C_4H_6NO_2^+$ ions. These ions nominally represent ISOP, MACR, and MVK, respectively, when using the NO^+ reagent ion. Results are shown both for HO_2- and NO-dominant conditions (Experiments #1 and #7).

The signal intensity for the $C_5H_8^+$ ion did not depend on trap temperature for either dominant oxidation pathway. The implication is that there was no chemical interference for isoprene detection via the $C_5H_8^+$ ion. Likewise, the signal intensities of the $C_4H_5O^+$ and $C_4H_6NO_2^+$ ions did not depend on temperature for the NO-dominant experiments, implying that these ions represented the instrument response to MACR and MVK in those experiments. By comparison, the signal intensities of the nominal $C_4H_5O^+$ and $C_4H_6NO_2^+$ ions depended strongly on temperature from 0 to -30 °C in the HO_2-dominant experiments, implying the presence of other molecular products that were removed at low temperature. The signal intensities were independent of temperature from -30 to -40 °C, meaning that the interference products were fully removed from the gas phase at the trap temperature below -30 °C and hence the $C_4H_5O^+$ and $C_4H_6NO_2^+$ ions

at -40 °C represented the instrument response to MACR and MVK. Temperature-dependent patterns of signal intensity using the H_3O^+ reagent ions (cf. Figure A-1 in Appendix A) were similar to the results shown in Figure 2-4 for the NO^+ reagent ions.

For the HO_2-dominant experiments, the signal intensities of the $C_4H_5O^+$ and $C_4H_6NO_2^+$ ions were stable at temperatures warmer than 0 °C. As the trap temperature cooled below 0 °C, the signal intensities first decreased and then returned to the original level. This dip-recovery behavior suggests adsorption on the cold inner walls of the trap coil followed by thermodynamic equilibration between partial and vapor pressures with time. As the trap temperature decreased further, the dip in signal intensity increased and the rate of recovery decreased, consistent with a longer approach to equilibrium for decreased vapor pressures at lower temperatures. For -30 °C, recovery was no longer observed, suggesting that the surface uptake process transitioned from adsorption to condensation.

With high plausibility, the condensing species can be inferred to be a mixture of organic hydroperoxides (ISOPOOH) and possibly epoxides (IEPOX) based on their physical properties and the dominant chemical pathways. There are two lines of evidence. (1) The condensing species were absent for the NO-dominant experiments, implying that the condensing products were produced exclusively by the HO_2 pathway. ISOPOOH ($C_5H_{10}O_3$) and IEPOX ($C_5H_{10}O_3$) isomers are oxidation products formed exclusively by the HO_2 pathway. Paulot et al. [2009b] reported a yield of >70% for ISOPOOH isomers from the reaction of HO_2 + ISOPOO and a yield of >75% for IEPOX isomers from further oxidation of ISOPOOH by OH. (2) The condensing species had lower volatilities than MVK and MACR because neither MVK nor MACR condensed at -40 °C (Table

2-2). Compared with MVK and MACR, the ISOPOOH and IEPOX species have multiple functional groups as well as an additional carbon atom. Correspondingly, their vapor pressures are lower than MVK and MACR [Pankow and Asher, 2008].

The expected SRI-TOF-MS product ions of ISOPOOH and IEPOX assuming no fragmentation were not observed in the chamber air using either H_3O^+ or NO^+ reagent ions. Therefore, either thermal decomposition in the instrument (60 °C) or fragmentation following ionization occurred to these two compounds in both modes. A set of experiments was carried out to investigate how the operating parameters of the SRI-TOF-MS might influence the fragmentation or the decomposition of the species that had condensed in the low-temperature trap. The results are included in Appendix A. The conclusion of the analysis is that ionization processes are the better explanation than thermal decomposition.

To further assess whether ISOPOOH and IEPOX isomers can fragment to ions at the same m/z ratio as the product ions of MVK and MACR, the fragmentation patterns for proxy compounds or authentic standards were tested. Trans-β-IEPOX (cf. Figure 1-3) was synthesized following the procedure of Zhang et al. [2012]. The ionization of β-IEPOX mainly led to $C_5H_7O^+$ ions in H_3O^+ mode and $C_5H_6O^+$ ions in NO^+ mode, which are different from the product ions of MVK and MACR. Under the assumption of similar fragmentation patterns for all the isomers of IEPOX, the conclusion is that IEPOX was not the condensing species that contributed to the same m/z ratio as the MVK and MACR ions (This statement was verified later when all the four IEPOX isomers were synthesized; cf. Figure 4-3).

Because no ISOPOOH standards were available, tert-butyl hydroperoxide ($M=C_4H_{10}O_3$) was instead tested as a proxy compound. The main product ions included $(M-(OOH))^+$, $(MH-(OH)-(CH_3))^+$, and $(MH-(H_2O))^+$ in the H_3O^+ mode. For the NO^+ mode, $(M-(OOH))^+$ and $(M\cdot NO-(OH)-(CH_3))^+$ were observed. As presented in Reaction (R2-5), the production of $(M\cdot NO-(OH)-(CH_3))^+$ in the NO^+ mode might be due to a loss of a β-carbon and an -OH from the -OOH group to produce a carbonyl compound upon reaction with NO^+. A similar pathway can produce $(MH-(OH)-(CH_3))^+$ in H_3O^+ mode. Under the supposition that similar chemical processes can occur for M=ISOPOOH, the product ions are identical to those produced by MVK and MACR in the PTR-TOF-MS analysis (Reactions (R2-6) and (R2-7)).

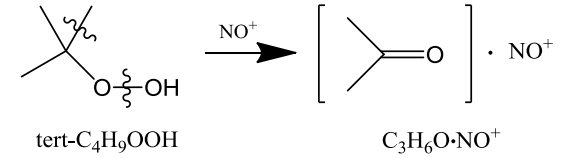

(R2-5)

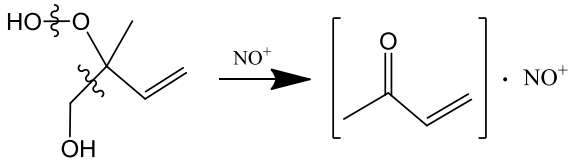

(R2-6)

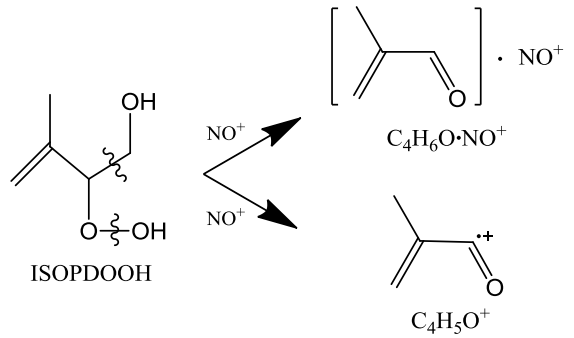

(R2-7)

A further line of evidence in favor of hydroperoxides is the variation of signal intensities with chamber residence time, as shown in Figure 2-5. The equivalent

concentrations of the interference for MVK and MACR (defined as the difference in the concentrations of MVK and MACR quantified at the trap temperature of 25 °C and those at -40 °C) were higher for shorter residence times, suggesting that the contributing compounds are first-generation products, i.e., hydroperoxides rather than epoxides.

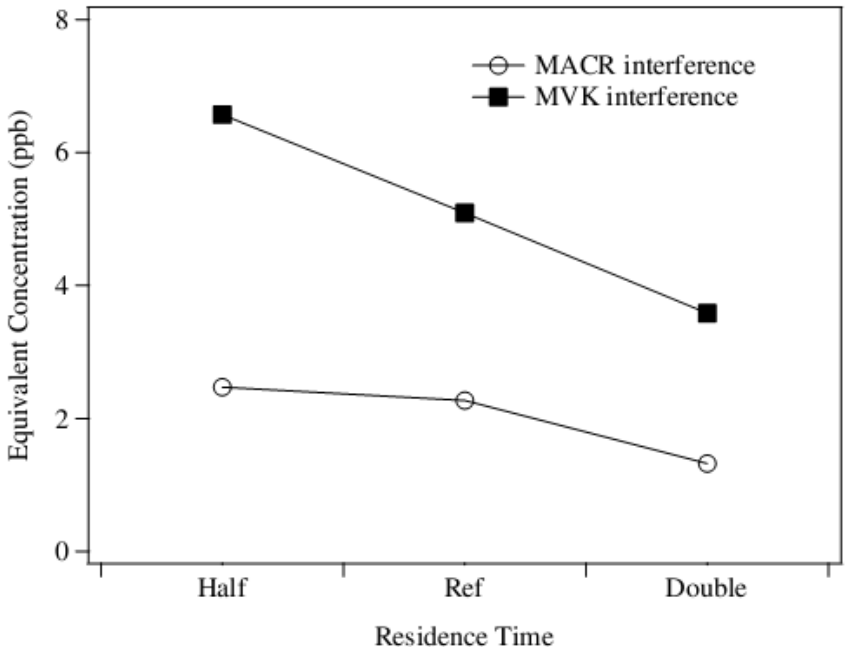

Figure 2-5 Change in the equivalent concentrations of the interference compounds to MVK and MACR with chamber residence time. The equivalent concentration of MVK/MACR interferences is defined as the difference of MVK/MACR concentration at the trap temperature of +25 °C and that at -40 °C. The residence time of reference experiment was 3.7 hr.

One year after our results was published [Liu et al., 2013], our hypothesis that ISOPOOH isomers, specifically ISOPBOOH and ISOPDOOH, are detected as the product ions of MVK and MACR in SRI-TOF-MS system was verified by using synthesized authentic ISOPOOH compounds [Nguyen et al., 2014b; Rivera-Rios et al., 2014]. These experiments suggest that this instrument bias is due to ISOPOOH decomposition via hemolytic peroxy bond cleavage on metals surface inside SRI-TOF-MS instruments [Rivera-Rios et al., 2014]. This proposed mechanism is consistent with

our experimental results shown in Appendix A. The interference signal was independent of the temperature of the inlet (no metal surface), the ionization energy of the drift tube, but increased slightly with the increase of the temperature of drift tube (metal surface).

2.3.3 Yields of MVK and MACR

The yield of MVK (MACR) is equal to the sum of the mathematical product of (i) the branching ratio leading to the precursor ISOPBOO (ISOPDOO) in the initial reaction of isoprene with OH and (ii) the branching ratios to the channels forming ISOPBO (ISOPDO) in the subsequent ISOPBOO (ISOPDOO) reactions (cf. Figure 2-1). The reactant and product concentrations in the CMFR at steady state can be incorporated in an analysis to determine MVK (MACR) product yields. The relationship of mass balance for the sources and sinks of MVK (MACR) is given by the following equation:

$$0 = \left(Y_{MVK}\, k_{ISOP+OH}\, [OH]_{ss} [ISOP]_{ss}\right)_{sources} - \left(k_{MVK+OH}\, [OH]_{ss}\, [MVK]_{ss} + \frac{1}{\tau}[MVK]_{ss} + k_{wall}\, [MVK]_{ss} \right)_{sinks} \quad (2\text{-}1)$$

in which $[M]_{ss}$ is the steady-state chamber concentration of compound M, Y_{MVK} is the yield of MVK from isoprene oxidation for one set of chamber conditions, τ is the mean residence time in the chamber, $k_{ISOP+OH}$ and k_{MVK+OH} are the reaction rate constants of ISOP and MVK with OH, and k_{wall} is the steady-state wall loss rate of MVK. Control experiments show that a photolysis sink for MVK (MACR) was negligible, at least for the conditions of the conducted experiments. Rearrangement of Equation (2-1) leads to the expression for the yield of MVK, as follows:

$$Y_{MVK} = \frac{(k_{MVK+OH}[OH]_{ss} + 1/\tau + k_{wall})[MVK]_{ss}}{k_{ISOP+OH}[OH]_{ss}[ISOP]_{ss}} \quad (2\text{-}2)$$

For Y_{MACR}, a direct analogy to Equation (2-2) exists.

For use of Equation (2-2), values of $k_{ISOP+OH}$ and k_{MVK+OH}, including their uncertainties, were taken from the IUPAC database [Atkinson et al., 2006]. A value of $k_{wall} = 0\ s^{-1}$ was used based on the results of wall-loss experiments for ISOP, MVK, and MACR that were performed separately in the HEC. The value of $[OH]_{ss}$ was calculated based on measurements of the isoprene concentration prior to the reaction (i.e., dark conditions) and at steady state (i.e., during photo-oxidation), as follows:

$$0 = \left(\frac{1}{\tau}[ISOP]_{in}\right)_{sources} - \left(k_{ISOP+OH}[OH]_{ss}[ISOP]_{ss} + \frac{1}{\tau}[ISOP]_{ss}\right)_{sinks} \quad (2\text{-}3)$$

in which $[ISOP]_{in}$ was the inflow concentration of isoprene to the HEC. The steady-state OH concentration inferred by use of Equation (2-3) varied from 1.8 to $2.0 \times 10^6\ cm^{-3}$ for Experiments #1 to #6.

Yields of MVK and MACR for each experiment are listed in Table 2-1. In the case of Experiment #1, the MVK and MACR yields by Equation (2-2) and its analog were (4.6 ± 0.7)% and (3.2 ± 0.6)%, respectively, for reaction at 25 °C and < 2% RH. The uncertainties (2σ) for Y_{MVK} and Y_{MACR} were estimated using a Monte Carlo method in which the values of all input parameters in Equations (2-2) and (2-3) were sampled from probability density functions of their individual values (i.e., their individual uncertainties). The uncertainties in the concentrations were based on calibrations. The uncertainties in the reaction rate coefficients were obtained from the IUPAC recommendations. A 6% 2σ-uncertainty was used for the chamber residence time based on the standard deviation in measured residence times for multiple experiments. The

ensembles of results for Y_{MVK} and Y_{MACR}, which can be approximated by normal distributions, were the basis of the reported statistical errors to the mean values.

In the case of Experiment #7 for NO-dominant conditions, MVK and MACR were produced in high yields as a result of the reaction of ISOPOO with NO [e.g., Tuazon and Atkinson, 1990]. Ozone produced as part of the NO_x photochemical cycle also reacted to a small extent with ISOP, MVK, and MACR in this experiment. Equations (2-1) to (2-3) were therefore expanded to include this chemistry, with rate constants taken from the IUPAC database. The ozone concentration (65 ppb) measured in the chamber outflow was used, resulting in a calculated OH concentration of 1.5×10^6 cm^{-3} with ozone correction. For these concentrations, 90% of isoprene reacted with OH and 10% with O_3. The ozonolysis of isoprene also provided an additional source term for MVK and MACR. This term, with MVK and MACR yields taken from Aschmann and Atkinson [1994], was also included in the calculation. The resulting MVK and MACR yields (Table 2-1) were (36.8 ± 4.4)% and (31.8 ± 3.9)% without ozone correction and (41.4 ± 5.5)% and (29.6 ± 4.2)% with the correction.

The source term in Equation (2-1) is written assuming that MVK is not produced through any process other than as a first-generation product of OH reaction with isoprene. Secondary oxidation processes of some isoprene oxidation products, like ISOPOOH ($C_5H_{10}O_3$) and IEPOX ($C_5H_{10}O_3$), isomers could conceivably also produce some MVK and MACR and therefore represent an additional source term. For example, the MCM suggests that photolysis of ISOPOOH can lead to ISOPO and hence MVK and MACR, although the modeled contribution of ISOPOOH photolysis is < 1% of the combined production rate of MVK and MACR in Experiment #1. As one test of the data against the

possibility of additional production by secondary sources (photolysis and otherwise), experiments were conducted for halved (#2; 1.9 hr) and doubled (#3; 7.4 hr) chamber residence times relative to Experiment #1. As expected, for an increase (decrease) in chamber residence time, the steady-state concentration of isoprene decreased (increased) while those of its oxidation products increased (decreased). The MVK and MACR yields were expected to remain constant only in the absence of significant secondary production; that is, significant secondary production would lead to non-linearity in the yields with respect to residence time. For halving the residence time (Experiment #2, Table 2-1; Figure 2-6A), however, these changes in concentration left the yield unchanged compared to Experiment #1. Doubling the residence time (Experiment #3, Table 2-1; Figure 2-6A) did increase the MVK and MACR yields. Therefore, secondary processes seemed to produce significant quantities of MVK and MACR only for $\tau \gg 3.7$ hr, and shorter residence times such as in Experiment #1 produced yields representative of first-generation products.

2.3.4 Verification of HO_2-dominant fate for isoprene-derived peroxyl radicals

The dominant regime for the fate of the ISOPOO radicals, whether that of HO_2, NO, RO_2, or isomerization reactions, was assessed both computationally with the assistance of MCM simulations and experimentally by empirical observation of the effects of varying the reaction conditions on the results. The HO_2 and $\sum RO_2$ concentrations modeled by the MCM, in conjunction with the upper limit of NO concentration based on measurement, were used to calculate the contribution of each pathway to the fate of ISOPOO in each experiment. The results are presented in Table 2-3. For Experiment #1, the modeled concentrations of HO_2 and $\sum RO_2$ were 540 ppt and 17 ppt, respectively, and the

measured NO was below the detection limit (70 ppt, 3σ), resulting in a calculated contribution of > 93% from the HO_2 pathway, < 6% from the NO pathway, and 1% for the RO_2 and isomerization pathways. The calculated contribution from the HO_2 pathway represents a lower limit because as a stringency test the calculation used an upper limit for the NO concentration (70 ppt). Actual NO concentration was likely lower because of titration by HO_2, perhaps on order of 3 ppt based on the MCM model simulation or 14 ppt based on inversion analysis (cf. Section 2.3.5).

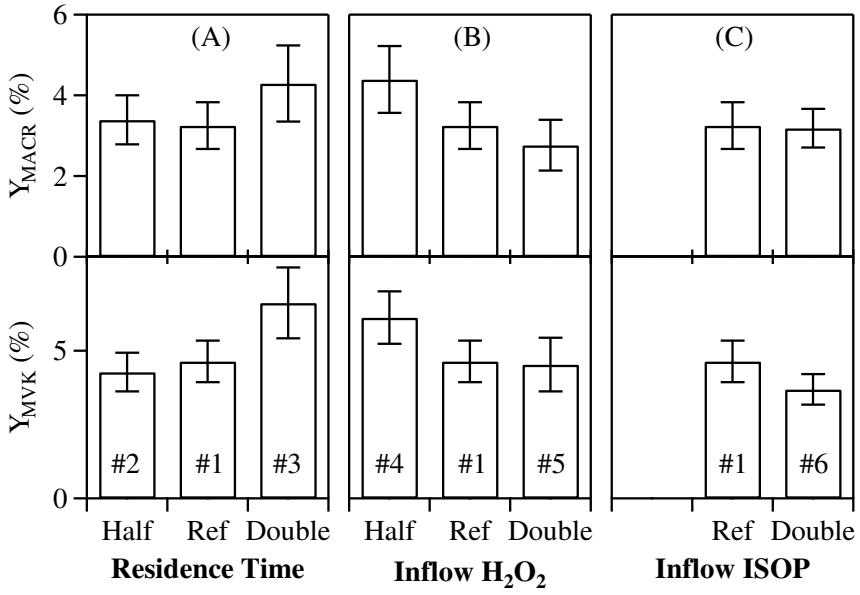

Figure 2-6 Yields of MACR (top) and MVK (bottom) for HO_2-dominant conditions. (A) Variable residence time. (B) Variable inflow concentration of H_2O_2. (C) Variable inflow concentration of ISOP. The labeled experiment numbers refer to Table 2-1.

The titration of NO by HO_2 was verified experimentally. A flow of 0.5 ppb NO was introduced with the chamber inflow for the same experimental conditions as Experiment #1. No change was observed in the NO signal (below detection limit) or the SRI-TOF-MS signals for major product ions. The NO_x concentration increased as expected, implying that NO was titrated by excess HO_2 to produce NO_2. This observation is consistent with the MCM simulations, which suggest a steady-state NO concentration

of 6 ppt in the presence of an inflow NO concentration of 0.5 ppb. Another line of evidence is that the nitrate-containing ion observed in the high-NO_x experiment (Experiment #7), which was the protonated ion of peroxyacetyl nitrate ($C_2H_4NO_5^+$) [Hansel and Wisthaler, 2000], was absent in all other experiments.

Table 2-3 Modeled relative importance of competing reaction pathways for Experiments #1 to #7.

	Mixing ratios (ppt)			Reaction rates with ISOPOO (10^{-2} s^{-1}) [3]				Contribution by pathway (%)			
	NO[1]	HO_2[2]	$\sum RO_2$[2]	NO	HO_2	RO_2	ISOM	NO	HO_2	RO_2	ISOM
#1	<70	541	17	1.5	23	0.1	0.2	<6	93	0.3	0.8
#2	<70	532	23	1.5	23	0.1	0.2	<6	93	0.4	0.8
#3	<70	540	13	1.5	23	0.1	0.2	<6	93	0.2	0.8
#4	<70	354	25	1.5	15	0.1	0.2	<9	89	0.7	1.2
#5	<70	795	12	1.5	34	0.1	0.2	<4	95	0.1	0.6
#6	<70	500	35	1.5	21	0.2	0.2	<7	92	0.7	0.9
#7	910	28	25	20	1.2	0.1	0.2	93	6	0.5	0.9

[1] Value measured by NO_x analyzer, which had a detection limit of 70 ppt.

[2] Value simulated using MCM v3.2 for the employed reaction conditions.

[3] Reaction rate coefficients of ISOPOO used here: 8.8×10^{-12} cm^3 $molec^{-1}$ s^{-1} for NO and 1.74×10^{-11} cm^3 $molec^{-1}$ s^{-1} for HO_2 [Atkinson et al., 2006]. A single effective reaction rate coefficient with value of 1.8×10^{-12} cm^3 $molec^{-1}$ s^{-1} was used for the RO_2 family. This value represents the average reaction rate coefficient of the ISOROO isomers weighted by their respective branching ratios in MCM v3.2. The isomerization rate coefficient measured experimentally (0.002 s^{-1}) by Crounse et al. [2011] was used. A higher contribution of isomerization pathway (4%) was expected using the rate coefficient predicted by Peeters and Muller (0.01 s^{-1}) [2010].

The accuracy of the foregoing modeling analysis, represented by Table 2-3, is subject to the uncertainties of the kinetic scheme of MCM v3.2 as well as pathways not included in the scheme, such as possible unaccounted-for wall loss rates or photolysis rates of reactive intermediates, principally ISOPOO. Experiments #4 to #6 were designed to supplement the modeling analysis by providing empirical verification that there was no considerable contribution to Experiment #1 from pathways other than HO_2.

Experiments #4 and #5 employed halved and doubled H_2O_2 inflow concentrations, respectively, thereby changing the steady-state concentration of HO_2 (cf. Table 2-3). As represented in the MCM (v3.2), the yields of MVK and MACR are 41.5% and 26.5% via the NO pathway and 35.5% and 24.5% via the RO_2 pathway, and the respective yields are predicted as 16% and 9% via the isomerization pathway [Peeters and Muller, 2010]. The observed yields in the HO_2-dominant experiments in the present study were much lower than either case above. Hence, in the case that other pathways significantly competed with HO_2, the MVK and MACR yields would have increased (decreased) with a decrease (increase) of the H_2O_2 and hence HO_2 concentrations. As shown in Figure 2-6B, doubling the H_2O_2 concentration (Experiment #5, Table 2-1) did not decrease the yield compared with Experiment #1, implying that pathways other than the HO_2 channel were not important for Experiments #1 and #5. These other channels did start to have an influence when the H_2O_2 concentration was halved, which increased the MVK and MACR yields (Experiment #4, Table 2-1).

Experiment #6 was designed as a further empirical test of the importance of the RO_2 pathway relative to the HO_2 pathway. Doubling the isoprene inflow concentration in Experiment #6 increased the steady-state concentration of RO_2 (cf. Table 2-1), yet the MVK and MACR yields did not increase (Figure 2-6C), supporting the conclusion that the RO_2 pathway was not significant in Experiment #1.

Two other possible reaction pathways of ISOPOO include wall collisions (i.e., leading to possible depositional loss or heterogeneous reaction) and photolysis. McMurry and Grosjean [1985] provided a formulation to estimate the lifetime of gas-phase species in a chamber against wall collisions. For the experimental conditions of the present study,

the estimate was on order 10^3 s. By comparison, the lifetime of ISOPOO against HO_2 was 5 s for the conditions of Experiment #1, suggesting that wall collisions were at most of minor importance for the fate of ISOPOO.

Although the absorption spectrum of ISOPOO radicals is not known specifically, oxygen-substituted organic peroxy radicals typically absorb across the range 200 to 300 nm [Lightfoot et al., 1992; Wallington et al., 1992]. By comparison, the employed lamps had negligible photo emission for wavelengths shorter than 310 nm. The data analysis therefore omits a photolysis channel. Even so, a caveat is that there is at least one case, represented by the $CH_3C(O)CH_2OO$ radical, for which absorption above 300 nm was reported [Cox et al., 1990].

The results of the high-NO_x experiment (#7) also provide evidence that wall collisions and photolysis were unimportant for the fate of ISOPOO. The yields $Y_{MVK,NO}$ and $Y_{MACR,NO}$ agreed with those reported in the literature for a wide range of reaction conditions (cf. Section 2.3.6). This agreement suggests an absence in Experiment #7 of significant ISOPOO wall collisions or photolysis. The lifetime of ISOPOO against NO (0.9 ppb) was 5 s for Experiment #7. Because the lifetime of ISOPOO against HO_2 for Experiment #1 was also 5 s, the logical inference is that wall collisions and photolysis were also unimportant fates of ISOPOO in that experiment.

2.3.5 Best Estimate for yields of MVK and MACR via the HO_2 pathway

The MCM simulations and empirical experiments both support qualitatively that there was a dominant contribution of HO_2 pathway to the fate of ISOPOO for Experiment #1 (Section 2.3.4). The present section provides a quantitative assessment of the possible effects of minor contributions from other pathways and the best estimate for Y_{MVK,HO_2} and

Y_{MACR,HO_2}. The focus of the analysis is on the competing NO pathway, established in Section 2.3.4 as the most significant pathway competing with HO_2 for the conditions of the experiments.

The possible minor contribution of the NO pathway to the yields of MVK and MACR in the HO_2-dominant experiments was estimated by constructing a kinetic model having branching ratios ξ_{HO2} and ξ_{NO} for the fate of ISOPOO with HO_2 and NO, respectively, and then applying a fit of the model to the observed yields from the three experiments using various H_2O_2 concentrations. The model is constructed as follows. In the case that MVK was produced only by HO_2 and NO reactions, $Y_{MVK} = Y_{MVK,HO_2}\,\xi_{HO2} + Y_{MVK,NO}\,\xi_{NO}$. For the case of ISOPOO loss only by these reactions, the branching ratios can be expanded, and the observed yield Y_{MVK} of MVK is then as follows:

$$Y_{MVK} = Y_{MVK,HO_2}\frac{k_{HO_2+ISOPOO}[HO_2]_{ss}}{k_{HO_2+ISOPOO}[HO_2]_{ss} + k_{NO+ISOPOO}[NO]_{ss}} + Y_{MVK,NO}\frac{k_{NO+ISOPOO}[NO]_{ss}}{k_{HO_2+ISOPOO}[HO_2]_{ss} + k_{NO+ISOPOO}[NO]_{ss}} \quad (2\text{-}4)$$

An analogous equation exists for Y_{MACR}. Terms in Equation (2-4) include the yields $Y_{MVK,NO}$ and Y_{MVK,HO_2} of MVK for the NO and HO_2 pathways, the reaction rates coefficients $k_{NO+ISOPOO}$ and $k_{HO_2+ISOPOO}$ of ISOPOO with NO and HO_2, and the steady-state concentrations $[NO]_{ss}$ and $[HO_2]_{ss}$ of NO and HO_2.

Any NO contamination in the chamber was taken to have a zero-order source term $k_{0,NO}$ independent of reactions conditions. For instance, there can be NO present in the inflow air (i.e., what passes through the pure air generator), or NO can diffuse from the outside chamber environment through the walls of the Teflon bag into the reaction

zone. Because NO was produced slowly but reacted quickly with the excess HO_2, we invoke the steady-state approximation and write:

$$0 = k_{0,NO} - k_{NO+HO_2}[NO]_{ss}[HO_2]_{ss} \tag{2-5}$$

where k_{NO+HO_2} is the reaction rate coefficient of NO and HO_2. Combining Equations (2-4) and (2-5), we have:

$$\begin{aligned} Y_{MVK} &= Y_{MVK,HO_2}\frac{[HO_2]_{ss}}{[HO_2]_{ss}+\frac{k'}{[HO_2]_{ss}}} + Y_{MVK,NO}\frac{\frac{k'}{[HO_2]_{ss}}}{[HO_2]_{ss}+\frac{k'}{[HO_2]_{ss}}} \\ &= Y_{MVK,HO_2}\left(1+\frac{k'}{[HO_2]_{ss}^2}\right)^{-1} + Y_{MVK,NO}\left(1+\frac{[HO_2]_{ss}^2}{k'}\right)^{-1} \end{aligned} \tag{2-6}$$

where $k' = \frac{k_{NO+ISOPOO}\,k_{0,NO}}{k_{HO_2+ISOPOO}\,k_{NO+HO_2}}$. There is an analogous equation (not shown) to Equation (2-6) for Y_{MACR}.

Regarding Equation (2-6), known terms include $Y_{MVK,NO}$ as determined in the high-NO_x experiment (#7), Y_{MVK} that was measured, and $[HO_2]_{ss}$ that was simulated by the MCM (Table 3). Unknown terms are Y_{MVK,HO_2} and k'. Experiments #1, #4, and #5 represent three realizations of Equation (2-6). Similarly, there are three realizations for Y_{MACR,HO_2} and k'. Overall, there are therefore six statements of equality and three terms Y_{MVK,HO_2}, Y_{MACR,HO_2}, and k'. These terms were numerically optimized by the Levenberg-Marquardt algorithm so as to minimize the sum-of-the-square of differences of the equality statements of the six realizations. Uncertainty estimates (2σ) in Y_{MVK,HO_2}, Y_{MACR,HO_2}, and k' were obtained by a Monte Carlo method of sampling from the

uncertainties in the input parameters and reevaluating the values of the optimized parameters. An uncertainty of 30% was used for the simulated HO_2 concentrations based on uncertainties in the reaction rate constants of the dominant source and sink of HO_2.

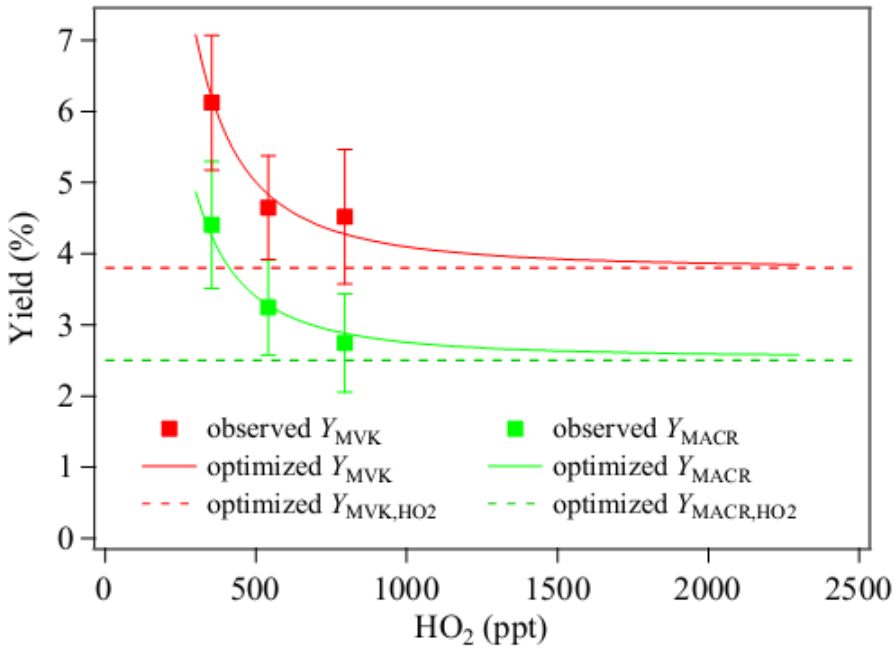

Figure 2-7 Optimization and sensitivity of Y_{MVK,HO_2} and Y_{MACR,HO_2} by Equation (2-6) to the yield data of MVK and MACR.

The fits after numerical optimization are shown in Figure 2-7 for Equation (2-6) compared to the data. Optimized values are as follows: Y_{MVK,HO_2} = (3.8 ± 1.3)% and Y_{MACR,HO_2} = (2.5 ± 0.9)%. The steady-state NO concentrations, corresponding to the obtained k' value ($7.5^{+14.1}_{-4.9} 10^3$ ppt^2), were 21^{+31}_{-13}, 14^{+26}_{-9}, and 9^{+21}_{-6} ppt for the conditions of half, reference, and double H_2O_2, respectively. For these results, Equation (2-6) implies that the branching ratios of ISOPOO to the HO_2 and NO pathways are 0.97 and 0.03, respectively, for Experiment #1.

2.3.6 Comparison with the literature

Laboratory studies investigating isoprene oxidation chemistry generally have been categorized as either "high-NO_x" or "low-NO_x" experiments [Tuazon and Atkinson, 1990; Paulson et al., 1992; Miyoshi et al., 1994; Benkelberg et al., 2000; Ruppert and Becker, 2000; Sprengnether et al., 2002; Lee et al., 2005; Karl et al., 2006; Paulot et al., 2009b; Crounse et al., 2011; Navarro et al., 2011]. Figure 2-8 shows a comparison of the yields of MACR and MVK via the HO_2 and NO pathway quantified in this study to the yields reported in earlier "low-NO_x" and "high-NO_x" experimental studies and also the yields represented in the MCM. The yields of MVK and MACR via the NO pathway quantified in the NO-dominant experiments are in good agreement with the yields reported in earlier "high-NO_x" experiments and also the yields used in the MCM for the NO pathway.

The yields of MVK and MACR reported herein for the HO_2 pathway are 60-90% lower than the yields reported in other "low-NO_x" experiments [Miyoshi et al., 1994; Benkelberg et al., 2000; Ruppert and Becker, 2000; Lee et al., 2005; Navarro et al., 2011]. Several factors may contribute to this difference. For all of the cited literature studies, the RO_2 pathway was expected to have a significant or even dominant contribution to the ISOPOO chemistry because initial isoprene concentrations of 1 to 100 ppm were used, compared to the <0.1 ppm concentrations of the present study. Miyoshi et al. [1994] found that the yields of MVK and MACR increased for higher isoprene:H_2O_2 ratios, an experimental parameter which regulated the ratio of RO_2 to HO_2. Navarro et al. [2011] observed that the yields of MVK and MACR dropped as the ratio of HO_2 to RO_2 increased from 0.1 to 1. Higher yields of MVK and MACR are expected from the RO_2 pathway than from the HO_2 pathway according to currently accepted

mechanisms, including the MCM (Figure 2-8). Hence, these findings suggest that both the RO_2 and the HO_2 channels contributed to the observed MVK and MACR production in these "low-NO_x" experiments. Another issue for some of the "low-NO_x" studies is that the background NO concentration was typically not well measured, e.g., < 100 ppb of NO_x reported in the study by Ruppert and Becker [2000]. NO_x and HONO off-gassing have been observed in many chamber systems [Carter et al., 2005; Rohrer et al., 2005]. Injection of H_2O_2 could also increase the measured NO_x level in the reactor depending on the concentration of nitrogen impurities in the H_2O_2 solution, as found in the present study. An unaccounted contribution from the background NO in the earlier "low-NO_x" experiments, therefore, could be another reason for the higher reported yields. The present study achieved low NO concentrations (verified experimentally to be below the detection limit of 70 ppt and inverse modeled as 10 to 20 ppt) by use of a high-purity H_2O_2 solution, of a chamber bag never exposed to high concentrations of NO_x, and operation in a CMFR configuration.

Paulot et al. [2009b] probed the HO_2 pathway using ppb-level isoprene concentrations and negative chemical ionization mass spectrometry (CIMS). A combined yield of MVK and MACR was reported because the CIMS instrument did not separately measure isomeric MVK and MACR. This yield was (12 ± 12)% via the HO_2 pathway, with the large uncertainty dependent on an initial amount of NO_x in the chamber [Paulot et al., 2009b]. The result of the present study, (6.3 ± 2.1)% for the combined yield of MVK and MACR, is consistent with the yield range of that study.

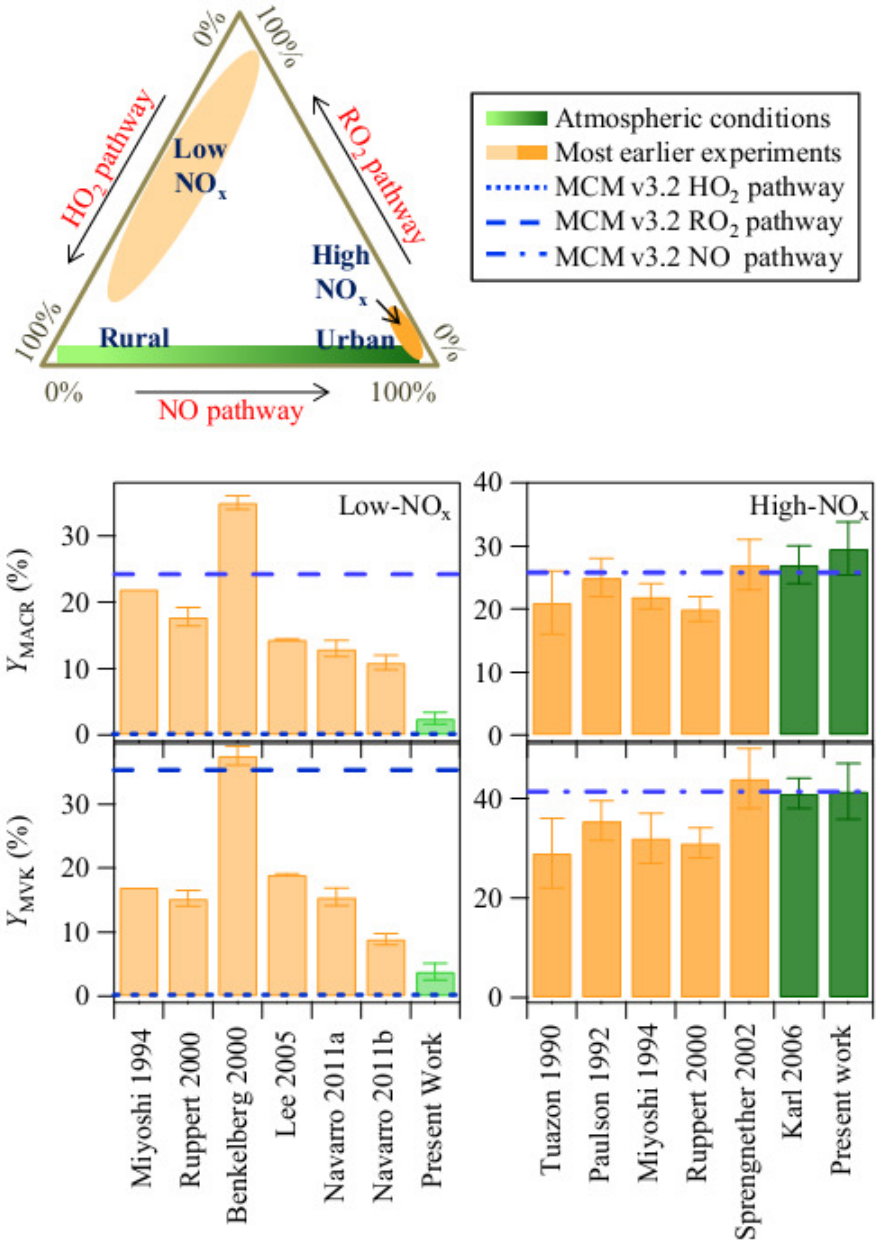

Figure 2-8 Comparison of the MVK and MACR yields of this study by ISOP photo-oxidation with those of earlier studies for conditions described in those studies as "low NO_x" and "high NO_x" (bar) and with those of RO_2, HO_2, or NO pathways represented in MCM (line). The inset triangle diagram represents environmental factors that can affect the dominant reaction pathways of isoprene-derived ISOPOO radicals in the atmosphere and in the laboratory studies. Isomerization pathway is not included due to its small contribution in most laboratory studies, although it could be important in remote atmospheric conditions. Cited studies: Tuazon and Atkinson [1990], Miyoshi et al. [1994], Paulson et al. [1992], Benkelberg et al. [2000], Ruppert and Becker [2000], Sprengnether et al. [2002], Lee et al. [2005], Karl et al. [2006], and Navarro et al. [2011]. The modeled ratio of HO_2 to RO_2 is 0.1 and 1 in Navarro 2011 Exp a and Exp b, respectively.

2.4 Conclusion and Atmospheric Implication

Photooxidation experiments of isoprene were conducted in a steady-state chamber for HO_2-dominant and NO-dominant conditions. The concentrations of ISOP, MVK, and MACR in the chamber were measured with a SRI-TOF-MS equipped with switchable H_3O^+ and NO^+ reagent ion capacities. The use of NO^+ allowed separate quantification of isomeric MVK and MACR, which was not possible using H_3O^+ alone. For both the H_3O^+ and NO^+ modes, some other oxidation products produced under HO_2-dominant conditions fragmented to ions having the same m/z ratios as the product ions of MVK and MACR.

These results have implications for the use of SRI-TOF-MS and its prototype proton-transfer-reaction mass spectrometer (PTR-MS; cf. Section 1.4) to elucidate isoprene chemistry in clean atmospheric environments, which are typically characterized by high HO_2:NO concentration ratios (i.e., favoring HO_2 dominant pathway) (Figure 2-8). The $C_4H_7O^+$ ions in H_3O^+ mode have been exclusively attributed to MVK and MACR [de Gouw and Warneke, 2007; Blake et al., 2009]. The results of the present study, showing interference compounds for HO_2-dominant conditions, indicate that analytical errors may occur. The interference compounds, plausibly attributable to organic hydroperoxides, have low volatility and were removed by adding a low-temperature trap (-40 °C) in the sampling line prior to the SRI-TOF-MS.

With respect to the yields of MVK and MACR, a steady-state approach was used in this study's analysis (Equation (2-1)). This approach was validated by the good agreement between the yields measured under high-NO_x conditions and those reported in the literature. For the low-NO_x conditions of the present study, both kinetic modeling and

inferential experimental evidence were consistent with the HO_2 pathway as the dominant fate of ISOPOO. Small contributions from other pathways to the measured MVK and MACR yields were assessed using experimental data, resulting in a yield for MVK of (3.8 ± 1.3)% and a yield for MACR of (2.5 ± 0.9)% for isoprene photo-oxidation via the HO_2 pathway for the present study.

These reported yields for the HO_2 pathway are 60 to 90% smaller than most other "low-NO_x" experiments. This difference is mainly attributed to significant contributions from the RO_2 pathway associated with the high isoprene concentrations (1-100 ppm) used in other studies (cf. Figure 2-8). In real atmospheric conditions, the RO_2 pathway is less important because of low atmospheric VOC concentrations, typically 10 ppt to 10 ppb (cf. Figure 2-8). Caution is therefore needed when directly applying the results from laboratory "low-NO_x" experiments to atmospheric "low-NO_x" conditions. Instead, it is recommended that the dominant reaction pathway, such as HO_2-dominant or NO-dominant, be specified in place of the more ambiguous descriptors of "low-NO_x" and "high-NO_x" conditions.

The production of MVK and MACR from ISOPOO through the HO_2 reaction pathway is concomitant with OH production, according to Reaction R1b. Therefore, the MVK and MACR yields via the HO_2 pathway imply a concomitant yield of hydroxyl radical from Reaction (R2-2) of (6.3 ± 2.1)%. The total OH yield from Reaction (R2-2) could be higher because only recycling of ISOPBOO and ISOPDOO are evaluated here. This value is consistent with the study of Taraborrelli et al. [2012] which constrained the OH yield from Reaction (R2-2) to <15%. Reactions (R2-3) and (R2-4), which are subsequent to Reaction (R2-2), produce HO_2 at a yield of (6.3 ± 2.1)% of the ISOPOO

and HO_2 initially reacted. Therefore, the HO_x recycling by the channel investigated in the present study is (12.6 ± 4.2)%, given that OH and HO_2 are both reactant and products.

A growing body of observational evidence suggests significant discrepancies in modeled and measured OH concentrations in atmospheric environments having high isoprene emissions and high HO_2:NO ratios [e.g., Lelieveld et al., 2008; Stone et al., 2011]. An OH-recycling channel for the reaction of ISOPOO and HO_2 (Reaction (R2-2)) was proposed to explain the discrepancy. Recycling of 200-300% OH radicals (i.e., amplification) was needed to close the gap between model predictions and atmospheric measurements over the coastal Amazon rainforest [Butler et al., 2008; Lelieveld et al., 2008] as well as in a Southeast Asian rainforest [Stone et al., 2011]. Therefore, the present study's result of (12.6 ± 4.2)% recycling of HO_x is insufficient to close the gap. Not all possible OH-recycling mechanisms for isoprene photo-oxidation are considered here, however [Peeters et al., 2009; Crounse et al., 2011]. Furthermore, a recent report on instrumental issues suggests that the gap between actual and modeled OH concentrations may not be as large as originally reported in some studies (Mao et al., 2012).

3. Reactive Uptake of Isoprene Photooxidation Products via the Hydroperoxy Pathway as Observed from the Gas Phase

3.1 Introduction

Secondary organic material (SOM) produced from atmospheric oxidation of volatile organic compounds constitutes a large fraction of the mass concentration of atmospheric particles [Zhang et al., 2007]. Widespread negative bias in the model prediction of SOM concentration has been a puzzle to atmospheric science community [Heald et al., 2005; Goldstein and Galbally, 2007]. One possible cause for the under-prediction of SOM concentration is missing chemical and physical processes that contribute to SOM formation but not accounted in the models [Carlton et al., 2009; Hallquist et al., 2009]. Non-oxidative reactive uptake of gaseous organic compounds, often catalyzed by acids, is considered as one type of such processes.

Laboratory studies have suggested that many types of organic compounds, including carbonyls [e.g., Jang and Kamens, 2001], hydroperoxides [e.g. Docherty et al., 2005], carboxylic acids [e.g., Hamilton et al., 2006], epoxides [e.g., Surratt et al., 2010], and even some hydrocarbons [e.g., Liggio et al., 2007], could undergo reactive uptake into the condensed phase. Various types of condensed-phase accretion reactions have been proposed [as summarized inKroll and Seinfeld, 2008; Hallquist et al., 2009; Ziemann and Atkinson, 2012], which leads to products with higher molecular weight and hence lower volatility (i.e. oligomers). These reactions are often catalyzed by acids [Ziemann and Atkinson, 2012]. Increased acidity of inorganic seed particles has been shown to lead to enhanced SOM production from individual organic compounds [e.g.,

Jang et al., 2002; Liggio and Li, 2008] and from photooxdiation and ozonolysis of various hydrocarbons [e.g., Czoschke et al., 2003; Surratt et al., 2006]. Whereas many of the previous laboratory studies have focused on product identification, an important yet less investigated question is the relative importance of the reactive uptake of the various gaseous organic compounds, given that atmospheric oxidation of a single hydrocarbon can often lead to many products with multi-functional groups [Atkinson and Arey, 2003].

The current study aims to evaluate the relative importance of the reactive uptake of isoprene and its oxidation products via the hydrperoxyl (HO_2) pathway for a wide range of acidities. Photooxidation of isoprene, particularly via the HO_2 pathway, is an important source of atmospheric SOM [Carlton et al., 2009]. A strong acid effect on SOM yield has been observed for isoprene photooxidation [Kleindienst et al., 2006; Surratt et al., 2007a]. Different from previous studies focusing on particle-phase products, the strategy of the current study is quantifying the change of gas-phase mass spectra before and after injecting acidic particles, in particular peaks arose from isoprene, isoprene-derived hydroxylhydroperoxides (ISOPOOH), and isoprene-derived epoxydiols (IEPOX). ISOPOOH and IEPOX isomers (Figure 1-3) are the major first-generation and second-generation products of isoprene OH-oxidation via the HO_2 pathway [Paulot et al., 2009b]. All the three types of compounds have been previously shown or suggested to contribute to SOM production by reactive uptake [e.g., Surratt et al., 2006; Liggio et al., 2007; Surratt et al., 2010].

3.2 Experimental

3.2.1 Serial-reactor set-up

In overview, two continuously mixed flow reactors were connected in series and operated at steady state as an experimental strategy to separate isoprene photooxidation from SOM production (Figure 3-1). In Reactor #1 (viz. the Harvard Environmental Chamber; HEC), gas-phase isoprene oxidation products were continuously produced. In Reactor #2, the outflow of the HEC was mixed with a flow of sulfate particles. As a result, the signal change of a gas-phase species in Reactor #2 was due to the molecular uptake or release of the species from the sulfate particles.

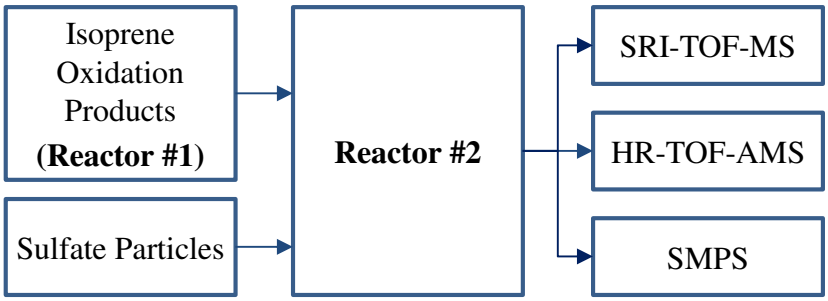

Figure 3-1 Schematic of experimental set-up. Abbreviations are defined in the main text.

Reactor #1 (i.e., the HEC) was operated as a continuously mixed flow reactor at steady state as described in Section 2.2.1. Photolysis of H_2O_2 by ultraviolet light produced OH radicals, initiating isoprene oxidation. The inflow and steady-state isoprene concentrations were 120 ± 5 ppb and 36 ± 1 ppb, respectively. The mean residence time was 3.7 ± 0.3 hr. No new particle production was observed inside Reactor #1, as confirmed by a condensation particle counter (CPC; < 0.5 particle cm^{-3}). Photooxidation in Reactor #1 corresponded to reaction conditions such that the isoprene-derived peroxyl (ISOPOO·) radicals reacted dominantly with HO_2 (cf. Section 2.3.4), which is the main

reaction pathway in unpolluted regions having sufficiently low NO_x concentrations [Lelieveld et al., 2008; Crounse et al., 2011; Xie et al., 2013].

Sulfate particles of variable acidities were generated using two methods. Highly acidic particles were produced from nucleation of sulfuric acid vapor. Sulfuric acid vapor was produced by heating a concentrated solution (96% w/w). The heater temperature was controlled at 67 °C to induce significant new particle production in the headspace over the solution. Adventitious NH_3 slightly neutralized the particles, as observed in the NH_4^+:SO_4^{2-} mass ratio determined by particle mass spectrometry. Less acidic sulfate particles were produced by exposing ammonium sulfate particles to sulfuric acid vapor. Size-selected crystalline ammonium sulfate particles were generated by using an atomizer, a diffusion dryer, and a differential mobility analyzer (DMA) in series. The central mobility diameters of particles carrying a single or double positive charge were 50 ± 2 and 72 ± 3 nm, respectively. The heater temperature of the sulfuric acid was controlled at 20-60 °C to avoid nucleation. The mass of depositing vapor on the ammonium sulfate particles was regulated by the heater temperature, ultimately determining the extent X of neutralization of the mixed particles. The quantity X is defined as $n(NH_4^+)/(2n(SO_4^{2-}))$ for ion mole concentration n(ion) (mol m^{-3}) and ranges from 0 for sulfuric acid to 1 for ammonium sulfate.

The flows of gas-phase oxidation products from Reactor #1 and of sulfate particles from the generator were mixed together in Reactor #2 (72 L, made of glass). Reactor #2 served as the second continuously mixed flow reactor, also operated at steady state. The temperature, relative humidity, and flow were 20 ± 1 °C, < 5%, and 0.87 Lpm, respectively. The reactor was covered in aluminum foil to avoid irradiation by laboratory

lighting. Particle injection was switched by adjusting the DMA voltage and heater temperature rather than altering flows. For photooxidation products measurable by the chemical ionization mass spectrometry employed in the present study (vide infra), no significant wall loss was observed in Reactor #2 at steady state in the absence of sulfate particles, as demonstrated by a comparison of the mass spectrum of air sampled directly from Reactor #1 with that sampled through Reactor #2 (Figure 3-2).

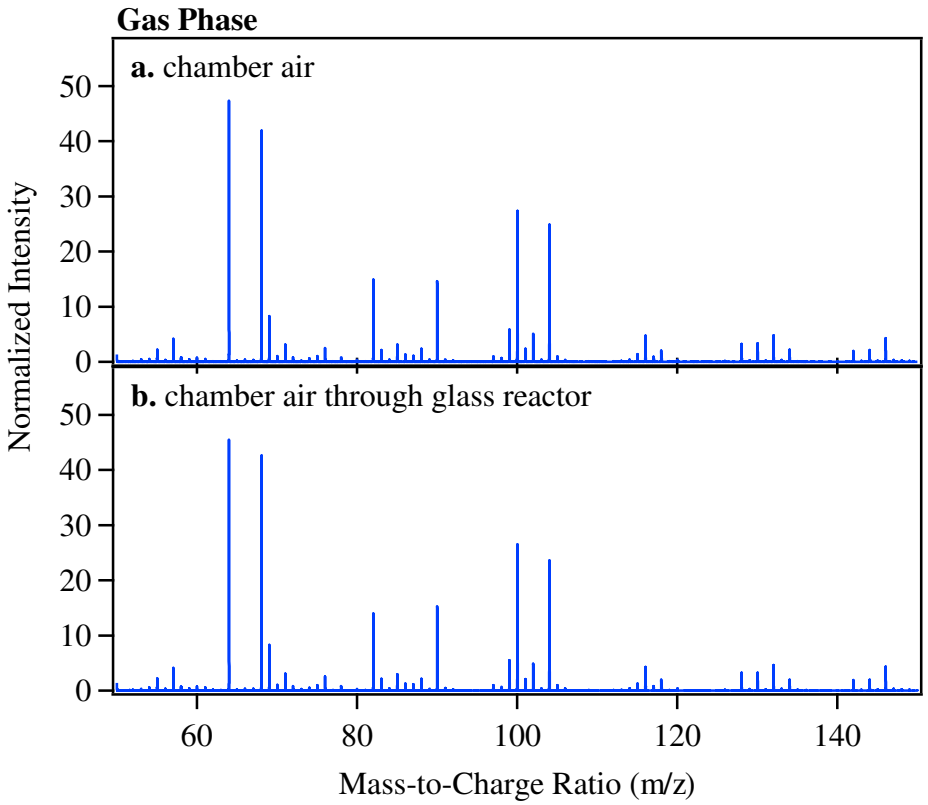

Figure 3-2 Mass spectra collected by SRI-NO^+-TOF-MS of HEC outflow. (a) Sampled directly and (b) sampled through the Reactor #2. The HEC condition was different from the main experiments in terms of initial isoprene concentration and residence time. HEC outflow was not diluted in Reactor #2.

3.2.2 Gas and particle measurements

Gas mass spectra of the outflow from Reactor #2 were recorded by a selective-reagent-ionization time-of-flight mass spectrometer (SRI-TOF-MS; NO^+ reagent; Ionicon

Analytik GmbH) [Jordan et al., 2009b; Jordan et al., 2009a]. Soft chemical ionization by NO^+ (9.26 eV) of the gas-phase sample typically resulted in one or a few product ions, and attribution of ions to specific molecules was possible [Smith and Spanel, 2005]. The SRI-NO^+-TOF-MS settings and data analysis procedures were as described in Section 2.2.2. Peaks over the whole high-resolution spectrum were fit, and their corresponding ion compositions were determined. Intensities of ion signals for isoprene and methacrolein were calibrated daily, and the observations indicated a stable instrument response during the experimental period. The ion transmission curve of the SRI-TOF-MS was measured using H_3O^+ as the reagent ion [Taipale et al., 2008]. Ion transmission was taken into account when comparing the intensities of any ions on the spectrum. A 2.0-μm pore size Teflon filter was used to remove particles upstream of the SRI-NO^+-TOF-MS, thereby avoiding complicating factors such as clogging of the inlet or wall deposition. Control studies suggested a negligible effect of the particle filter on the measured gas-phase signals of the outflow of Reactor #2 (cf. Appendix B).

Particles of the outflow from Reactor #2 were sampled by a high-resolution time-of-flight Aerosol Mass Spectrometer (HR-TOF-AMS; Aerodyne Research Inc.) [DeCarlo et al., 2006] and a Scanning Mobility Particle Sizer (SMPS; TSI Inc.). HR-TOF-AMS were used to quantify the extent X of neutralization of the sulfate particles and the mass concentration M_{SOM} of the produced SOM. Ammonium nitrate was used for calibration of the ionization efficiency, which is the major factor affecting quantification of mass concentration. Both mass concentration and unit resolution mass spectra were analyzed using the data analysis software package Sequential Igor Data Retrieval (ver. 1.51H). High resolution data analysis was performed by Peak Integration by Key Analysis (ver.

1.10H). SMPS was used to measure the number-diameter distribution of the particle population. The SMPS consisted of a DMA (TSI 3081) and a CPC (TSI 3776). The DMA voltage was scanned from 32 to 6358 V, corresponding to a diameter range of 25.5 to 487 nm for a sheath flow of 3.0 Lpm and a sample flow of 0.3 Lpm. The scanning time of the DMA was 100 s. The overall time resolution of the measurement was 120 s.

3.2.3 Tests with extended residence time

Separate experiments were conducted to investigate whether the reactive uptake processes is kinetically limited in Reactor #2. Flows of acidic particles and oxidation products of isoprene were mixed in Reactor #2 as described above. When steady state was achieved in Reactor #2, DMA and heating of sulfuric acid was turned off, so that no more particles were injected into the second reactor. The inflow rates to Reactor 2 were not altered so that the inflow concentrations of isoprene oxidation products kept the same. The residence time of particles in Reactor #2 increased with time, whereas the number concentration of particles kept dropping. Size distribution of particles was monitored by a SMPS for 8 hours after stopping the particle injection, in order to investigate whether and by how much the particles could further grow.

3.3 Results and Discussion

3.3.1 Particle measurements

A general overview of the experiments and observations by HR-TOF-AMS is presented in Table 3-1. The extent X of neutralization listed in the second column corresponds to the sulfate particles injected into Reactor #2. Upon injection and mixing with the isoprene photooxidation products, secondary organic material was produced (M_{SOM}; fourth

column). The rows of Table 3-1 correspond to a series of experiments that varied X stepwise from 0.97 ± 0.07 to 0.016 ± 0.005, corresponding to sulfate concentrations of 1.2 ± 0.1 to 8.2 ± 0.5 μg m^{-3}. Sulfate particles were generated by condensation of sulfuric acid vapor to ammonium sulfate particles without leading to nucleation in Experiment #2-#8 and by nucleation of sulfuric acid vapor in Experiment #9. The entries in Table 3-1 show that SOM production was insignificant for solid neutral particles (X = 0.97 ± 0.07) and increased for aqueous acidic particles from 2.1 ± 0.1 μg m^{-3} for X = 0.69 ± 0.04 to 42.5 ± 1.9 μg m^{-3} for X = 0.39 ± 0.02 [Kuwata et al., 2014]. The sections below probe the SOM production processes from the perspective of gas mass spectrometry measurements.

Table 3-1 Summary of experimental conditions and AMS observations

Experiment	X	$M_{sulfate}$ (μg m^{-3})	M_{SOM} (μg m^{-3})
#1	N.A.[1]	<MDL[2]	<MDL
#2	0.97 ± 0.07[3]	0.8 ± 0.1	<MDL
#3	0.69 ± 0.04[4]	1.2 ± 0.1	2.1 ± 0.1
#4	0.64 ± 0.04	1.3 ± 0.1	4.0 ± 0.1
#5	0.57 ± 0.03	1.8 ± 0.1	8.1 ± 0.2
#6	0.50 ± 0.03	2.1 ± 0.1	13.1 ± 0.3
#7	0.46 ± 0.03	2.8 ± 0.1	17.8 ± 0.4
#8	0.39 ± 0.02	3.5 ± 0.1	24.9 ± 0.3
#9	0.016 ± 0.005	8.2 ± 0.5	42.5 ± 1.9

[1] Not Applicable (N.A.).

[2] Method Detection Limit (MDL).

[3] Sulfate particles are solid.

[4] Sulfate particles are at least partially aqueous [Schlenker and Martin, 2005; Mifflin et al., 2009]

Additional experiments (Section 3.2.3) showed that diameter growth of the particle population in Reactor #2 ceased when the injection of sulfate particles was stopped. The implication is that reactions went to completion for majority particles within

the residence time in Reactor #2. This result is important for data interpretation of the main experiment (Section 3.3.3) and evaluation of filter effect (Appendix B). One possible reason of the observed reaction completion is that acids were consumed by organosulfate formation. Decrease of acidity with reaction time has also been reported for SOM formation from α-pinene ozonolysis on acidic sulfate particles previously [Jang et al., 2008]. Acids are often considered as catalyst for the reactive uptake processes, it is often neglected that they could also serve as reactants of some particle-phase reactions and be consumed.

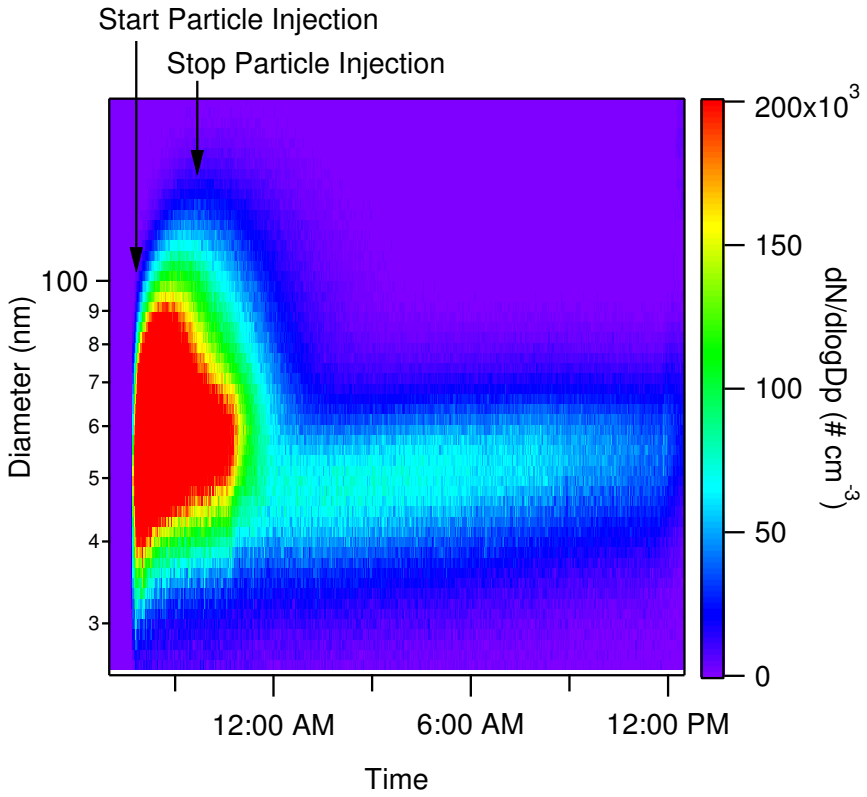

Figure 3-3 Evolution of particle number-diameter distribution following termination of sulfate particle injection in Reactor #2. The extent X of neutralization of injected sulfate particle was 0.02. The Injection of isoprene oxidation products was continued after termination of particle injection.

3.3.2 Uptake or release revealed from gas mass spectra change

The steady-state conditions of the Reactor #1 and #2 enables directly relating the gas mass spectral change to uptake by particles. The mass balance of sources and sinks of any gas-phase species in Reactor #2 in the absence and presence of particles are given by the following equations:

$$\frac{[X]_{in}}{\tau} - \left(\frac{1}{\tau} + k_{wall}\right)[X]_{ss,without\ particles} = 0 \quad (3\text{-}1)$$

$$\frac{[X]_{in}}{\tau} - \left(\frac{1}{\tau} + k_{particles} + k_{wall}\right)[X]_{ss,with\ particles} = 0 \quad (3\text{-}2)$$

where $[X]_{in}$ is the inflow concentration of X to the Reactor #2 (# cm^{-3}), which was constant through the experiment because of the steady-state condition of Reactor #1; $[X]_{ss,\ without\ particles}$ and $[X]_{ss,\ with\ particles}$ are the steady-state concentrations of X in the Reactor #2 without and with particle injection, respectively; τ is the residence time in Reactor #2; $k_{particles}$ and k_{wall} are the particle-loss and wall-loss rate coefficients of species X (s^{-1}) in Reactor #2, respectively. At steady-state and dry condition in Reactor #2, k_{wall} of any species X is considered as zero because of the agreements of SRI-NO^+-TOF-MS signals of the outflow from Reactor #1 sampled directly and through Reactor #2 (Figure 3-2).

Combination of Equations (3-1) and (3-2) leads to the expression of the particle-loss rate coefficient $k_{particles}$ in Reactor #2 as follows:

$$k_{particles} = \frac{1}{\tau}\frac{[X]_{ss,without\ particles} - [X]_{ss,with\ particles}}{[X]_{ss,with\ particles}} = \frac{1 - R_{conc}}{\tau R_{conc}} \quad (3\text{-}3)$$

where R_{conc} is the ratio of steady-state concentration of X with particles to that without particles, defined as $R_{conc} = [X]_{ss,\ with\ particles} / [X]_{ss,\ without\ particles}$. R_{conc} can be estimated using the ratio of peak intensities of the corresponding ion on the SRI-NO^+-TOF-MS spectrum.

Examples of gas-phase unit-mass-resolution spectra collected by sampling the outflow from Reactor #2 by the SRI-TOF-MS are shown in Figure 3-4. The two spectra correspond to the absence and the presence of highly acidic particles (X = 0.02), respectively. The ratios R of peak intensities of the two spectra (i.e., in the presence of acidic particles vs. in the absence of particles) were also presented in Figure 3-4 as approximations of the concentration ratios R_{conc} of respective compounds. The intensities of many peaks decreased following the injection of acidic sulfate particles (R < 1), such as those of $C_4H_6O{\cdot}NO^+$ (m/z 100) and $C_5H_6O^+$ (m/z 82). Some peak intensities did not change significantly following the injection of acidic sulfate particles (R ~ 1), such as those of $C_5H_8^+$ (m/z 68) originating from isoprene and $H_2O_2{\cdot}NO^+$ (m/z 64) from hydrogen peroxide. The former and latter cases indicate significant and insignificant uptake of the corresponding compounds by the acidic particles, respectively.

An unexpected observation of the mass spectral change is that the intensities of a few peaks increased following the injection of acidic particles (R > 1), such as that of $C_5H_8NO_4^+$ (m/z 146). Separate measurements of the particle flow upstream of Reactor #2 suggested that these ions were not from the particle flow itself. Observed increase of peak intensities on the gas mass spectrum upon exposure to acidic particles, therefore, indicates that some products from the particle-phase reactions can partition back into the

gas phase. Degassing of particle-phase products under acidic condition has been reported for α- and β-pinene oxides previously [Iinuma et al., 2013]. To our knowledge, the current study provides the first evidence that similar degassing process could also occur to particle-phase reactions of isoprene oxidation products under acidic condition. The chemical properties of degassed species are discussed further below.

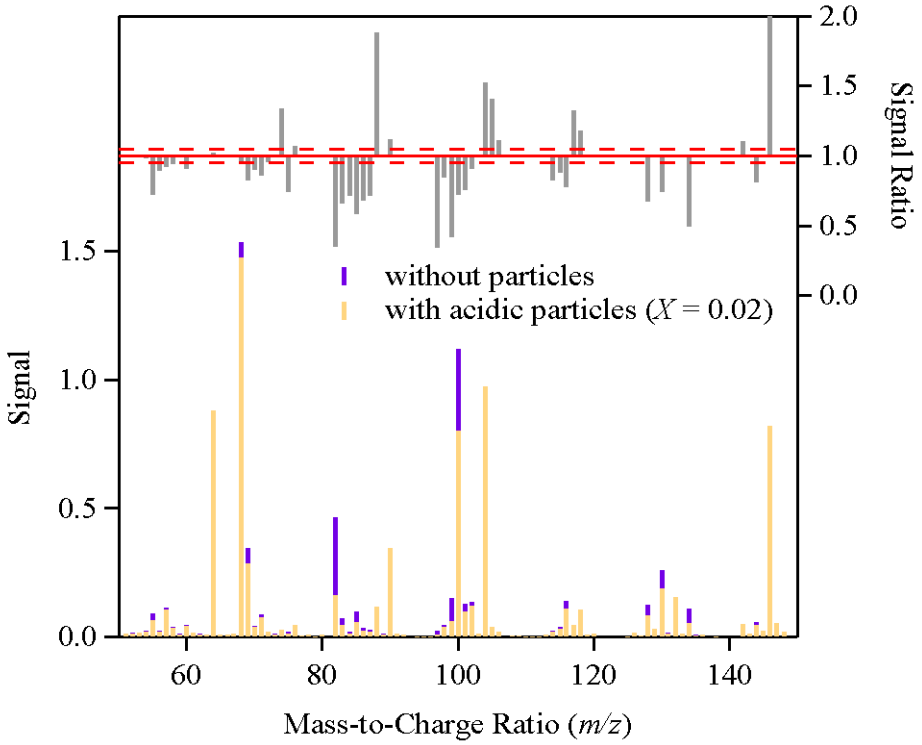

Figure 3-4 Unit-mass-resolution spectra collected by SRI-NO^+-TOF-MS of the outflow of Reactor #2. Mass spectrum in the presence (orange) and absence (purple) of acidic particles (X = 0.02) and the signal ratio R of the two spectra (grey). Spectrum intensities are normalized to the signal intensity of the NO^+ reagent ion. Solid lines represent a signal ratio of 1:1 The regions between dashed lines approximates 99.7% confidence intervals of systematic variation of signal ratio in the absence of particles.

3.3.3 Acidity-dependent uptake of isoprene, isoprene-derived hydroperoxides (ISOPOOH), and isoprene-derived epoxydiols (IEPOX)

Figure 3-5 presents the change of peak intensities of $C_5H_8^+$, $C_4H_6NO_2^+$, and $C_5H_6O^+$ ions with the extent X of neutralization of sulfate particles. $C_5H_8^+$ ion arose from isoprene (cf.

Section 2.3.1). Under the employed experimental condition, 80% intensity of $C_4H_6NO_2^+$ ion originated from ISOPOOH isomers and the rest 20% from methyl vinyl ketone (MVK) and methacrolein (MACR) (cf. Section 2.3.2). $C_5H_6O^+$ was dominantly attributed to IEPOX isomers (cf. Section 4.3.1).

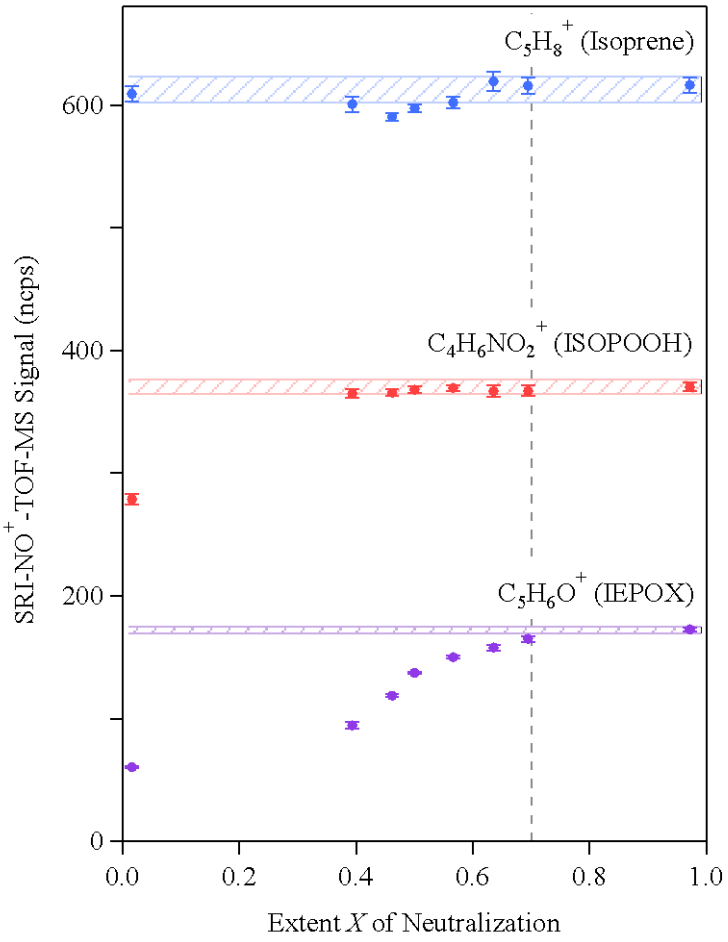

Figure 3-5 Dependence of ion intensities of $C_5H_8^+$, $C_4H_6NO_2^+$, and $C_5H_6O^+$ measured by SRI-NO^+-TOF-MS on the extent X of neutralization of particles. The three ions are mainly attributed to isoprene, ISOPOOH, and IEPOX isomers, respectively, under the employed experimental condition. The shadow areas represent the 99.7% confidential intervals (±3δ) of the intensities of individual ions in the absence of particles. Except $C_5H_8^+$ ion itself, the peak intensities of the other ions were normalized to the intensity of $C_5H_8^+$. The dotted line represents the threshold of X = 0.7, which is the transition point of the sulfate particles from aqueous to solid.

Upon exposure to acidic particles, the signal changes of isoprene, ISOPOOH, and IEPOX in the gas phase had a vast difference in term of the extent and the dependence on

particle acidities. The gas-phase signals of isoprene ($C_5H_8^+$) in the presence of particles at various acidities agreed to greater than 95% with the value in the absence of particles. The random variation of <5% most likely resulted from drifts of the rates of the inflows into Reactor #2 since similar variation was observed for other ions (not shown). The absence of significant change of $C_5H_8^+$ ion indicates no observable uptake of isoprene under the experimental conditions employed. The signals of $C_4H_6NO_2^+$ and $C_5H_6O^+$ ions shown in Figure 3-5 are corrected for flow variations using the measured $C_5H_8^+$ signal. A 25% decrease of $C_4H_6NO_2^+$ ion intensity was observed at the highest acidity employed (X = 0.02) but no significant change was observed at higher X investigated, suggesting that reactive uptake of ISOPOOH was significant only at highly acidic conditions. For IEPOX, signal decrease of $C_5H_6O^+$ ions (i.e., uptake) was observed for the whole range of X in the presence of liquid phase. The signal decrease was greater at a lower X.

The results can be compared with previous studies qualitatively and quantitatively. Qualitatively, non-oxidative reactive uptake of isoprene, ISOPOOH isomers, and IEPOX isomers has all been suggested as important sources of SOM previously. Liggio et al. [2007] reported direct polymerization of isoprene on acidic sulfate particles and suggested that in ambient conditions the produced polymeric mass from isoprene could be comparable to methylbutanetetrols, key tracers of SOM from isoprene photooxidation [Claeys et al., 2004]. Since a high level of organic peroxides was detected in the SOM samples generated from isoprene photooxidation [Surratt et al., 2006], ISOPOOH isomers were also speculated as important direct SOM precursors [Kroll et al., 2006; Surratt et al., 2006], likely via peroxyhemiacetal formation with aldehydic species as observed for other hydroperoxides [Tobias and Ziemann, 2000;

Docherty et al., 2005]. Recent laboratory findings demonstrate that reactive uptake of IEPOX isomers could produce many molecular tracers of isoprene SOM identified earlier in the ambient air and that the mass spectra of IEPOX-derived SOM had some features similar with a statistical factor of ambient SOM spectra tentatively attribute to isoprene photooxidation [Budisulistiorini et al., 2013]. The results shown in Figure 3-5 provided a direct comparison of the importance of the three possible direct SOM precursors at atmospheric relevant concentrations. Gas-phase signal drop due to reactive uptake of IEPOX isomers was much larger than those of isoprene and ISOPOOH, which were not observed in most cases. This observation suggested a much more important role of the non-oxidative uptake of IEPOX isomers as compared with isoprene and ISOPOOH isomers for the whole acidity range investigated.

Quantitatively, the results shown in Figure 3-5 could be used to estimate the reactive uptake coefficient γ of the respective compounds, given by

$$\gamma = \frac{4Vk_{particles}}{cS} = \frac{4V}{cS\tau}\frac{I_{ss,without\ particles} - I_{ss,with\ particles}}{I_{ss,with\ particles}} \quad (3\text{-}4)$$

where S is the reactive surface area (cm^2); V is the volume of the reactor (cm^3); c is the mean molecular speed of X (cm/s); $I_{ss,without\ particles}$ and $I_{ss,\ with\ particles}$ are the signal intensity of X measured by SRI-NO^+-TOF-MS in Reactor #2 without and with particle injection.

The key of to determine γ is to determine the reactive surface area S. Due to the reaction for majority particles in Reactor #2 went to completion within the residence time (Section 3.3.1), the total reactive surface area was smaller than at least 50% of the measured particle surface area corrected for wall loss (cf. Section 4.3.3). A lower-limit of reactive uptake coefficient γ could hence be estimated.

The estimated lower limit of uptake coefficients γ_{IEPOX} of IEPOX ranged from 0.08 to 0.20 for the investigated acidities. As a comparison point, a γ_{IEPOX} of 0.10±0.01 at X=0.5 and 30% RH was reported recently [Gaston et al., 2014]. In this study, γ_{IEPOX} was determined to be > 0.10 at X=0.5 and <5% RH. The two results are consistent considering higher reactive uptake coefficient at lower RH [Gaston et al., 2014].

For isoprene, the absence of signal change was also consistent with the low reactive uptake coefficient γ_{ISOP} of isoprene reported previously. γ_{ISOP} was determined to be 10^{-3} to 10^{-4} onto 78-93 wt % sulfuric acid film [Connelly and Tolbert, 2010] and 10^{-6} to 10^{-7} onto water surface at 1<pH<3 [Enami et al., 2012]. Taking the upper limit of γ_{ISOP} (10^{-3}) reported in the literature and the upper limit of reactive surface area (0.5 $S_{particles,\ wall\ corrected}$) estimated for the current study into Eq. (3-4), the predicted signal drop of isoprene due to reactive uptake was at maximum 1% in the current study, below the random variation of $C_5H_8^+$ ion (5%). For ISOPOOH, no kinetic data was available for comparison.

3.3.4 Uptake and production of other products

In addition to $C_5H_8^+$, $C_4H_6NO_2^+$, and $C_5H_6O^+$ ions, there are many other carbonaceous ions on the gas mass spectra (Figure 3-1). It is difficult to determine the precursor compounds of all the ions, since there are many isomers among known oxidation products of isoprene and fragmentation often occurs to highly oxygenated organic compounds upon their reaction with NO^+ (cf. Section 2.3.2). Nevertheless, general features of the X-dependence of the ion signals across the spectrum are discussed here to provide references and directions for future studies.

Table 3-2 List of ions following each of the six types of X-dependent signal change.

X-dependence [1]	Ions (normalized signal change corrected for transmission[2], in ncps)
I	**$C_5H_8^+$**, $C_3H_4NO_3^+$, $C_4H_6NO_4^+$
II	**$C_4H_6NO_2^+$** (-84), $C_4H_5O^+$ (-21), $C_5H_6NO_3^+$ (-9), $C_4H_6NO_3^+$ (-7), $C_4H_7O^+$ (-4), $C_4H_4NO_4^+$ (-3), $C_4H_6O^+$ (-1)
III	**$C_5H_6O^+$** (-78), $C_5H_7O_2^+$ (-9), $C_4H_8NO_4^+$ (-5), $C_5H_8NO_3^+$ (-7), $C_4H_5O_2^+$ (-5), $C_4H_7^+$ (-4), $C_5H_5O_2^+$ (-1), $C_5H_9O^+$ (-2), $C_4H_6O_2^+$ (-2), $C_5H_6NO_4^+$ (-2), $C_4H_7O_2^+$ (-1), $C_5H_6O_2^+$ (-1), $C_4H_8O_2^+$ (-2), $C_3H_5O^+$ (-1)
IV	**$C_3H_6NO_3^+$** (+104), $C_6H_8NO_5^+$ (+8), $C_5H_8NO_5^+$ (+5), $C_7H_{12}NO_5^+$ (+4), $C_6H_{10}NO_5^+$ (+1), $C_5H_4NO_4^+$ (+1), $C_6H_8NO_6^+$ (+1)
V	**$C_5H_8NO_4^+$** (+17), $C_3H_6NO_2^+$ (+4), $C_2H_4NO_3^+$ (+3),$C_5H_6NO_5^+$ (+1), $C_3H_4NO_4^+$ (+3), $CH_2NO_3^+$ (+1)
VI	**$C_5H_9O_3^+$** (4), $C_5H_9O_2^+$ (-6), $C_5H_7O_3^+$ (0), $C_2H_3O^+$ (0)

[1]An example of each type (in Bold) is shown in Figure 3-5 and Figure 3-6.

[2]The number in the parenthesis shows the signal change of the respective ion with and without particles at X=0.02 for Type II, IV, and VI and at X=0.39 for Type III and V.

The carbonaceous ions across the spectrum can be categorized into six types according to the X-dependence of their signal changes. A complete list of ions of each type is presented in Table 3-2. The signal intensities of some ions showed insignificant increase or decrease in the investigated range of X (Type I), such as $C_5H_8^+$ (Figure 3-5). For some ions, decrease of peak intensities occurred only at highly acidic conditions (X = 0.02 in this case; Type II), such as $C_4H_6NO_2^+$ (Figure 3-5). For some other ions, their signal intensities showed an decrease for a wide range of X and more decrease was observed under lower X (Type III), such as $C_5H_6O^+$ (Figure 3-5). Likewise, for ions showed an increase in peak intensity (Fig. 1), some increased only at highly acidic conditions (Type IV), such as $C_3H_6NO_3^+$ (Figure 3-6a), whereas some others increased

for a wide range of X with more increase under lower X (Type V), such as $C_5H_8NO_4^+$ (Figure 3-6b). Moreover, the peak intensities of a few ions decreased in the presence of acidic particles at higher X but increased at lower X (Type VI), such as $C_5H_9O_3^+$ (Figure 3-6c). X-dependence of Type VI is possibly a combination of Type III and Type IV.

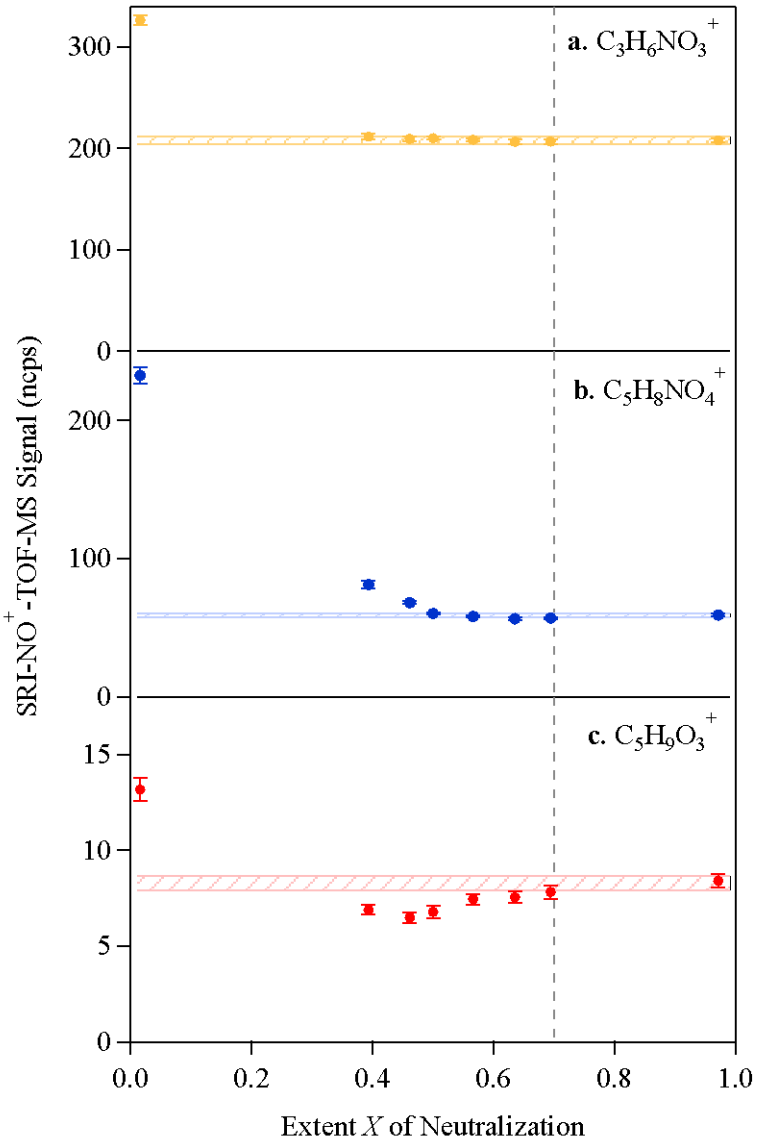

Figure 3-6 Dependence of ion intensities of (a) $C_3H_6NO_3^+$, (b) $C_5H_8NO_4^+$, and (c) $C_2H_3O^+$ measured by SRI-NO^+-TOF-MS on the extent X of neutralization of particles. The shadow areas represent the 99.7% confidential intervals (±3δ) of the intensities of individual ions in the absence of particles.

Compounds corresponding to ions of Type III can have a large contribution to SOM production by reactive uptake (i.e., kinetically favorable) under atmospheric-relevant acidic conditions. As shown in, $C_5H_6O^+$ ion, attributed to IEPOX isomers, showed the most significant drop in peak intensities among ions of Type III. The contribution of uptake of IEPOX isomers to SOM production was quantitatively evaluated at $0.4 < X < 0.7$ in Section 4. The next largest drop of peak intensities occurred to $C_5H_7O_2^+$ ion (Table 3-2). One possible parent compound of $C_5H_7O_2^+$ ion among others is hydroxyl aldehydic epoxide ($C_5H_8O_3$), a proposed C_5 OH-oxidation product of IEPOX compounds [Jacobs et al., 2013; Bates et al., 2014]. Reactions of $C_5H_8O_3$ with NO^+ possibly give rise to $C_5H_7O_2^+$ by hydroxide ion transfer, $((C_5H_8O_3)\text{-}OH)^+$, which is a common reaction pathway with NO^+ for compounds with a hydroxyl group [Smith and Spanel, 2005]. There are also a few other ions of Type I, although their signal drops were much smaller (< 7% of $\Delta C_5H_6O^+$).

Compounds corresponding to ions of Type V were likely produced from particle-phase reactions of compounds corresponding to ions of Type III. There were both C_5 and C_1-C_3 ions (Table 3-2). The largest signal increase occurred to $C_5H_8NO_4^+$ ion. The precursor compounds of C_5 ions are likely produced from acid-catalyzed isomerization reactions of some C_5 isoprene oxidation products. Particle-phase isomerization reactions catalyzed by acids have been previously observed for epoxides [Lin et al., 2011] and 1,4-hydroxylcarbonyls [Lim and Ziemann, 2009]. The C_1-C_3 ions could arise from small molecules produced by particle-phase decomposition reactions or from fragmentation of bigger molecules upon the ionization by NO^+. Further studies are warranted to investigate the precursor compounds of $C_5H_8NO_4^+$ ion and its formation mechanism.

3.3.5 Possible particle-phase reaction mechanism of ISOPOOH isomers

Among ions of Type II, $C_4H_6NO_2^+$ ion, mainly attributed to ISOPOOH isomers, had the largest signal drop. The second largest drop occurred to $C_4H_5O^+$ ion. This ion also originated mainly from ISOPOOH isomers under the experimental conditions (cf. Section 2.3.2). The observation that reactive uptake of ISOPOOH isomers only occurred at highly acidic conditions in this study is consistent with the inertness of aliphatic alkyl hydroperoxides at low acidity in organic chemistry literatures. Aliphatic alkyl hydroperoxides are not only generally stable in 5-50% aqueous sulfuric acids, but are usually prepared under such conditions [Deno et al., 1970]. Possible reactions of organic hydroperoxides in strong acids include acid-catalyzed decomposition [Deno et al., 1970; Bushick, 1971; Turner, 1971] and reactions with carbonyls to form peroxyhemiacetal and peroxyacetal [Docherty et al., 2005; Surratt et al., 2006].

Acid-catalyzed decomposition might be the major fate of ISOPOOH isomers in the particle phase. Decomposition of hydroperoxides usually starts from acid-cleavage of the oxygen-to-oxygen bond and followed by 1,2 akyl shift of resultant RO^+. Among ISOPOOH isomers, a progressively higher decomposition rate was expected for tertiary (ISOPBOOH), secondary (ISOPDOOH), and primary (ISOPAOOH and ISOPCOOH) hydroperoxides, since increased substitution of α-carbon makes O-O bond more vulnerable to electrophilic attack [Deno et al., 1970]. In case of ISOPBOOH, the most reactive and most abundant ISOPOOH isomer (44% predicted by Mater Chemical Mechanism, cf. Figure 1-3), hydroxyacetone ($C_3H_6O_2$) is expected to be produced along with acetaldehyde (C_2H_4O) as follows:

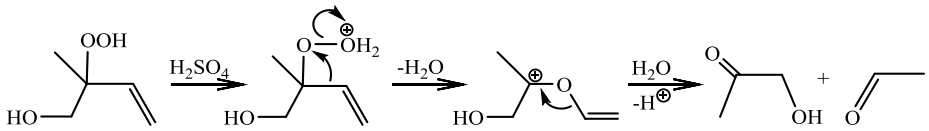

(R3-1)

Hydroxyacetone has a high vapor pressure [Pankow and Asher, 2008] and is expected to produce $C_3H_6NO_3^+$ ion upon the reaction with NO^+ via cluster formation [*Španěl et al.*, 1997]. Consistent with the proposed reaction, $C_3H_6NO_3^+$ had the largest signal increase among ions of Type IV (i.e., those increased only at highly acidic conditions). For the other accompanying product, acetaldehyde, the observed signal of the expected ion ($C_2H_3O^+$) [*Španěl et al*., 2002; Mochalski et al., 2014] was also elevated at highly acidic condition, but to a much less extent compared with $C_3H_6NO_3^+$. This might be related to higher ionization energy (IE) of acetaldehyde (10.23 eV) compared with hydroxyacetone (10.00 eV) and hence a lower reaction rate coefficient with NO^+ (IE: 9.26 eV). Another possibility is that other compounds might also fragment to $C_2H_3O^+$ [Mochalski et al., 2014]. Further study using authentic ISOPOOH compounds is needed to confirm the proposed mechanism.

Among ions of Type IV, there are also some highly oxygenated C_6-C_7 ions, such as $C_6H_8NO_5^+$, $C_7H_{12}NO_5^+$, $C_6H_{10}NO_5^+$, and $C_6H_8NO_6^+$. The presence of ions with a carbon number greater than five suggested that accretion reactions between organic compounds occurred at highly acidic conditions. Peroxyhemiacetal and peroxyacetal formation from the reaction of hydroperoxides and aldehydes could be one possible reaction mechanism among others, especially considering the large drop in signal intensities of ions originated from ISOPOOH isomers at highly acidic condition.

Overall, the particle-phase reactions of ISOPOOH isomers did not seem to contribute to SOM formation significantly even at highly acidic condition. The total gas-phase signal of ISOPOOH ions ($C_4H_6NO_2^+$ and $C_4H_5O^+$, Type II) decreased for 105 ncps (Table 3-2) at X = 0.02 as compared with no significant decrease at X = 0.39. The decrease for IEPOX ion ($C_5H_6O^+$, Type III) was 112 ncps at X = 0.02 and 78 ncps at X = 0.39. By comparison, the produced SOM was 42 ± 0.3 μg m^{-3} at X = 0.02 and 25 ± 0.3 μg m^{-3} at X = 0.39 (Table 3-1). The relative increase in the concentration of produced SOM from X = 0.39 to X = 0.02 was much smaller than the corresponding total decrease of gas-phase signals of ISOPOOH and IEPOX ions. This observation is also consistent with that a great amount of particle-phase products (Type IV), in particular those might originate from ISOPOOH decomposition, were degassed at X = 0.02 as discussed earlier.

3.4 Conclusion and Atmospheric Implication

In conclusion, by using two steady-state reactors in series, the current study provided a direct evaluation of the relative importance of reactive uptake of isoprene and its oxidation products via the HO_2 pathway under a variety of acidities. Although isoprene, ISOPOOH isomers, and IEPOX isomers have all been previously suggested as possible direct SOM precursors via reactive uptake, the current study showed that uptake of IEPOX isomers is much more important than that of the other two compounds under atmospheric-relevant acidities. This observation is quantitatively consistent with the reactive uptake coefficient of isoprene and IEPOX isomers recently reported in the literature.

Given that laboratory studies have suggested that reactive uptake could occur to many types of organic compounds, it is important to pick out atmospheric-relevant

reactive uptake processes in a multi-component system like photooxidation of hydrocarbons. The unique experimental set-up used in this study is shown to be a useful approach to identify key species undergoing reactive uptake in a complex system. It could serve as a pre-selection step for further kinetic studies.

4. Uptake of Gas-phase Epoxydiol (IEPOX) Isomers Accounts for Half of the Particle-Phase Material Produced from Isoprene Photooxidation via the Hydroperoxyl Pathway

4.1 Introduction

Atmospheric particles are linked to adverse human health effects [Pope III and Dockery, 2006], visibility impairment [Charlson, 1969], and anthropogenic changes to Earth's energy balance [Jacob, 1999]. Secondary organic material (SOM) accounts for a large and sometimes dominant fraction of the mass concentration of submicron atmospheric particles [Zhang et al., 2007; Hallquist et al., 2009]. SOM is produced as a result of the oxidation of volatile organic compounds (VOCs) [Hallquist et al., 2009]. There are multiple parallel production pathways, including gas- and condensed-phase processes [Kroll and Seinfeld, 2008]. Because of the complexity of the processes involved, a quantitative and predictive understanding of SOM production is a major challenge in atmospheric chemistry research [Hallquist et al., 2009].

The reaction pathways of a single species, namely isoprene, are estimated to contribute at least 25 to 50% of the annual global average of SOM production [Henze and Seinfeld, 2006; Hoyle et al., 2007; Heald et al., 2008; Lin et al., 2012]. Predominantly emitted by vegetation, isoprene is the single largest source of non-methane VOCs to the atmosphere [Guenther et al., 2006]. Under atmospheric conditions, oxidation of isoprene is initiated primarily by hydroxyl radicals (OH) followed by the addition of molecular oxygen (O_2) to produce a population of reactive peroxyl radical intermediates (ISOPOO) [Archibald et al., 2010]. The subsequent fate of these RO_2 radicals can follow multiple

pathways, resulting in many different products in the gas and particle phases. Molecular tracers of isoprene oxidation, such as 2-methylbutanetetrols, C_5-alkene triols, organosulfates, and oligomeric species, have been identified in SOM sampled at locations worldwide [Claeys et al., 2004; Wang et al., 2005; Surratt et al., 2006; Surratt et al., 2007b; Chan et al., 2010; Froyd et al., 2010].

A quantitative understanding of the multiple reaction pathways that contribute to SOM production from isoprene photooxidation is a critical step in the formulation of accurate models of atmospheric particle mass concentrations [Carlton et al., 2009]. Recent laboratory and ambient findings demonstrate that isoprene epoxydiol (IEPOX) isomers, which are produced by the further reactions of the population of ISOPOO intermediates with hydroperoxyl (HO_2) and then hydroxyl radicals [Paulot et al., 2009b], serve as at least one set of important products to produce SOM [Cole-Filipiak et al., 2010; Surratt et al., 2010; Lin et al., 2011; Budisulistiorini et al., 2013; Gaston et al., 2014; Nguyen et al., 2014a], especially by reactive uptake to acidic sulfate particles [Cole-Filipiak et al., 2010; Surratt et al., 2010; Lin et al., 2011; Gaston et al., 2014]. The IEPOX isomers include trans-β-IEPOX, cis-β-IEPOX, δ1-IEPOX, and δ4-IEPOX (Figure 1-3), of which the β isomers dominate (>97%) for typical reaction conditions [Bates et al., 2014]. Known IEPOX-derived particle-phase molecules account for at least 20% of the mass of isoprene-derived SOM in the laboratory [Surratt et al., 2010]. The result is a lower limit given that not all IEPOX-derived products are known (i.e., an incomplete set of molecular tracers).

The quantitative determination of the relative contribution of the IEPOX pathway to SOM production from isoprene photooxidation is the goal of the present study.

Although the IEPOX pathway has been suggested as an important pathway for SOM production from isoprene photooxdation, direct quantitative evidence nevertheless remains lacking, and other reaction pathways might also be quantitatively important [Surratt et al., 2006; Chen et al., 2011].

4.2 Experimental

The present study is based on the same set of main experiments as in Section 3 and further supporting experiments to quantitatively evaluate the contribution of IEPOX to SOM production in the main experiments. Detailed description of the main experiments is presented in Section 3.2.1 and 3.2.2. In overview, two continuously mixed flow reactors were connected in series and operated at steady state as an experimental strategy to separate isoprene photooxidation from SOM production as described in Section. In Reactor #1, gas-phase isoprene oxidation products were continuously produced. In Reactor #2, the outflow of the HEC was mixed with a flow of sulfate particles. The gas-phase and particle-phase mass spectra of the outflow from Reactor #2 were recorded by a switchable-reagent-ionization time-of-flight mass spectrometer using NO^+ as reagent ions ($SRI\text{-}NO^+\text{-}TOF\text{-}MS$) and a high-resolution time-of-flight aerosol-mass-spectrometer, respectively. The signal change of a gas-phase species in Reactor #2 was due to the molecular uptake or release of the species from the sulfate particles. The supporting experiments for the present study are described as below.

4.2.1 Instrument calibration using authentic IEPOX compounds

All the four IEPOX isomers were synthesized [Ebben et al., 2014]. The purity of the IEPOX compounds was confirmed by nuclear magnetic resonance (NMR) spectroscopy.

Reference mass spectra were obtained by sampling a gas flow containing individual IEPOX isomers into the SRI-NO^+-TOF-MS.

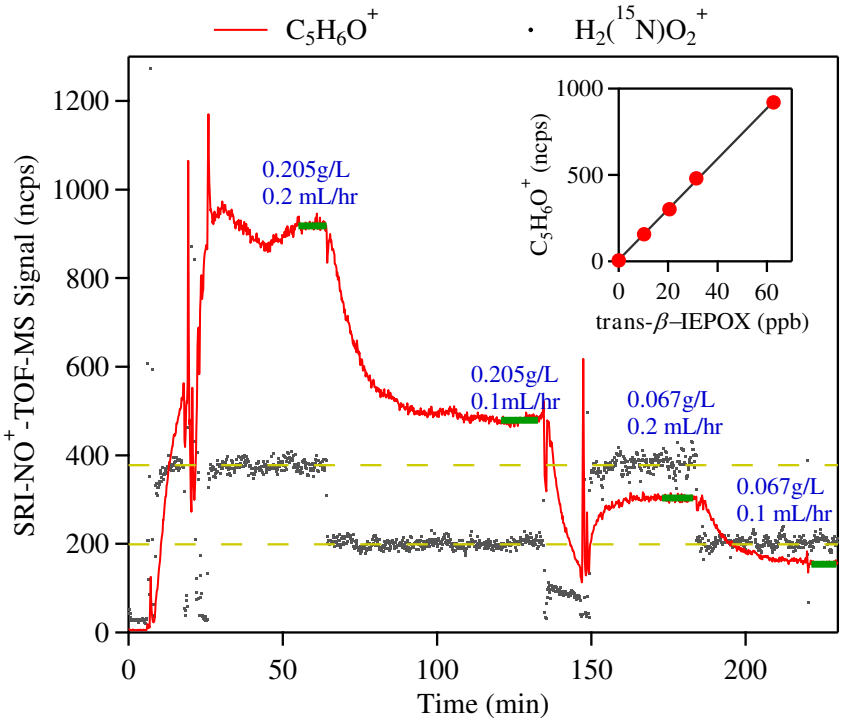

Figure 4-1 Time series of ion signals during the calibration of trans-β-IEPOX. $C_5H_6O^+$ is the dominant product ion of trans-β-IEPOX reacting with NO^+. $H_2(^{15}N)O_2^+$ is a unique isotope ion of $H_2O{\cdot}NO^+$ ion, arising from the reaction of water vapor with NO^+. The signal intensity of $H_2(^{15}N)O_2^+$ ion is magnified for four times. Four calibration points are shown, indicated with respective concentrations and injection rates of IEPOX (aq) fed into the nebulizer. The inset plot shows the correlation between calculated IEPOX concentration in the calibration flow and the measured signal intensity of $C_5H_6O^+$ ion.

In addition to the reference mass spectra, the sensitivity of the SRI-NO^+-TOF-MS to the trans- and cis-β-IEPOX isomers was determined, as follows. An aqueous solution (0.05-0.2 g L^{-1}) containing one IEPOX isomer was nebulized (Meinhard TR-30-A1). The nebulizer was fed (0.1-0.2 mL hr^{-1}) using a gastight syringe (Hamilton 1002LT) placed in a syringe pump (Chemyx Fusion 200). The gas flow into the nebulizer was 1 sLpm. The nebulizer outflow was further mixed with a purified air flow at 1 sLpm in a glass mixing flask (100 mL) to allow full evaporation of the nebulized droplets to take place. No liquid

condensation was visible on the walls of the flask. After sufficient time, steady signals were observed by SRI-NO^+-TOF-MS (Figure 4-1), indicating that equilibrium with the walls was attained (all surfaces were glass or Teflon). The steady-state gas-phase IEPOX concentration in the outflow of the mixing flask (10 to 65 ppb) was calculated based on the solution concentration and the several dilution flows. The calibration was done later than the experiments, but the SRI-NO^+-TOF-MS was operated at the same E/N ratio. Drift of the instrument sensitivity to IEPOX with time was corrected based on the changes in the sensitivities to isoprene and MACR, which were by the same factor.

A combined sensitivity for IEPOX isomers, S_{IEPOX}, was used to convert the peak intensities of $C_5H_6O^+$ ion to IEPOX concentrations, given by $S_{IEPOX} = (S_{cis\text{-}\beta\text{-}IEPOX} + 2.5\ S_{trans\text{-}\beta\text{-}IEPOX}) / 3.5 = 22$ ncps $ppb^{-1} = 4.5$ ncps $\mu g^{-1}\ m^3$, where $S_{cis\text{-}\beta\text{-}IEPOX}$ (19 ncps ppb^{-1}) and $S_{trans\text{-}\beta\text{-}IEPOX}$ (23 ncps ppb^{-1}) are the measured sensitivities of cis- and trans-β-isomers, respectively. The analysis assumed 100% production of β isomers compared to δ isomers (by comparison, > 97% suggested by Bates et al. [2014]) and a ratio of 1:2.5 for the concentrations of cis- and trans-β-IEPOX in the conducted experiments. The latter was estimated based on the ratio of production yields (1:2.3) and OH reaction rates (1.5:1) of cis- and trans-β-IEPOX [Bates et al., 2014]. The uncertainty of S_{IEPOX}, which is a systematic error for the whole set of experiments, is estimated to be 10%. The major source of the uncertainty is the time delay between the chamber experiments and the calibration.

4.2.2 Cold-trapping and re-evaporation of oxidation products

The relative volatilities of gas-phase oxidation products present in the outflow from Reactor #1 were examined by cold trapping and re-evaporation. The outflow from

Reactor #1 passed through a 1-m Teflon PFA coil immersed in a liquid bath at -40 °C for 4 hr. After this collection period, the coil was purged using a flow of dry purified air while increasing the bath temperature at 5 °C hr^{-1}. The flow was sampled by the SRI-NO^+-TOF-MS. Molecules of progressively lower vapor pressures sequentially evaporated into the purified air, and the time series analysis of the mass spectra provided characterization of the products. The main purpose of these experiments was to show cross-check consistency for the assignment of the $C_5H_6O^+$ ion as IEPOX compounds (vide infra).

4.2.3 Uptake experiments using IEPOX compounds

For selected experiments, instead of using photooxidation products from Reactor #1, a gas flow containing trans-β-IEPOX was injected into Reactor #2. For volatilization, a drop of trans-β-IEPOX was placed inside of a Teflon T-fitting. The fitting was flushed by purified air, thereby producing a gas stream containing a trace amount of trans-β-IEPOX. These experiments provided reference spectra of IEPOX-derived SOM, as a comparison point for the SOM spectra collected in the main experiments. The IEPOX signal in the gas-phase flow into Reactor #2 was, however, not stable enough to allow for quantitative analysis.

4.3 Results and Discussion

The three sections of the results and discussion are organized from the perspectives of the gas phase, the particle phase, and the link between the gas and particle phases, respectively, all aiming to assess the relative contribution of the IEPOX pathway to SOM production from isoprene photooxidation.

Table 4-1 Summary of experimental conditions and observations.

Experiment	HR-TOF-MS		SRI-NO^+-TOF-MS		
	X	M_{SOM} [1] ($\mu g\ m^{-3}$)	$\Delta_{C_5H_6O^+} / \sum \Delta$ [2] (%)	$[IEPOX]_{gas}$ [3] ($\mu g\ m^{-3}$)	M_{IEPOX}/M_{SOM} [4] (%)
1	N.A.[5]	<MDL	N.A.	38.5 ± 0.5 (7.7)	N.A.
2	0.97 ± 0.07[7]	<MDL	<MDL	38.5 ± 0.4 (7.7)	<MDL
3	0.69 ± 0.04[8]	2.1 ± 0.1 (3 ± 1)	72 ± 13 (19)	36.8 ± 0.5 (7.4)	54 ± 26
4	0.64 ± 0.04	4.0 ± 0.1 (7 ± 1)	60 ± 8 (16)	35.4 ± 0.5 (7.1)	49 ± 17
5	0.57 ± 0.03	8.1 ± 0.2 (14 ± 3)	63 ± 5 (14)	32.7 ± 0.3 (6.5)	45 ± 12
6	0.50 ± 0.03	13.1 ± 0.3 (22 ± 4)	55 ± 3 (13)	29.7 ± 0.2 (5.9)	43 ± 11
7	0.46 ± 0.03	17.8 ± 0.4 (30 ± 6)	47 ± 3 (13)	25.4 ± 0.3 (5.1)	47 ± 11
8	0.39 ± 0.02	24.9 ± 0.3 (42 ± 8)	56 ± 3 (13)	20.6 ± 0.5 (4.1)	46 ± 11
			59 ± 17 (21)[9]		**46 ± 11**[10]

[1] M_{SOM} is the measured particle organic mass concentration. The number in the parenthesis is the wall-loss corrected particle organic mass concentration.

[2] $\Delta_{C_5H_6O^+} / \sum \Delta$ is the contribution of the decrease of $C_5H_6O^+$ signal to the total of signal decreases across the full spectrum. It is used as an estimate of the contribution of IEPOX isomers to the total loss of organic species in the gas phase (molecular counts). There is an increase in the uncertainty for the latter (shown in parenthesis) to take into account of the differences in the NO^+ reaction rate coefficients with different compounds.

[3] $[IEPOX]_{gas}$ is the steady-state gas-phase concentration of IEPOX isomers in Reactor #2. The presented uncertainty reflects twice the standard deviation of IEPOX signal in each experiment to facilitate inter-experimental comparison. The number in the parenthesis is the uncertainty considering additional systematic error associated with the IEPOX sensitivity applied to the whole set of experiments.

[4] M_{IEPOX}/M_{SOM} is the contribution of IEPOX isomers to the production of isoprene SOM. M_{IEPOX} was the SOM produced from IEPOX pathways, estimated using the decrease of gas-phase mass concentration of IEPOX isomers (cf. Main Text).

[5] Not Applicable (N.A.).

[6] Method Detection Limit (MDL).

[7] Sulfate particles are solid.

[8] Sulfate particles are at least partially aqueous [Schlenker and Martin, 2005; Mifflin et al., 2009].

[9] An estimate for the complete set of experiments by bootstrapping the results of individual experiments.

[10] An estimate for the complete set of experiments by fitting M_{SOM} vs. $[IEPOX]_{gas}$ (Figure 4-7(a)).

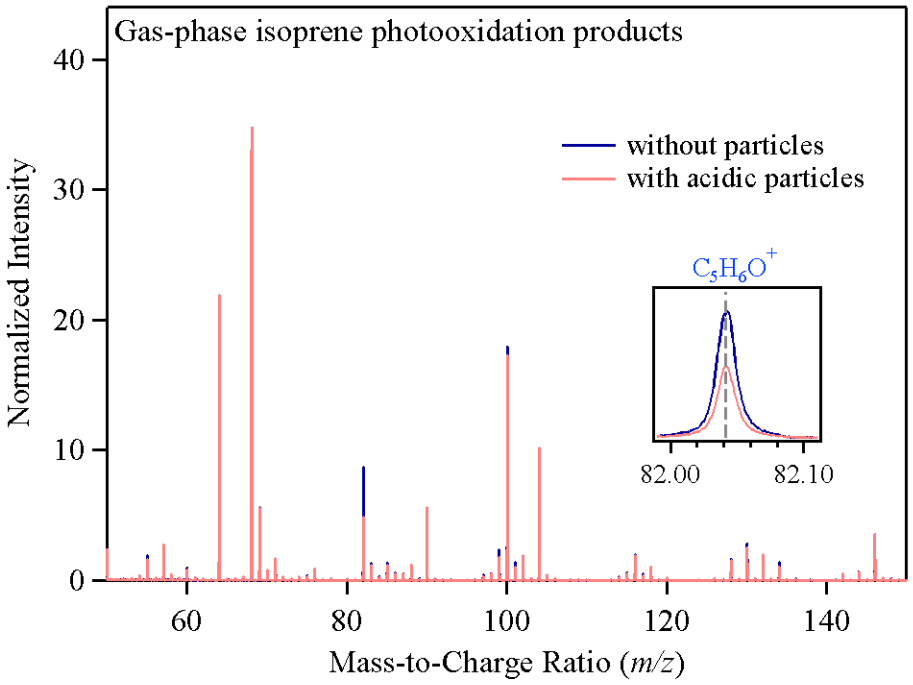

Figure 4-2 Mass spectra collected by SRI-NO^+-TOF-MS of outflow of Reactor #2. Light red and blue lines show the mass spectrum in the presence and absence of acidic particles (X = 0.4), respectively. Inset shows an expansion near m/z 82, corresponding at m/z 82.0413 to $C_5H_6O^+$. Spectrum intensities are normalized to the signal intensity of the NO^+ reagent ion.

A general overview of the experiments and observations is presented in Table 4-1. The extent X of neutralization listed in the second column corresponds to the sulfate particles injected into Reactor #2. Upon injection and mixing with the isoprene photooxidation products, secondary organic material was produced (M_{SOM}; fourth column). Corresponding changes in the gas-phase composition are listed in the subsequent columns of Table 4-1. The rows of Table 4-1 correspond to a series of experiments that varied X stepwise from 0.97 ± 0.07 to 0.39 ± 0.02. The experiment using highly acidic sulfate particles (X = 0.016 ± 0.005, Experiment #9 in Table 3-1) is not included in this study due to less atmospheric relevance and much more complicated chemistry (Section 3.3.4). The entries in Table 4-1 show that SOM production was insignificant for solid neutral particles (X = 0.97 ± 0.07) and increased for aqueous acidic

particles from 2.1 ± 0.1 μg m^{-3} for X = 0.69 ± 0.04 to 24.9 ± 0.3 μg m^{-3} for X = 0.39 ± 0.02. The accompanying changes in the gas-phase species (Table 4-1) reveal two results (vide infra): the IEPOX isomers comprised (59 ± 21)% (molecular count) of the loss of monitored gas-phase species, and the mass concentration of IEPOX isomers lost from the gas phase accounted for (46 ± 11)% of the produced SOM mass concentration.

4.3.1 Loss of gas-phase species

Figure 4-2 shows two examples of high-resolution mass spectra collected by sampling of the gas-phase outflow from Reactor #2. The two spectra correspond to the absence and the presence of acidic particles (X = 0.39 ± 0.02) in Reactor #2. Many peak intensities did not change significantly following the injection of acidic particles, such as those for ions originating from unreacted isoprene ($C_5H_8^+$, m/z 68.0621), hydrogen peroxide ($H_2O_2 \cdot NO^+$, m/z 64.0029), and some oxidation products (e.g., $C_3H_6NO_3^+$, m/z 104.034). By comparison, some other peak intensities, mostly those arising from C_4^+ and C_5^+ ions of isoprene oxidation products, such as $C_5H_6O^+$ (m/z 82.0413) and $C_5H_7O_2^+$ (m/z 99.0441), decreased following the injection of acidic particles. The change of -81 ncps in normalized signal intensity of the $C_5H_6O^+$ ion was eight times greater than the next largest change, which was-10 ncps for $C_5H_7O_2^+$. The unit ncps is the signal in counts per second (cps) normalized (n) to a NO^+-reagent-ion signal of 10^6 cps.

On the basis of characterization using authentic compounds, the $C_5H_6O^+$ ion is attributed to the ionization of *β*-IEPOX (i.e., trans-*β*-IEPOX + cis-*β*-IEPOX; $C_5H_{10}O_3$). Specifically, $C_5H_6O^+$ was the dominant product ion for authentic *β*-IEPOX isomers, as obtained using the NO^+ reagent ion (Figure 4-3). The ion arose from charge transfer of NO^+ with *β*-IEPOX followed by dehydration (i.e., $((C_5H_{10}O_3)\text{-}2(H_2O))^+$). Although this

ion also appeared as one fragment of the two δ-IEPOX isomers (Figure 4-3), Bates et al. [2014] found that the δ isomers accounted for <3% of the IEPOX isomers produced from isoprene photooxidation.

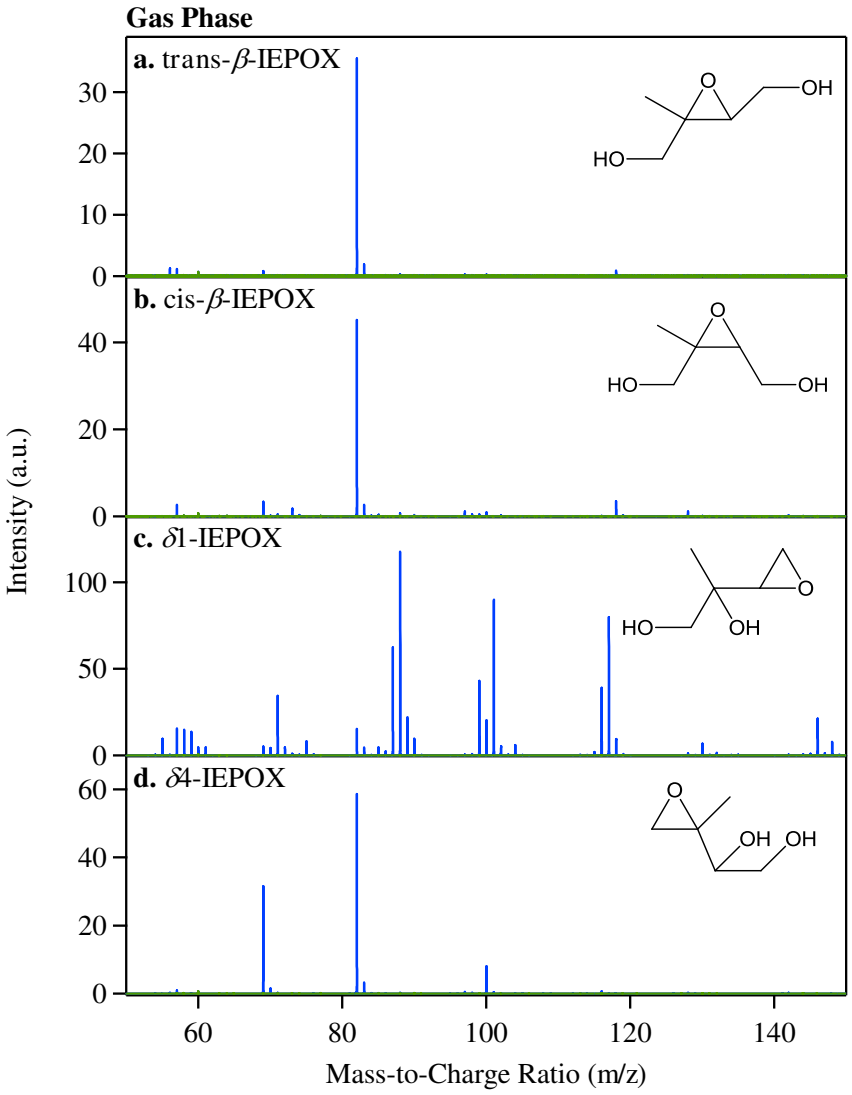

Figure 4-3 Mass spectra of IEPOX isomers collected by SRI-TOF-MS (NO^+). (a) trans-β-IEPOX, (b) cis-β-IEPOX, (c) δ1-IEPOX, and (d) δ4-IEPOX (Blue) in comparison with zero air (green). One dominant product ion at $C_5H_6O^+$ (m/z 82.0413) was observed for trans-β-IEPOX and cis-β-IEPOX. The major fragment ions for δ1-IEPOX include $C_4H_8O_2^+$ (m/z 88.0519), $C_5H_9O_2^+$ (m/z 101.060), and $C_5H_9O_3^+$ (m/z 117.055); and for δ4-IEPOX include $C_4H_5O^+$ (m/z 69.0335) and $C_5H_6O^+$. The additional fragment ions for the δ isomers as compared to the β isomers are explained by the less substituted and hence less stable epoxide rings.

Another data set, based on cold trapping and re-evaporation of the isoprene photooxidation products exiting Reactor #1, gives further support that the $C_5H_6O^+$ ion arose dominantly from IEPOX isomers, rather than other possible known oxidation products. Methyl furan (C_5H_6O) is an oxidation product of isoprene which also gives rise to $C_5H_6O^+$ upon reaction with NO^+. In control studies, methyl furan obtained as a pure compound was not trapped at the temperature employed (results not shown). For the outflow from Reactor #1, over 95% of the $C_5H_6O^+$ signal intensity was removed by the cold trap, implying that methyl furan was not a major contributor to this ion. Figure 4-4 shows the spectra recorded upon heating the trap. $C_5H_6O^+$ arose dominantly from compounds having long retention times and hence low vapor pressures, as expected for IEPOX isomers (~0.3 Pa) [Pankow and Asher, 2008]. By comparison, many other trapped products, such as the isoprene-derived hydroperoxide precursors of the IEPOX isomers [Paulot et al., 2009b], had shorter retention times, as expected for these higher-volatility compounds (~0.6 Pa) [Pankow and Asher, 2008]. Even so, the possibility remains that unknown reaction products might have vapor pressures similar to those of the IEPOX isomers and might also give rise to the $C_5H_6O^+$ ion.

The decreases in peak intensities observed by SRI-NO^+-TOF-MS upon mixing with sulfate particles were analyzed to estimate the contribution of IEPOX isomers to the total loss of gas-phase species. The decrease (ncps) at each ion peak was calculated. Decreases greater than three times the standard deviation of the noise at each signal were taken as significant. The sum (ncps) across all significant decreases was calculated. The combined decreases of the $C_4{}^{12}CH_6O^+$ and $C_4{}^{13}CH_6O^+$ signals (i.e., common $C_5H_6O^+$ isotopologues) accounted for (56 ± 3)% of the total for the experiment shown in Figure

4-2 and (59 ± 17)% across all experiments (Table 4-1). By comparison, the next largest contribution for the experiment shown in Figure 4-2 was (7 ± 3)% ($C_5H_7O_2^+$). Uncertainties are given to 2σ (95%) unless stated otherwise. Further information on uncertainty estimates is provided in Appendix C.

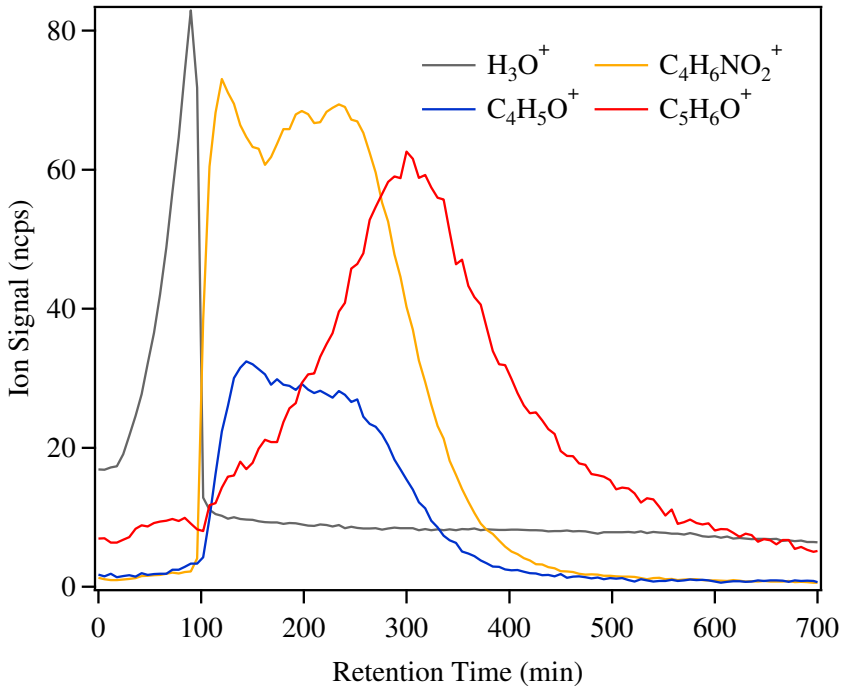

Figure 4-4 Evaporation spectrum of H_3O^+, $C_4H_5O^+$, $C_4H_6NO_2^+$, and $C_5H_6O^+$ ions for outflow from Reactor #1 trapped at -40 °C. H_3O^+ was attributed to water vapor, $C_4H_5O^+$ and $C_4H_6NO_2^+$ were dominantly from isoprene-derived hydroperoxides (cf. Section 2.3.2). The ion signals of H_3O^+, $C_4H_6NO_2^+$, and $C_5H_6O^+$ are scaled by a factor of 0.1, 0.5, and 2, respectively. Note that the signal of these individual ions integrated over time during the evaporation process agreed with their respective total signal drop during the cold-trapping process by 98%, suggesting that the integrity of the corresponding precursor compounds were kept during the cold-trapping and evaporation processes.

For the present study, the percent contributions in the decreases of peak intensities of the SRI-NO^+-TOF-MS spectrum are assumed as equivalent to the percent contributions in actual concentrations. This assumption is believed reasonable within the uncertainties because the ionization reactions of NO^+ with oxygenated organic compounds are usually collision limited [Smith and Spanel, 2005]. The uncertainty

estimate in the percent contributions for the concentrations takes into account possible differences in the NO^+ reaction rate constant among the different compounds (± 50%) and hence is larger than that for the signal intensities (Table 4-1). For the estimate using the whole set of experiments, uncertainty increased from 17% for signal intensity to 21% for concentration. Further discussion is provided in Appendix C.

The finding is that IEPOX isomers accounted for (59 ± 21)% of the total gas-phase species concentrations (molecular count) removed on exposure to acidic sulfate particles. This finding implies that IEPOX likewise accounted for (59 ± 21)% of the SOM produced during isoprene photooxidation in the presence of acidic particles. This estimate is based on molecular count rather than mass. An estimate based on mass concentration is presented further below.

4.3.2 Chemical composition of particulate organic material

The mass spectrum of SOM produced by the uptake of isoprene photooxidation products was compared to that obtained for SOM produced by the uptake of *β*-IEPOX, both in the presence of acidic particles. The unit mass resolution spectrum of isoprene-derived SOM had marker peaks at m/z 82 ($C_5H_6O^+$) and 101 ($C_5H_9O_2^+$) (Figure 4-5(a)). There were also peaks (m/z < 60) at m/z 27, 28, 29, 39, 41, 43, 44, 53, and 55. These characteristic peaks, described both by the m/z values as well as the intensities relative to one another, were similar to those present in the mass spectrum of *β*-IEPOX SOM, both as recorded in the current study (Figure 4-5(b)) as well as reported in the literature [Budisulistiorini et al., 2013; Nguyen et al., 2014a]. The fraction of m/z 82, which has been used as a marker ion in the interpretation of ambient data [Robinson et al., 2011; Slowik et al., 2011; Budisulistiorini et al., 2013; Chen et al., 2014], was (2.9 ± 0.1)% for SOM derived from

chamber oxidation products and (3.6 ± 0.1)% for that derived from β-IEPOX. The similarity of the mass spectrum of isoprene-derived SOM to that of β-IEPOX SOM provides further support for the conclusion that IEPOX isomers were the dominant carbon contributors to SOM production during isoprene photooxidation, at least for the conditions of this study (i.e., HO_2-dominant reaction conditions in the presence of acidic particles at low relative humidity).

The mass spectrum of isoprene-derived SOM obtained from this study can be compared with results obtained for ambient particles in or nearby isoprene source regions. Available data sets include those from Borneo [Robinson et al., 2011], the central Amazon [Chen et al., 2014], Atlanta [Budisulistiorini et al., 2013], and Ontario [Slowik et al., 2011]. Positive-matrix factorization (PMF) of the mass spectra collected in these locations resolved in all four cases a statistical factor attributed at least in part to isoprene-derived SOM (cf. Figure 4-5(c-f)). The factors have in common a characteristic peak at m/z 82, which was also present in the isoprene-derived SOM of the present study (Figure 4-5(a)). High-resolution analysis of these mass spectra shows that the $C_5H_6O^+$ ion was the dominant contributor to this peak [Robinson et al., 2011; Slowik et al., 2011; Chen et al., 2014].

Figure 4-6(a-d) present correlation plots between the mass spectrum of isoprene-derived SOM and the PMF factors. For the Borneo data, there is close clustering along the 1:1 line, with an exception for m/z 44 (Figure 4-6(a)). Good correlation with the Amazon factor is also apparent except for m/z 44 and m/z 28 (Figure 4-6(b)). The differences at m/z 44 might arise from additional oxidation and photochemical processing during the particle atmospheric lifetime, i.e., processes which were not captured in the

current laboratory study. Overall, there is positive but nevertheless weaker correlation with the factors from Atlanta (Figure 4-6(c)) and Ontario (Figure 4-6(d)).

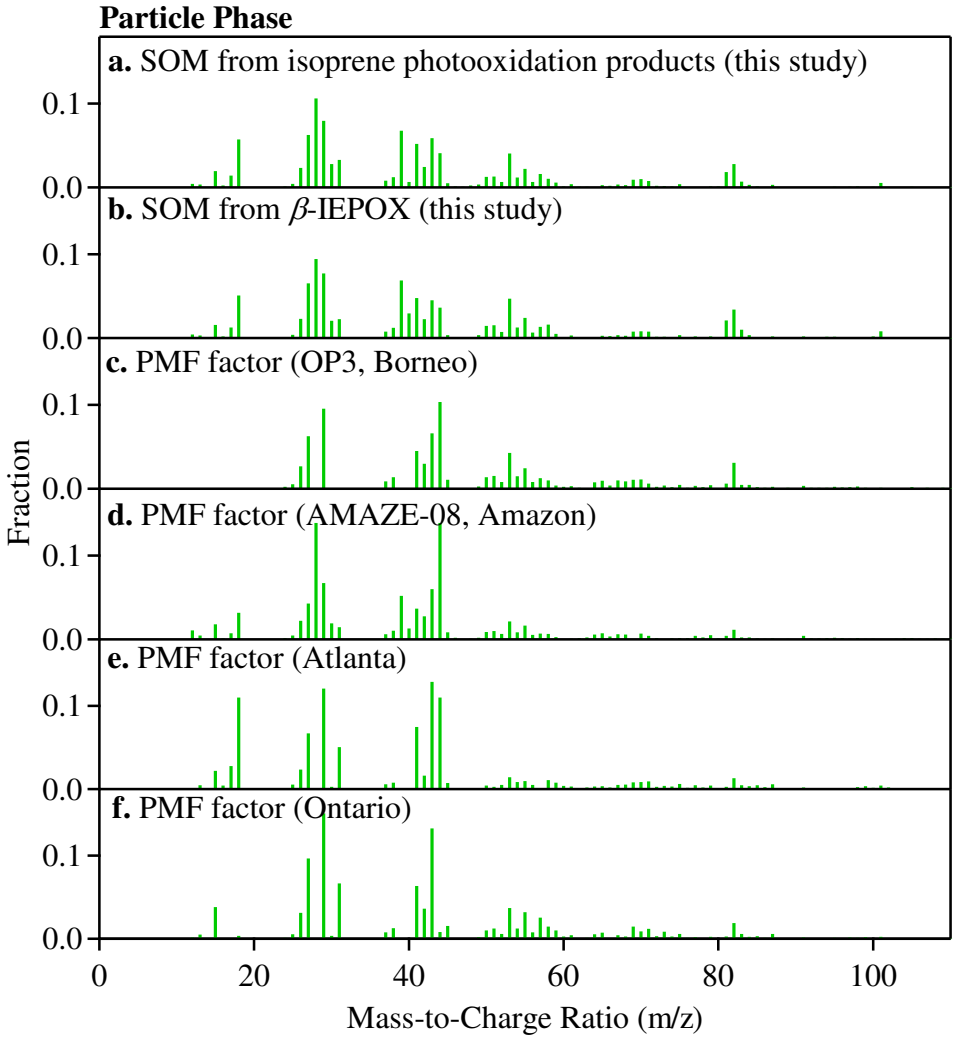

Figure 4-5 Mass spectra collected by HR-TOF-AMS of outflow of Reactor #2. (a) SOM produced by isoprene photooxidation products in the presence of acidic particles (X = 0.6). (b) SOM produced from tran-β-IEPOX in the presence of acidic particles (X = 0.6). (c) Isoprene-related PMF factor from Borneo (OP3) [Robinson et al., 2011]. (d) Isoprene-related PMF factor collected during the wet season of the central Amazon (AMAZE-08) [Chen et al., 2014]. (e) Isoprene-related PMF factor from Atlanta [Budisulistiorini et al., 2013]. (f) Isoprene-related PMF factor from Ontario [Slowik et al., 2011]. There was no significant change in the fractional contributions of the major peaks in panels a and b with extent X of neutralization for the conducted experiments (results not shown).

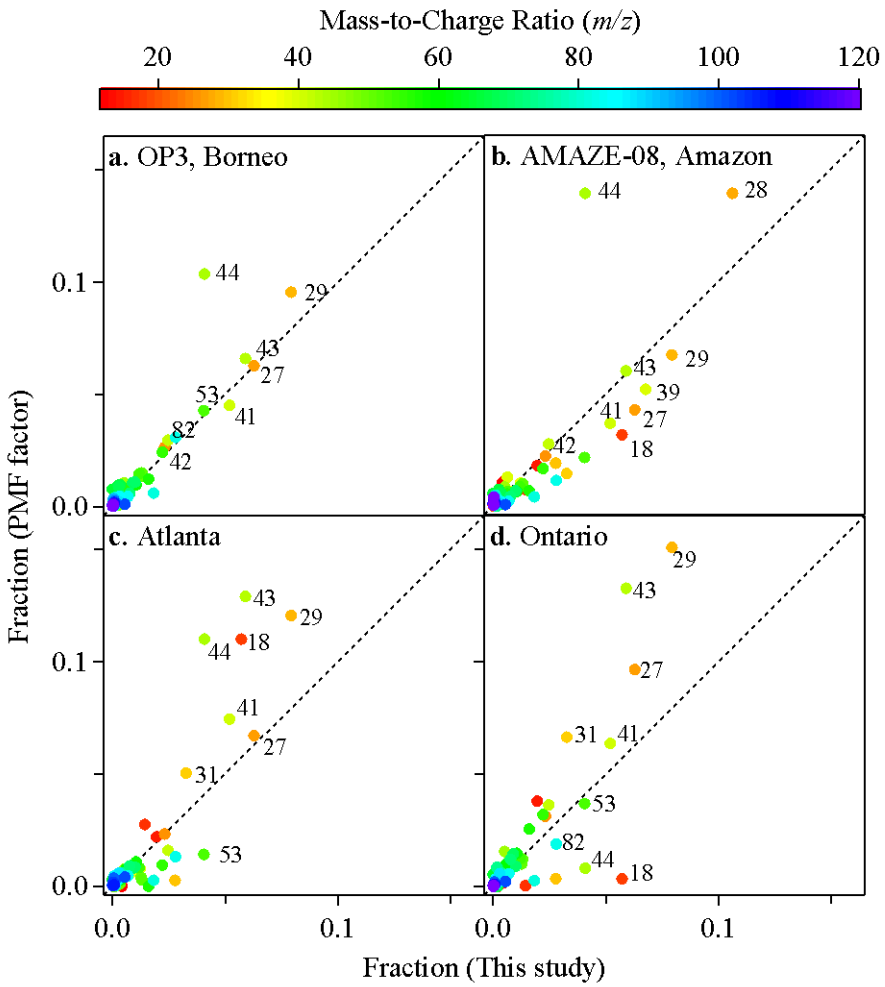

Figure 4-6 Correlation plot between the normalized mass spectrum of isoprene-derived SOM from this study (X = 0.6) and the isoprene-related PMF factors from ambient data sets. The data sets were obtained in (a) Borneo (OP3) [Robinson et al., 2011], (b) the Amazon (AMAZE-08)[Chen et al., 2014], (c) Atlanta [Budisulistiorini et al., 2013], and (d) Ontario [Slowik et al., 2011]. Correlation plots are based on unit-mass-resolution spectra.

One possible explanation for the different levels of correlation in the panels of Figure 4-6 is that the SOM of the present study corresponds to fresh production from isoprene photooxidation via the HO_2 pathway in the presence of acidic particles whereas the range of atmospheric conditions and processes is broader. These laboratory conditions might more closely resemble remote isoprene source regions like Borneo and Amazon than to regions having large urban influences like Atlanta and Ontario (i.e., more NO_x

and more NH_3). The overall caveat must also be kept in mind that all four study locations were subject to complex local environmental and chemical factors not captured in the present laboratory study, such as differences in relative humidity (<5% in present study) as well as possible interactions with the multiple organic species in the atmosphere. A second caveat is that the presented results cannot rule out the possibility that other isoprene reaction pathways, as yet uninvestigated, might also give rise to a similar mass spectrum as IEPOX uptake under laboratory conditions and that these other SOM production processes might thereby also contribute to the observed PMF factors. These two caveats notwithstanding, however, the positive correlations of Figure 4-6 do substantially underpin that the PMF factors identified for atmospheric data sets can be associated at reasonable likelihood with reactive uptake under acidic conditions of isoprene oxidation products along the HO_2 pathway, in particular IEPOX isomers.

4.3.3 Uptake of IEPOX isomers and production of particulate organic material

Figure 4-7(a) shows a scatter plot between the steady-state mass concentration $[IEPOX]_{gas}$ of IEPOX isomers in the gas phase and the mass concentration M_{SOM} of SOM in the outflow of Reactor #2. $[IEPOX]_{gas}$ was calculated from the intensities of the $C_5H_6O^+$ ion using a sensitivity for IEPOX isomers (4.5 ± 0.4 ncps μg^{-1} m^3) derived from the measured sensitivities of cis- and trans-β-IEPOX. The plot shows that the production of M_{SOM} correlated ($R^2 = 0.99$) with the loss of gas-phase IEPOX isomers across the range of investigated X. The correlation further confirms that the reactive uptake of IEPOX isomers, which were present in the suite of isoprene photooxidation products produced in Reactor #1, was a contributing process to SOM production.

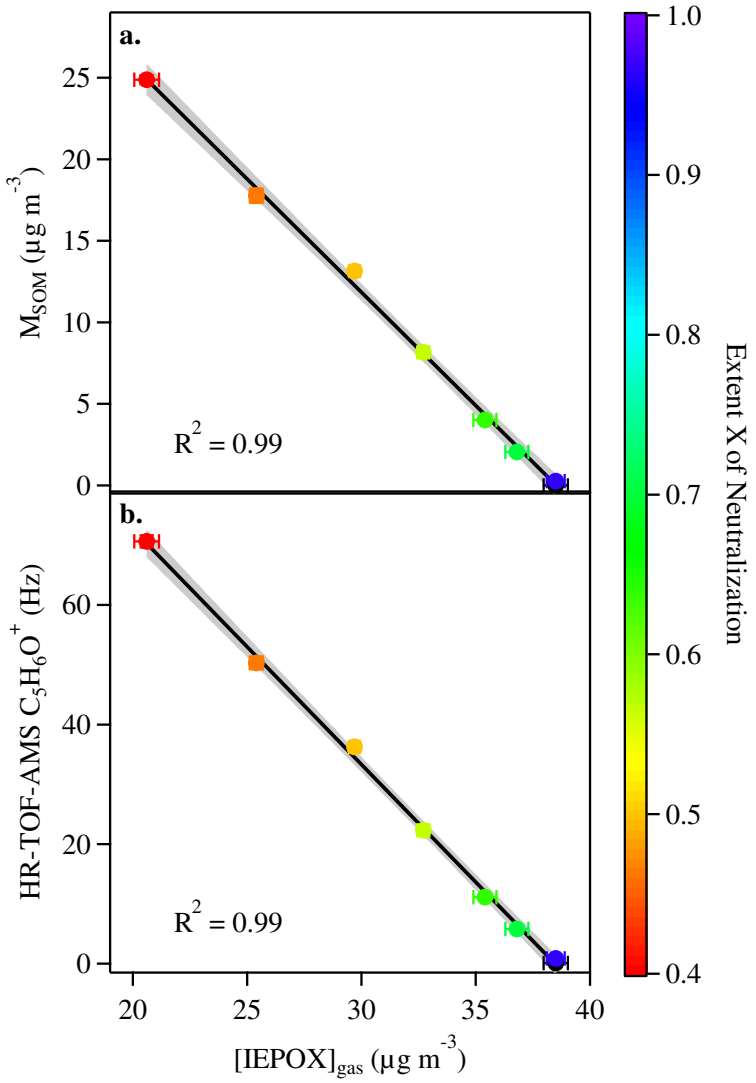

Figure 4-7 Correlation plot between the steady-state concentration of IEPOX isomers in the gas phase, [IEPOX]$_{gas}$, measured by SRI-NO$^+$-TOF-MS and data sets recorded by HR-TOF-AMS of the outflow of Reactor #2. (a) Particle organic mass concentration, M_{SOM}. (b) AMS $C_5H_6O^+$ signal. The experiments are conducted using isoprene oxidation products produced in Reactor #1. Black lines show a linear fit of experimental data, and the grey region represents the 95% confidence interval of the fit. Data points are colored by extent X of neutralization. The black data points represent experiments conducted when sulfate particles were not injected.

The relative contribution of IEPOX isomers to SOM production, compared to other possible contributors, was estimated by comparing on a mass basis the gas-phase loss of IEPOX isomers to SOM production. The SOM production was based on the mass concentration measured by the HR-TOF-AMS and corrected for wall loss in Reactor #2.

Of the sulfate particles injected, (41 ± 4)% were lost to the walls based on the particle number concentrations measured upstream and downstream of Reactor #2, implying a wall-loss correction factor for M_{SOM} of 1.7 ± 0.3. The assumption in this analysis is that the particles deposited to the walls were similar to those in the outflow (i.e, no further growth given a longer exposure time), as justified by additional experiments showing that diameter growth of the particle population in Reactor #2 ceased when the injection of sulfate particles was stopped (Figure 3-3). The stated uncertainty (0.3) takes this assumption into account. The mass concentration of SOM produced from IEPOX isomers was estimated based on the decrease in gas-phase IEPOX concentration measured by SRI-NO^+-TOF-MS and corrected for the stoichiometric change due to condensed-phase reactions, such as the addition of a water molecule. By this analysis, the decrease in gas-phase IEPOX mass concentration corresponded to (46 ± 11)% of the produced organic mass concentration (including wall-loss correction) across the experiments. The stated uncertainty includes a 5% uncertainty in the fitted slope of Figure 4-6(a), a 20% uncertainty in the wall-loss correction for M_{SOM}, a 10% uncertainty in the sensitivity factor for gas-phase IEPOX detection, and an 8% uncertainty in the stoichiometric change of condensed-phase reactions of IEPOX compounds. Within the stated uncertainties, this result of an IEPOX contribution of (46 ± 11)% by consideration of gas-phase mass loss and particle-phase mass increment was consistent with the estimate of an IEPOX contribution of (59 ± 21)% (molecular counts) based on the total loss of gas-phase species. The two separate analyses lead to the common conclusion that the reactive uptake of IEPOX isomers accounted for half of the produced SOM, at least for isoprene photooxidation under HO_2-dominant conditions in the presence of acidic particles.

The experiments also showed that the absolute loss of gas-phase IEPOX isomers and the associated production of SOM were greater for more acidic particles (i.e., lower X), even as the relative contribution of IEPOX to gas-phase loss and particle-phase production remained constant within the stated uncertainties. One possibility is that greater acidity promoted the reactive uptake of IEPOX isomers [Cole-Filipiak et al., 2010; Eddingsaas et al., 2010; Gaston et al., 2014]. Another possibility is that for the conducted experiments the sulfate mass concentration, which has been suggested as a controlling factor of SOM production from the reactive uptake of epoxy compounds [Iinuma et al., 2009], was higher for more acidic particles. Further experiments are needed to differentiate between these two possible explanations.

Figure 4-7(b) shows a scatter plot between the gas-phase concentration of IEPOX isomers and the corresponding intensity of the $C_5H_6O^+$ signal measured by the HR-TOF-AMS for the particle phase over a range of X. The decrease of the gas-phase IEPOX concentration and the increase of HR-TOF-AMS $C_5H_6O^+$ were correlated ($R^2 = 0.99$), suggesting that the HR-TOF-AMS $C_5H_6O^+$ signal of isoprene-derived SOM was directly related to the reactive uptake of IEPOX isomers. Given that the AMS uses electron-impact ionization, the AMS $C_5H_6O^+$ ion should not be interpreted as indicative of the direct presence of IEPOX isomers in the particle phase but rather of the possible presence of IEPOX isomers as well as their derivatives and other oxidation products having similar base structures that can all fragment to $C_5H_6O^+$. The correlation apparent in Figure 4-7(b) does, however, provide further positive support of the link between isoprene photooxidation products (in particular IEPOX isomers) and the HR-TOF-AMS $C_5H_6O^+$ signal (m/z 82). This signal has recently emerged in the literature as a suggested tracer

fragment ion of isoprene-derived SOM in the atmosphere [Robinson et al., 2011; Slowik et al., 2011; Budisulistiorini et al., 2013; Chen et al., 2014].

The results presented thus far have provided strong evidence from two different perspectives that the SOM production pathways tied to IEPOX isomers accounted for half of the SOM mass concentration for the investigated reaction conditions. The further open question is what the carbon sources of the other half of the produced SOM were. The signal decreases of the SRI-NO^+-TOF-MS mass spectra occurred across many ion peaks, in addition to that from $C_5H_6O^+$ ion (Figure 4-2). Due to fragmentation of oxygenated isoprene products (e.g., IEPOX isomers and ISOPOOH isomers) [Liu et al., 2013; Nguyen et al., 2014b] and the existence of many isomers among known isoprene products, inference of the precursor compounds associated with the other ions (i.e., besides $C_5H_6O^+$) remains highly uncertain at the present time. A study using standard compounds would be needed for definitive insights.

4.4 Conclusion and Atmospheric Implication

The simultaneous monitoring of the loss of gas-phase species and the production of particle-phase mass establishes that the uptake of IEPOX isomers explains (46 ± 11)% of the SOM mass concentration produced from isoprene photooxidation for HO_2-dominant conditions in the presence of acidic particles at low relative humidity. Atmospheric chemistry models have recently begun to incorporate isoprene-derived SOM production via reactive uptake, with a focus on IEPOX isomers [Lin et al., 2012; Pye et al., 2013]. An uncertainty, however, in the validity of these treatments has been the importance of IEPOX relative to other products of isoprene photooxidation for SOM production. The results of the present study provide a direct experimental basis to support the

appropriateness of these recent additions to models by finding that IEPOX isomers account for half of SOM produced under laboratory conditions and demonstrating that SOM production in the particle phase is proportional to IEPOX loss from the gas phase.

Although the present study explored a range of particle acidity, the experiments were conducted only for low relative humidity (< 5%). The result is a relatively low particle water content. For instance, pure sulfuric acid at 10% RH and 20 °C has half as much absorbed water as at 50% RH [Wexler and Clegg, 2002]. The implication is that acid-catalyzed reactions might be faster at <5% RH compared to elevated RH. Another possibility, however, is that other competing mechanisms, which are less important at elevated RH, can become kinetically favorable at the higher ionic strength of the lower RH. Given the close connections between IEPOX reactivity and acidity on the one hand and acidity and water content on the other hand, further laboratory studies are warranted across the range of atmospheric humidities.

5. Separate Measurements of Isoprene-derived Hydroperoxides (ISOPOOH) from Methyl Vinyl Ketone (MVK) and Methacrolein (MACR) over Amazonia

5.1 Introduction

By abundance, isoprene (C_5H_8) is the dominant non-methane biogenic volatile organic compound (VOC) emitted to the atmosphere. The reactive chemistry of isoprene has a large influence on the oxidation capacity of the atmosphere and the formation of secondary organic material (SOM) of atmospheric particles. Atmospheric oxidation of isoprene is initiated primarily by hydroxyl radicals (OH) followed by the addition of molecular oxygen (O_2) to produce a population of reactive peroxyl radical intermediates (ISOPOO). The subsequent chemistry of the ISOPOO radicals proceeds along several competing pathways, which lead to different sets of products in the gas and particle phases and hence different environmental impacts [Archibald et al., 2010].

The NO and HO_2 pathways are suggested as the major competing reaction pathways affecting the fate of ISOPOO in the atmosphere [Crounse et al., 2011; Xie et al., 2013]. The reaction with NO dominates in polluted, urban regions of the planet. In many isoprene source regions, particularly remote tropical forests, NO_x concentrations could be sufficiently low [e.g., Lelieveld et al., 2008; Hewitt et al., 2010] that the HO_2 pathway becomes equally important or dominant. Accurate measurements of isoprene oxidation products via the HO_2 and NO pathways, particularly in low-NO regions, are crucial for evaluating the impact of isoprene chemistry on local atmospheric oxidation capacity and SOM formation.

Recent laboratory studies have revealed an unexpected instrumental bias for the measurement of isoprene oxidation products using both gas chromatography (GC) and proton-transfer-reaction mass spectrometry (PTR-MS) [Liu et al., 2013; Rivera-Rios et al., 2014], which have been the most commonly-used two techniques to measure VOCs and their oxidation products in ambient air. Isoprene-derived hydroxylhydroperoxides (ISOPOOH; $C_5H_{10}O_3$), the major first-generation products via the HO_2 pathway, are detected as their equivalent NO-pathway products, methyl vinyl ketone (MVK, C_4H_6O) and methacrolein (MACR, C_4H_6O). This instrument bias was first discovered in our chamber study of isoprene photochemistry using PTR-MS [Liu et al., 2013] and later verified using authentic ISOPOOH compounds and shown to occur to GC systems [Rivera-Rios et al., 2014]. These findings suggest that the previously reported ambient concentrations of MVK and MACR in low-NO regions might be overestimated. Several important scientific findings based on these observations, therefore, might need to be revisited, including those regarding to the oxidation capacity of the atmosphere [e.g., Kuhn et al., 2007] and the budget [e.g., Di Carlo et al., 2004] and surface-atmosphere exchange [e.g., Karl et al., 2010] of the reactive carbon.

Given this instrument bias, quantifying the respective contributions of ISOPOOH isomers and MVK/MACR to the observed apparent MVK/MACR signals in low-NO atmospheres is a crucial next step to advance our knowledge of isoprene photochemistry and to reexamine the scientific conclusions based on previous MVK/MACR measurements. Here we present preliminary results of the separate measurements of ISOPOOH and MVK/MACR in Amazonia by deploying a cold trap upstream of a proton-transfer-reaction time-of-flight mass spectrometer (PTR-TOF-MS). To our

knowledge, this study provides the first field evaluation of ISOPOOH contributions to apparent MVK/MACR signals. The implication of the findings is discussed.

5.2 Experimental

5.2.1 Measurement site

Measurements were made as part of the Green Ocean Amazon campaign (GoAmazon 2014/5) at T3 site (3°12'47.82"S, 60°35'55.32"W) in Central Amazon. T3 site is a terrestrial site located in a pasture area surrounded by tropical rainforests, 60 km to the west of the city of Manaus, Brazil (Figure 5-1). The pasture area has a maximum length of 6 km (north-south) and maximum width of 2 km (west-east). The distances from the T3 site to the nearby forests range from 200 m (west) to 4 km (north). Since grass has a low emission factor of isoprene [Guenther et al., 2006], the observed isoprene and its oxidation products at T3 have a predominant origin of upwind forests. Back-trajectory analyses suggest that the fetch of T3 site oscillates between the extremes of a clean atmosphere and the interactions of heavy pollution from Manaus with the natural environment. That is, oxidation products of isoprene observed at T3 could be produced under either clean or polluted conditions or in between, depending on the wind direction. Measurements were carried out during separate 2-month Intensive Observation Periods (IOP) in the wet season (IOP1) and in the dry season (IOP2), respectively, in 2014. Only IOP-1 data is presented here since complicating factors such as biomass burning has a negligible influence on isoprene chemistry in the wet season.

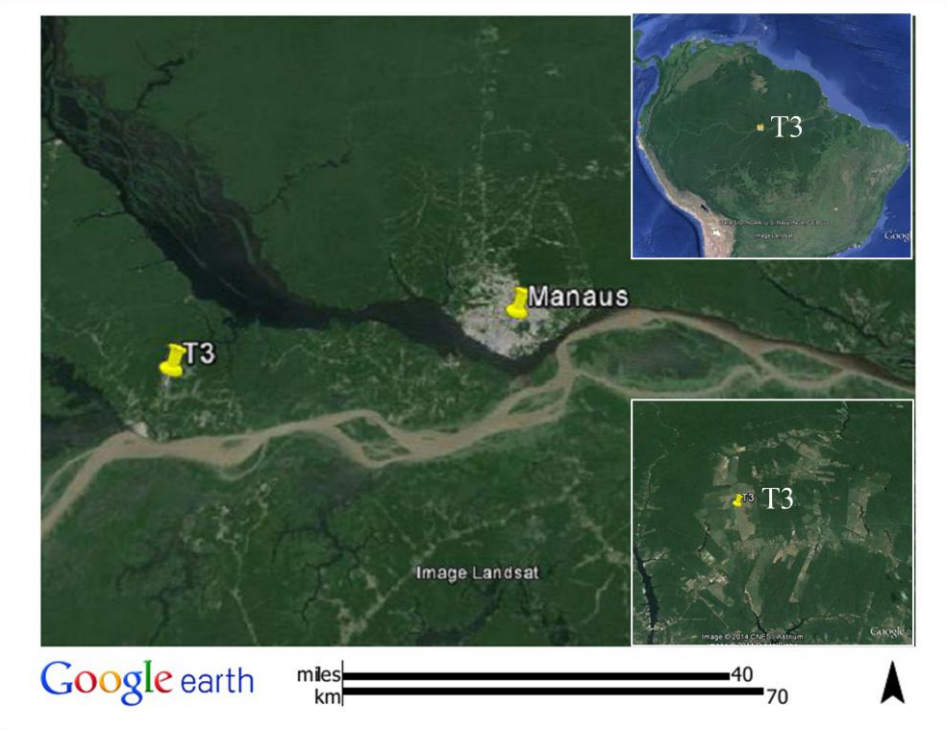

Figure 5-1 Overview of the observation site (T3). Inset figures show the zooming-out (top) and zooming-in view (bottom) of T3 site.

5.2.2 Instrumentation

The PTR-TOF-MS used in this study is part of the Mobile Aerosol Observing System (MAOS; Department of Energy). MAOS is physically contained in two 20' SeaTainers custom adapted to provide a sheltered laboratory environment for operators and instruments even under harsh conditions. The main trace-gas inlet (1/2" PFA; ~13 L/min) is fixed at 10 meter above the ground. To prevent condensation in the inlet lines inside the container, the room temperature was kept at 27 °C. By comparison, the maximum dew point of ambient air during IOP1 was calculated as 24 °C based on measured ambient temperature and relative humidity.

The PTR-TOF-MS instrumentation has been described in detail elsewhere [Jordan et al., 2009b]. The instrument was operated at a drift tube temperature of 80 °C

and a drift tube pressure of 2.2 mbar. The drift tube voltage was set to 550 V, resulting in an E/N = 132 Td (E, electric field strength; N, number density of air in the drift tube; unit, Townsend, Td; 1 Td = 10^{-17}V cm^2). The PTR-TOF-MS spectra were collected at a time resolution of 1 min.

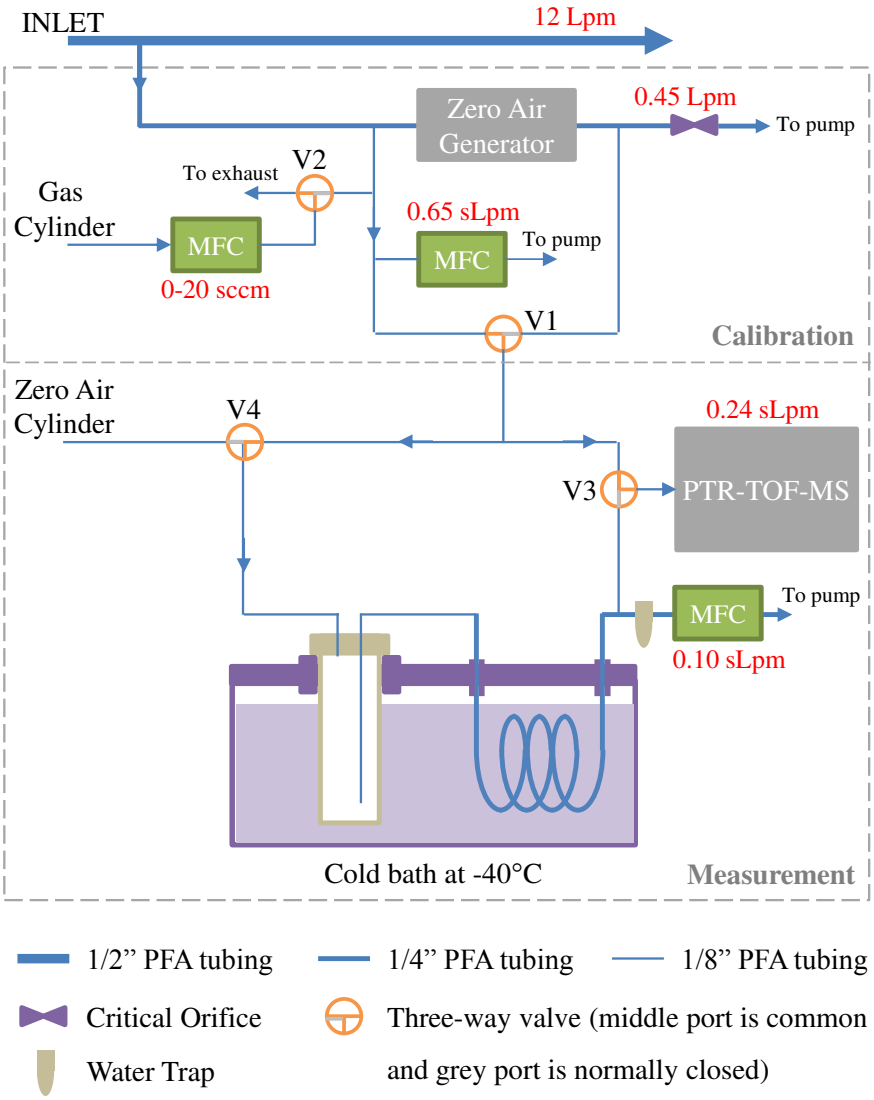

Figure 5-2 Schematic diagram of the gas inlet system for the PTR-TOF-MS. The top and bottom sections are calibration and measurement set-ups, respectively.

Figure 5-2 show the schematic diagram of the inlet system of PTR-TOF-MS. The system subsampled from the main trace-gas sampling line and consisted of two sections:

calibration and measurement. Three-way valves (NResearch; contact surface made of PTFE) were used to switch between the various calibration and measurement modes.

The calibration system enabled measurements of instrument background and sensitivity at ambient humidity. Instrument background was determined by removal of the analyte molecules in the sample air using a zero air generator (Parker Balston 75-83NA). The humidity drop through the zero air generator was typically less than 5% based on the measured signal change of water cluster ion ($H_5O_3^+$). Laboratory tests prior to the campaign suggested that signals of interested compounds in the outflow of the zero air generator was as low as in ultra-high-purity zero air (Airgas). Instrument sensitivity was determined by addition of gas standards (5.14 ppm ISOP and 5.14 ppm MVK in N_2 or 5.4 ppm MACR and other BVOCs in N_2; Air Liquide) into the sample flow at controlled flow rates. A metal-sealed mass flow controller (MFC; MKS 1479A) was used to eliminate the reactions of ketones with Viton o-rings of normal MFCs.

The outflow from the calibration system was measured by the PTR-TOF-MS through or bypass a cold trap. The cold trap consisted of a cylindrical glass bottle (ChemGlass CG-1140; 35×100 mm) and a 1/4" PFA coil in series, both immersed in a cold bath (Lauda ECO RE 1050) at -40 °C. Sampling through a length of tubing kept at -40 °C has been used to selectively remove ISOPOOH isomers in our and other laboratory systems [Liu et al., 2013; Nguyen et al., 2014b; Rivera-Rios et al., 2014]. The tubing could, however, be easily clogged by ice formation when the sample flow was humid. In this study the sample flow was, therefore, preconditioned in the glass bottle (with a large cross section) to remove majority of water vapor upstream of the PFA tubing. The glass bottle was sealed to a mobile phase cap (Alltech; PTFE insert; 2 ports

for 1/8" tubing) with an FEP-coated O-ring. All the contact surfaces of the sample flow were glass or Teflon. A side flow (0.1 sLpm) was constantly taken from the cold trap to reduce the equilibrium time needed when switching from non- trap to trap measurement. The cold trap could be optionally purged by dry zero air from cylinders, usually when cooling the bath. Due to power instability at the site, the cold bath was only run during daytime under the supervision of the operator. Condensed ice in the glass bottle was manually removed at the end of the day.

The measurement procedure was controlled by PTR Manager software and recorded into the data file of PTR-TOF-MS. The control was achieved by powering the three-way valves on and off using analogy output of PTR-TOF-MS. A 15-min background measurement was done every few hours. A 15-min single-point sensitivity check was done once a day. When the cold trap was operated, ambient measurement was alternatively switched between non-trap and trap modes every 15 mins.

5.2.3 Calibration and tests using authentic ISOPOOH compounds

At the end of IOP2, ISOPBOOH, the most abundant ISOPOOH isomer (cf. Figure 1-3), was synthesized in Manaus [Rivera-Rios et al., 2014] and used to calibrate the instrument and test the performance of the cold trap at T3 site. Air flow carrying a certain concentration of ISOPBOOH was generated using a nebulizer system as described in Section 4.2.3. To simulation the ambient humidity, the dilution flow to the mixing flask was humidified using a bubbler. The humidity of the ISOPBOOH-carrying flow was varied by changing the ratios of humid dilution flow and the dry flow to the nebulizer.

5.3 Results and Discussion

5.3.1 Quantification of ISOPOOH

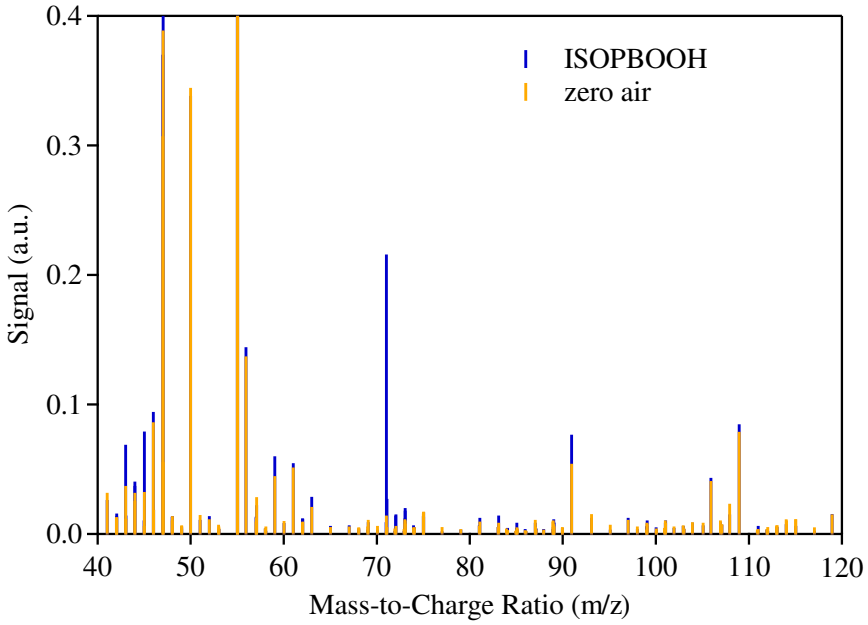

Figure 5-3 Unit-resolution mass spectrum of ISOPBOOH measured by PTR-TOF-MS. Reference spectrum of zero air used as carrier gas of ISOPBOOH is also shown. High background level of the zero air measurement arose from impurity in the zero air cylinder purchased locally.

Figure 5-3 shows the PTR-TOF-MS spectrum of synthesized ISOPBOOH standard. $C_4H_7O^+$ (m/z 71) was found as the dominant peak, in agreement with the PTR-MS characterization of ISOPBOOH in an earlier laboratory study [Rivera-Rios et al., 2014]. Rivera-Rios et al. [2014] suggested that ISOPBOOH decomposes to MVK via hemolytic peroxy bond cleavage on metal surfaces inside the PTR-TOF-MS instrument, and hence detected as $C_4H_7O^+$. For standard measurement in the present study, a dominant portion of $C_4H_7O^+$ was believe to originate from ISOPBOOH instead of possible impurities MVK or MACR, since the signal intensity of $C_4H_7O^+$ ion could drop approximately to background level after passing through the cold trap at low humidity (cf. Figure 5-5 (b)).

Minor peaks on the mass spectrum include $C_2H_3O^+$ (m/z 43; 0.11 $I_{C_4H_7O^+}$) and $C_2H_5O^+$ (m/z 45; 0.13 $I_{C_4H_7O^+}$). These two ions at high likelihood arose from residual solvents used for the synthesis, acetyl acetate and ether. Since facility for nuclear magnetic resonance analysis was not available, the purity of the synthesized standard was estimated as (80 ± 10)% by mass based on the PTR-MS measurements. A caveat about the purity determined by PTR-MS analysis is the negligence of the compounds having lower proton affinity than water.

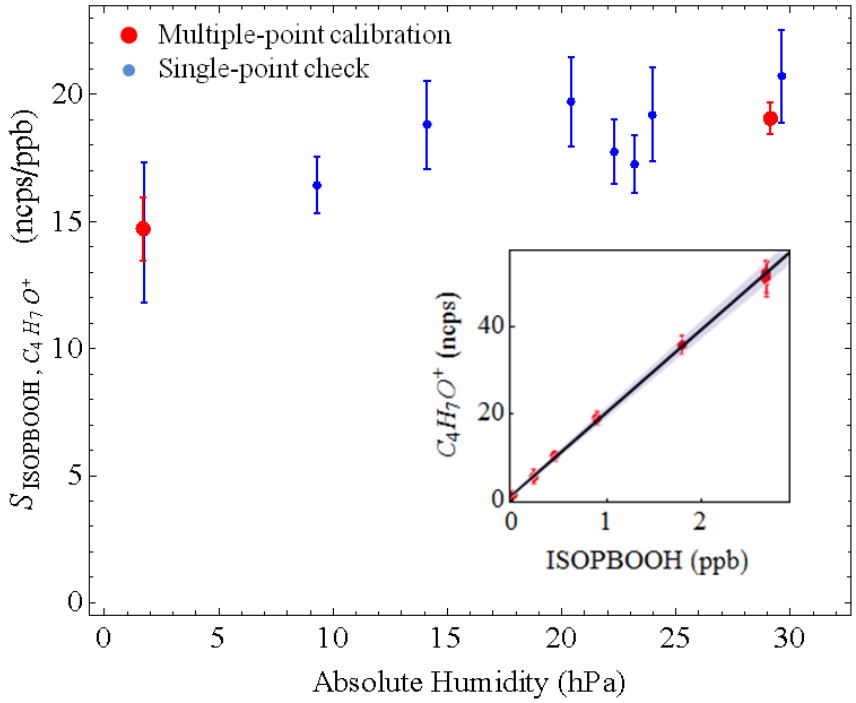

Figure 5-4 Dependence of the sensitivity of ISOPBOOH to $C_4H_7O^+$ ion on absolute humidity. Larger errors of the sensitivity values derived from single-point checks are due to instable room temperature. Inset figure shows the result of the multiple-point calibration at absolute humidity of 29 hPa.

Figure 5-4 present the measured sensitivities of ISOPBOOH to $C_4H_7O^+$ ion. The sensitivity depended on the humidity of the sample flow. At absolute humidity smaller than 15 hPa, the sensitivity increased with humidity. At absolute humidity greater than 15 hPa, the sensitivity leveled off at around 19 ncps/ppb. Similar humidity dependence has

been observed for organic acids in our earlier laboratory experiments (not shown here), possibly related to competitive uptake by walls inside the stainless-steel drift tube of the PTR-TOF-MS instrument (i.e. at sufficiently high humidity, water molecules dominated over the analyte molecules for occupying certain reactive sites on the instrument walls and hence reduced the wall loss of analyte molecules). Since ambient humidity during the measurement period ranged from 24 to 29 hPa, a single calibration factor of 19.0±0.6 ncps/ppb measured at 29 hPa by multi-point calibration (Figure 5-4) was applied for the whole humidity range. The same sensitivity was assumed for ISOPDOOH which decomposed to MACR inside of PTR-TOF-MS instrument [Rivera-Rios et al., 2014].

An unexpected finding of the cold-trap tests of ISOPBOOH standard was that the signal intensity of $C_4H_7O^+$ ion did not drop to background level through the cold trap at humid condition. The observed cold-trap $C_4H_7O^+$ signal depended on ISOPBOOH concentration and humidity of the sample flow, as shown in Figure 5-5 (a). The relation could be fitted well using the following equation:

$$f_{C_4H_7O^+}([ISOPBOOH], AH) = a\,[ISOPBOOH]([ISOPBOOH] + b)(AH + c) \quad (5\text{-}1)$$

where $f_{C_4H_7O^+}([ISOPBOOH], AH)$ is the signal intensity of $C_4H_7O^+$ ion in ncps measured for ISOPBOOH-carrying flow after the cold trap. [ISOPBOOH] is the concentration of ISOPBOOH in the sample flow in ppb; AH is the absolute humidity of the sample flow in hPa; a, b, and c are fitting parameters. Figure 5-5 (a) and (b) show the comparison of measured and fitted data of all the experiments.

The observed cold-trap $C_4H_7O^+$ signal most likely resulted from certain reaction of ISOPBOOH inside the cold trap involving water vapor. There are a few lines of evidence: (1) the $C_4H_7O^+$ signal was not proportional to the calculated concentration of

ISOPBOOH and could drop to close to background level at low humidity (Figure 5-5 (b)). There is hence less chance that the observed ion signal arose from volatile impurities contained in the synthesized standard. (2) $C_4H_7O^+$ signal increased with the increase of residence time in the cold trap (Not shown here), which favored the possibility of production of MVK/MACR through certain reactions of ISOPBOOH inside the cold trap instead of insufficient removal of ISOPBOOH by the cold trap. (3) $C_4H_7O^+$ signal intensity was proportional to humidity (Figure 5-5 (a)), which indicated that water vapor was involved in the possible reaction of ISOPBOOH. Further studies are needed to understand the possible reaction mechanism and the role of water, considering that ISOPBOOH has been found stable in aqueous solution at ambient temperature.

Despite of the nonideal performance of the cold trap, Figure 5-5 (b) shows that at ambient humidity the $C_4H_7O^+$ signal from ISOPOOBH measurement through the cold trap was still smaller than the signal bypassing the cold trap. As a result, it is still possible to estimate the ISOPOOH concentration in the ambient air based on the difference of $C_4H_7O^+$ signal from non-trap measurements to cold-trap measurement, although with a lower sensitivity than expected. The measured signal intensities $I_{C_4H_7O^+,nontrap,ambient}$ of $C_4H_7O^+$ ion bypass the cold trap and $I_{C_4H_7O^+,coldtrap,ambient}$ through the cold trap are given by

$$I_{C_4H_7O^+,nontrap,ambient} = I_{bg,C_4H_7O^+} + S_{MVK/MACR,C_4H_7O^+}([MVK+MACR]) + S_{ISOPOOH,C_4H_7O^+}[ISOPOOH] \quad (5\text{-}2)$$

$$I_{C_4H_7O^+,coldtrap,ambient} = I_{bg,C_4H_7O^+} + S_{MVK/MACR,C_4H_7O^+}([MVK+MACR]) + f_{C_4H_7O^+}([ISOPOOH],AH) \quad (5\text{-}3)$$

where $I_{bg,C_4H_7O^+}$ is the background signal intensity of $C_4H_7O^+$ ion in ncps,

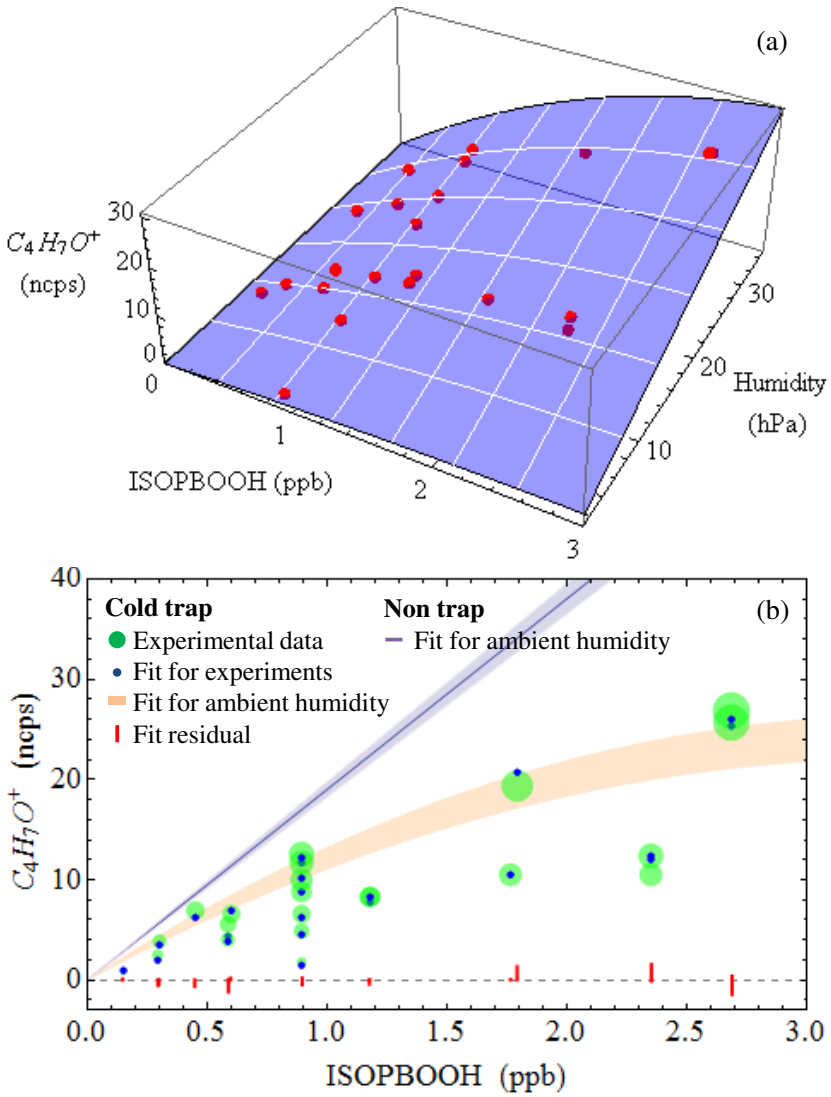

Figure 5-5 Dependence of cold-trap signal intensity of $C_4H_7O^+$ ion on humidity and ISOPBOOH concentration. Panel (a) shows a comparison of measured and fitted data in 3D plot and panel (b) shows the comparison and fitting residual in 2D plot. The signal intensities of $C_4H_7O^+$ ion shown in figures are background-corrected. The point size of experimental data shown in Panel (b) is scaled by the absolute humidity.

$S_{MVK/MACR,C_4H_7O^+}$ is the combined sensitivity of MVK and MACR; [MVK+MACR] is the sum concentration of MVK an MACR; [ISOPOOH] is the sum concentration of ISOPBOOH and ISOPDOOH, which are both detected as $C_4H_7O^+$ ion in PTR-TOF-MS; $S_{ISOPOOH,C_4H_7O^+}$ is the combined sensitivity of ISOPBOOH and ISOPDOOH;

$f_{C_4H_7O^+}([ISOPOOH], AH)$ is the after-trap signal intensity of $C_4H_7O^+$ ion as a function of [ISOPOOH] and absolute humidity (AH).

For use of Equations (5-2) and (5-3), $I_{C_4H_7O^+,nontrap,ambient}$ and $I_{C_4H_7O^+,coldtrap,ambient}$ were from ambient measurements. $S_{MVK/MACR,C_4H_7O^+}$ and $I_{bg,C_4H_7O^+}$ were determined by using MVK/MACR standards and pure air generator. For both of the two values, there was insignificant difference between nontrap and cold-trap measurements. Assuming that the sensitivity and coldtrap behavior of ISOPDOOH is the same as ISOPBOOH, $S_{ISOPOOH,C_4H_7O^+}$ and $f_{C_4H_7O^+}([ISOPOOH], AH)$ are equivalent to those derived for ISOPBOOH as above. By solving Equations (5-2) and (5-3), [MVK+MACR] and [ISOPOOH] could be determined.

5.3.2 Ambient measurements

Figure 5-6 shows the measurements on March 10, 2014 as one example how anthropogenic pollution changed the relative production of MVK/MACR and ISOPOOH from isoprene photochemistry. March 10 was one of the sunny days during IOP1 in the wet season. As shown in Figure 5-6 (a), NO concentration ranged from a few hundred ppt to 1 ppb in the morning, and dropped to below detection limit in the afternoon, indicating a transition of air mass over T3 site from polluted condition to clean condition. At high NO level in the morning, NO pathway was expected to dominate the fate of ISOPOO radicals, Consistently, the cold-trap signal of $C_4H_7O^+$ ion agreed with non-trap signal (Figure 5-6 (b)), suggesting that the measured signal had a dominant origin from highly volatile precursors, i.e., MVK and MACR. As NO level dropped with time, the cold trap

signal of $C_4H_7O^+$ started to be consistently lower than the non-trap signal, suggesting that ISOPOOH isomers started to contribute to the measured $C_4H_7O^+$ ion.

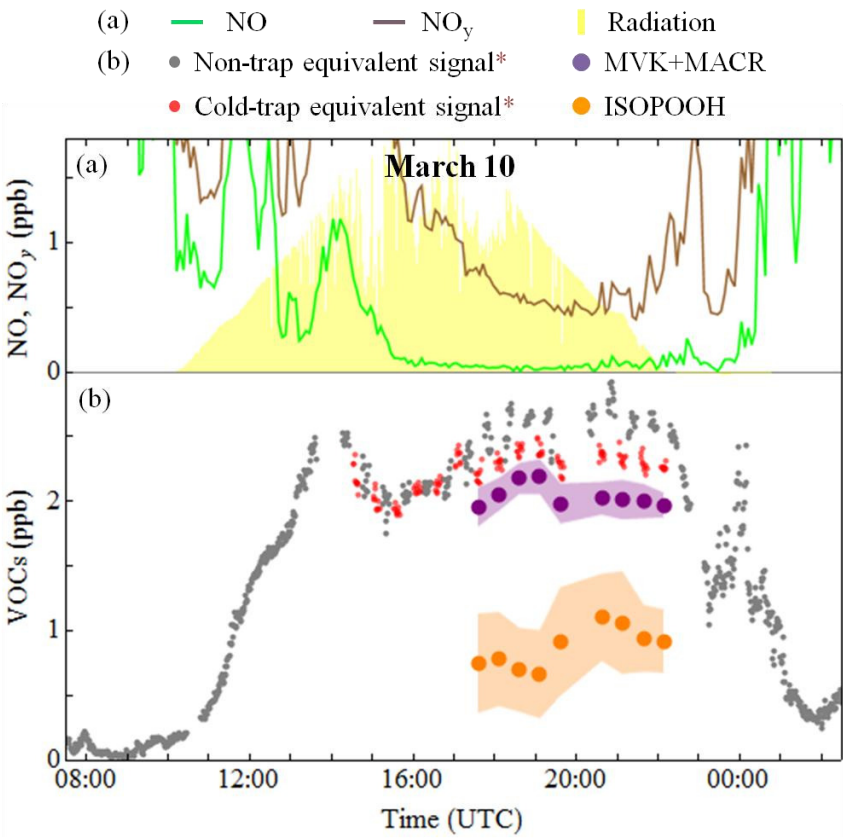

Figure 5-6 One case study on March 10, 2014 of changed chemistry with anthropogenic influence. (a) NO and NO_y concentrations and solar radiation; (b) concentrations of MVK+MACR and ISOPOOH isomers. *The cold-trap and non-trap equivalent signals represent the cold-trap and non-trap $C_4H_7O^+$ signals scaled by the sensitivity of MVK/MACR, respectively. The shadow areas of the concentrations of MVK+MACR and ISOPOOH isomers represent the estimated errors at 1σ.

The concentration of ISOPOOH isomers and the sum concentration of MVK and MACR were calculated for the cold-trap runs which had significant lower $C_4H_7O^+$ signal than the adjacent non-trap runs ($p < 0.001$). For Figure 5-6 (b), nine cold-trap runs reached this criterion. The ISOPOOH concentration and the sum concentration of MVK and MACR for each run were calculated by applying the measured cold-trap signal and adjacent non-trap signal of $C_4H_7O^+$ ion into Equations (5-2) and (5-3). The uncertainties

(1σ) of the calculated concentrations were estimated by Monte Carlo methods. The uncertainty estimate considered the uncertainty of $C_4H_7O^+$ signals from the cold-trap and non-trap measurements, the uncertainty of ISOPOOH sensitivity via non-trap measurement, the uncertainties of fitting parameters of Equation (5-1), and the uncertainty of measured ambient humidity. The measured concentrations were in the range of 0.7 ± 0.3 to 1.1 ± 0.3 ppb for ISOPOOH isomers and 2.0 ± 0.2 to 2.2 ± 0.1 ppb for MVK and MACR. The calculated sum concentration of MVK and MACR were 74-84% of the measured values without correction from the contribution from ISOPOOH isomers (i.e. normal PTR-MS operation).

For the whole IOP1, there were 283 cold-trap runs in total. 52 runs were used for concentration calculation. The selection was based on a few data filters in addition to the difference test of cold-trap signal and non-trap signal. For example, slope test by the signal difference between the contiguous non-trap measurements was used to take out the data points when the MVK and MACR concentration was in a rapid increasing or decreasing trend. Coincidence test was used to take out the data points which stand alone among contiguous cold-trap measurements to be significant lower than nontrap measurements. Plume test using high concentrations of both NO and toluene as an indicator screened out the data points at high-NO_x conditions.

Figure 5-7 summarized the calculated results as the fraction $f_{ISOPOOH}$ of ISOPOOH of the total concentration of MVK, MACR and ISOPOOH. Although the measured total concentration of MVK, MACR and ISOPOOH ranged from 0.3 ppb to 3.3 ppb, $f_{ISOPOOH}$ fell in a relative narrow range. The absence of $f_{ISOPOOH}$ values below 0.2 relate to the intrinsic high detection limit of the current method (i.e. a small difference of

two big numbers might be below the noise level). In addition, the sensitivity for ISOPOOH, defined as the difference non-trap and cold-trap signal in Figure 5-5 (b) was also lower for lower ISOPOOH concentration at certain humidity. The absence of $f_{ISOPOOH}$ values above 0.6 might relate to the nature of isoprene chemistry under low-NO conditions. At low-NO conditions, RO_2 and isomerization pathways could also become important in addition to the HO_2 pathway. The RO_2 pathway has been experimentally proved to produce MVK and MACR [e.g., Navarro et al., 2011]. The isomerization pathway was theoretically proposed to produce MVK and MACR although definite experimental evidence still lacks [Peeters et al., 2014]. In addition, depending on the NO level in the clean condition, a trace amount of NO (~ 40 ppt) could make the NO pathway equally important as the HO_2 pathway. The lack of high values of $f_{ISOPOOH}$ indicates that even at clean condition other pathways besides HO_2 pathway could still be important.

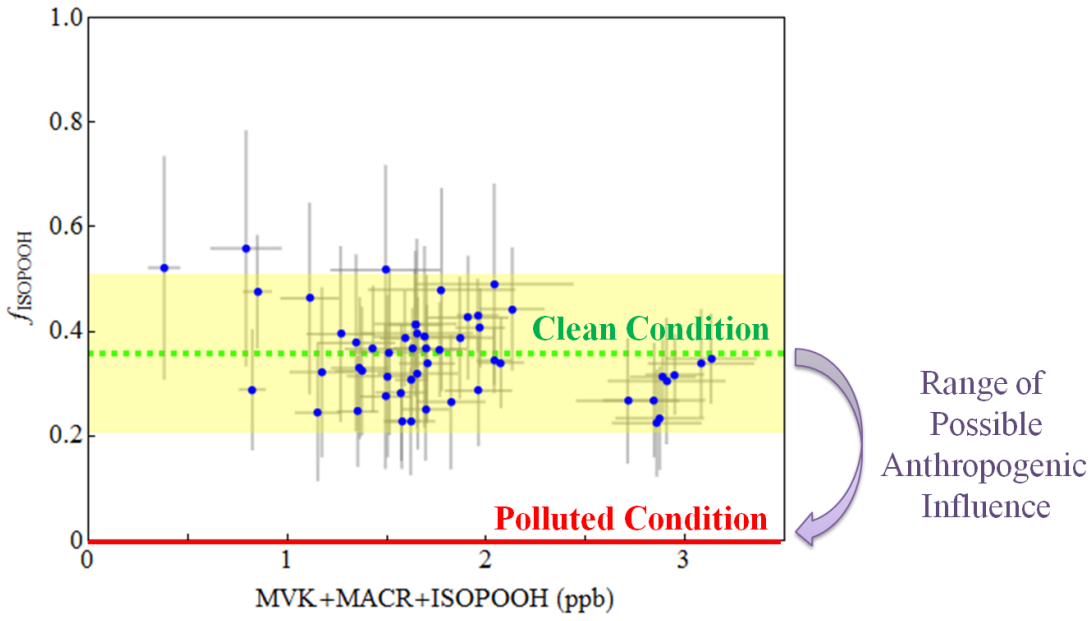

Figure 5-7 The fraction $f_{ISOPOOH}$ of ISOPOOH isomers in the total concentration of MVK, MACR and ISOPOOH measured during IOP1. The green dashed line and light yellow region represent mean and uncertainty (1σ) of estimated background $f_{ISOPOOH}$.

The observation that all the measured $f_{ISOPOOH}$ values lie in a certain range makes it possible to estimate $f_{ISOPOOH}$ under clean conditions. The relatively high detection limit of the current method served as a filter to screen out the data points in transition state between cleaned and polluted conditions. The background $f_{ISOPOOH}$ value was, therefore, estimated as 0.36 ± 0.15 (1σ) using the 52 data points and considering the uncertainties of each data point.

5.4 Conclusions and Atmospheric Implication

By deploying a cold trap upstream of a PTR-TOF-MS and calibrating the instrument using authentic standard, the present study separately measured the concentration of ISOPOOH isomers and the sum concentration of MVK and MACR. Preliminary analysis constrained the fraction of ISOPOOH concentration in the total concentration of MVK, MACR and ISOPOOH isomers to be 0.36 ± 0.15 over Amazonia under clean condition. One limitation of the current study is the uncertainties associated with the purity of the synthesized ISOPBOOH standards due to lack of NMR facility in the region. To further consolidate the results, calibration and cold-trap tests presented in Section 5.3.1 are going to be repeated in the lab using better quantified ISOPOOH standards under the experimental conditions employed in Amazon.

Despite of the uncertainties, the result has important implication for evaluating possible anthropogenic influence on isoprene chemistry over Amazonia. The high NO level in anthropogenic plume simply shifts the isoprene RO_2 chemistry to be dominant by NO pathway (i.e., $f_{ISOPOOH} \rightarrow 0$), the key to evaluate the anthropogenic influence is to understand isoprene RO_2 chemistry under clean condition. Relative contributions of the different pathways under clean condition are, however, difficult to evaluate, due to

technical challenges to measure trace amounts of NO, HO_2, and RO_2 correctly and large uncertainties of the reaction rate coefficients used. By measuring the fraction of ISOPOOH concentration in the total concentration of the major first-generation products (i.e., MVK, MACR and ISOPOOH) under clean condition, the present study provide an important constrain of isoprene RO_2 chemistry under clean condition and defines the range of possible anthropogenic influence, that is, an change of $f_{ISOPOOH}$ from 0.36 ± 0.15 to close to zero.

The current results also have important implications for interpreting the previous MVK/MACR measurements by providing a reference correction factor. An ISOPOOH fraction of 0.36 ± 0.15 under clean condition in Central Amazon suggested that the previously reported concentrations of MVK and MACR under similar clean conditions could be overestimated by 15%-40%, assuming the ratio of ISOPOOH sensitivity to MVK/MACR sensitivity is consistent for different PTR instruments. The contribution of ISOPOOH to previously measured deposition flux of MVK and MACR could be even larger, considering ISOPOOH has much smaller vapor pressure and is more soluble in water than MVK and MACR. The previous scientific conclusions based on MVK/MACR concentration measurements might be adjusted based on the parameterization provided in the current study, but those based on MVK/MACR flux measurements would require further investigation.

6. Conclusion and Outlook

Isoprene photooxidation plays an important role in tropospheric chemistry. The laboratory and field studies presented in the current thesis provided new perspectives for the gas-phase chemistry of isoprene and production of secondary organic material (SOM) in the particle phase under clean conditions. The results improved the current understanding of isoprene photooxdiation, provided important parameterization for accurate modeling of isoprene chemistry, and led to re-evaluation of some previous scientific findings.

In Chapter 2, the production yields of methyl vinyl ketone (MVK, C_4H_6O) and methacrolein (MACR, C_4H_6O) as first-generation products of isoprene photooxidation via the hydroperoxyl (HO_2) pathway were quantified as (3.8 ± 1.3)% and (2.5 ± 0.9)%, respectively, at +25 °C and < 2% relative humidity. Production of MVK and MACR via the HO_2 pathway implies concomitant production of hydroxyl ((6.3± 2.1)%) and hydroperoxyl ((6.3± 2.1)%) radicals, meaning a HO_x recycling of (12.6 ± 4.2)% given that HO_2 was both a reactant and product.

Another important finding in Chapter 2 is that some low-volatility oxidation products of isoprene via the HO2 pathway, believed to be mostly isoprene-derived hydroperoxides (ISOPOOH), were detected as the same product ions as MVK and MACR by Switchable-Regent-Ionization Time-of-Flight Mass Spectrometer (SRI-TOF-MS) using both H_3O^+ and NO^+ as reagent ions. These products were selectively removed from the gas phase by placement of a cold trap (-40 °C) inline prior to the SRI-TOF-MS. This finding has been confirmed very recently with synthesized standards by another group. This implication of this finding is that some scientific conclusions based on

previous ambient measurements of MVK and MACR using similar instruments under clean condition need to be re-evaluated.

In addition to gas-phase reaction mechanism, SOM production from isoprene photochemistry was also investigated, by using a novel serial-reactor set-up. In Chapter 3, the relative importance of possible intermediates of isoprene SOM production was evaluated under a wide range of acidities by comparing the gas-phase mass spectral change upon the injection of particles. Although isoprene, ISOPOOH isomers, and isoprene-derived epoxydiols (IEPOX) have all been previously suggested as possible direct SOM precursors via reactive uptake, the current study showed that uptake of IEPOX isomers is much more important under atmospheric-relevant acidities. In addition, the gas-phase mass spectral change revealed some particle-phase reaction products can partition back into the gas phase.

In Chapter 4, the contribution of IEPOX pathways to the production of isoprene SOM was quantitatively evaluated. IEPOX isomers lost from the gas phase accounted for (46 ±11)% of the produced SOM mass concentration. The IEPOX isomers comprised (59± 21)% (molecular count) of the loss of monitored gas-phase species. The implication is that for the investigated reaction conditions the SOM production pathways tied to IEPOX isomers accounted for half of the SOM mass concentration.

To evaluate the laboratory findings in atmospheric condition, a field study of isoprene chemistry over Amazonia was also carried out, as presented in Chapter 5. One goal is to separately measure MVK/MACR and ISOPOOH. Preliminary data analysis determined the fraction $f_{ISOPOOH}$ of ISOPOOH concentration in the total concentration of MVK, MACR and ISOPOOH isomers as 0.36 ± 0.15 under clean conditions. This value

could define the possible range of anthropogenic influence on isoprene chemistry over Amazonia ($f_{ISOPOOH}$ -> 0 under polluted condition) and serve as an important bench mark for evaluation of previous MVK/MACR measurements. Further calibration and analysis is underway to consolidate the results. In addition, there are still many other ways to explore the field observational data in combination with the laboratory data. I will continue to analyze the GoAmazon 2014/5 data sets along this direction as a postdoctoral scholar after my graduation.

Appendix A: Additional Tests for Interference Compounds

Changes in the signal intensities of $C_5H_9^+$ and $C_4H_7O^+$ ions produced using the H_3O^+ reagent ion are shown in Figure A-1 for stepwise decreases in trap temperature from +25 to -40 °C. The intensities of the two ions nominally represent the concentration of ISOP, the sum concentration of MACR and MVK, respectively. Consistent with the temperature-dependent patterns of signal intensity using the H_3O^+ reagent ions (Figure 2-4), the data in Figure A-1 show that in the HO_2-dominant experiments additional species contributed to these ions for trap temperatures warmer than -30 °C.

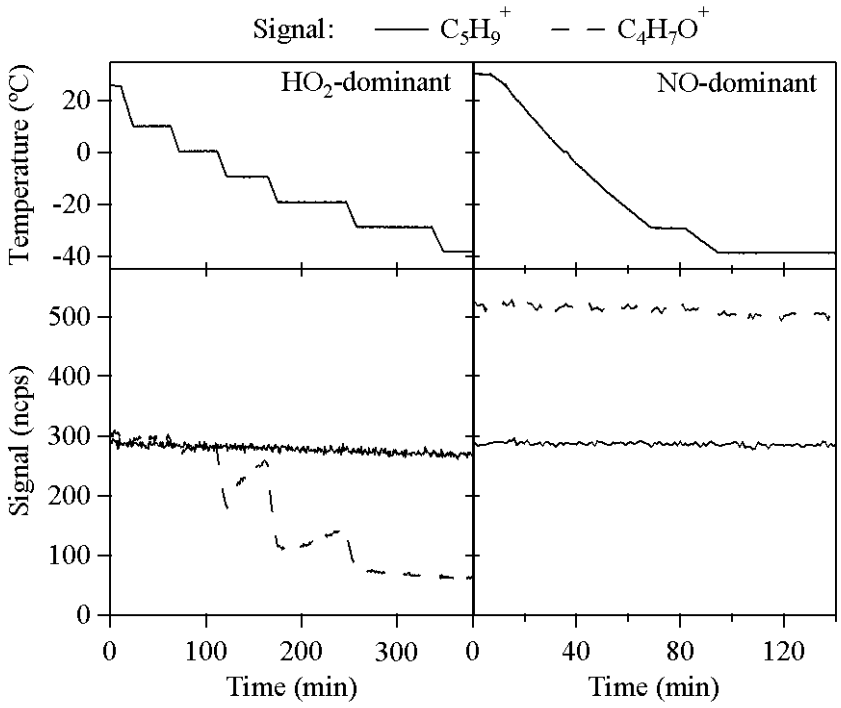

Figure A-1 Change in the signal of selected ion for steady-state chamber air measured with H_3O^+ reagent ions as the trap temperature dropped from room temperature to -40 °C in discrete steps. Left column shows the time series of temperature (top) and of ion signals (bottom) in Experiment #1 under HO_2-dominant conditions, and right column shows results for Experiment #7 under NO-dominant conditions. Solid line and dashed line in the bottom panels represent the ion signal of $C_5H_9^+$ and $C_4H_7O^+$, respectively.

To understand whether thermal decomposition of the condensing compounds, possibly ISOPOOH, occurred in the instrument (60 °C), the change in ion signals of steady-state chamber air was monitored at a low drift tube temperature of 30 °C as the inlet temperature was varied from 30 °C to 80 °C. The trap temperature was kept at 25 °C. The residence time of the sample air in the drift tube and in the inlet line was comparable (60-80 ms). No significant change in ion signals was observed, suggesting that thermal decomposition of other oxidation products inside the instrument did not contribute to the ions at the same m/z ratio as MVK and MACR product ions.

Measurements of steady-state chamber air have been made at various E/N ratios in both NO^+ and H_3O^+ mode. The apparent concentrations of isoprene, MVK, and MACR were quantified with respective calibrations at each E/N ratio. Here the apparent concentrations are defined as the equivalent concentrations of isoprene, MVK, and MACR assuming no interference compounds. As shown in the top panels of Figure A-2, the apparent MVK and MACR concentrations were independent on E/N ratio in the range of 15-70 Td in the NO^+ mode and 20-120 Td in the H_3O^+ mode. This observation indicates that the fragmentation of the interference compounds was not very sensitive to the collision energy we used.

As shown in the bottom panels of Figure A-2, the apparent concentrations of MVK and MACR showed some decrease as the temperature of the drift tube decreased. The apparent concentrations were quantified using respective calibrations at each temperature. The decrease of the apparent concentration of MVK + MACR at the NO^+ mode was bigger than that at the H_3O^+ mode. This observation suggests that fragmentation of the condensing compounds was thermally driven, which seems

inconsistent with the independence of the E/N ratio. Further investigation is hence needed to fully understand the mechanism.

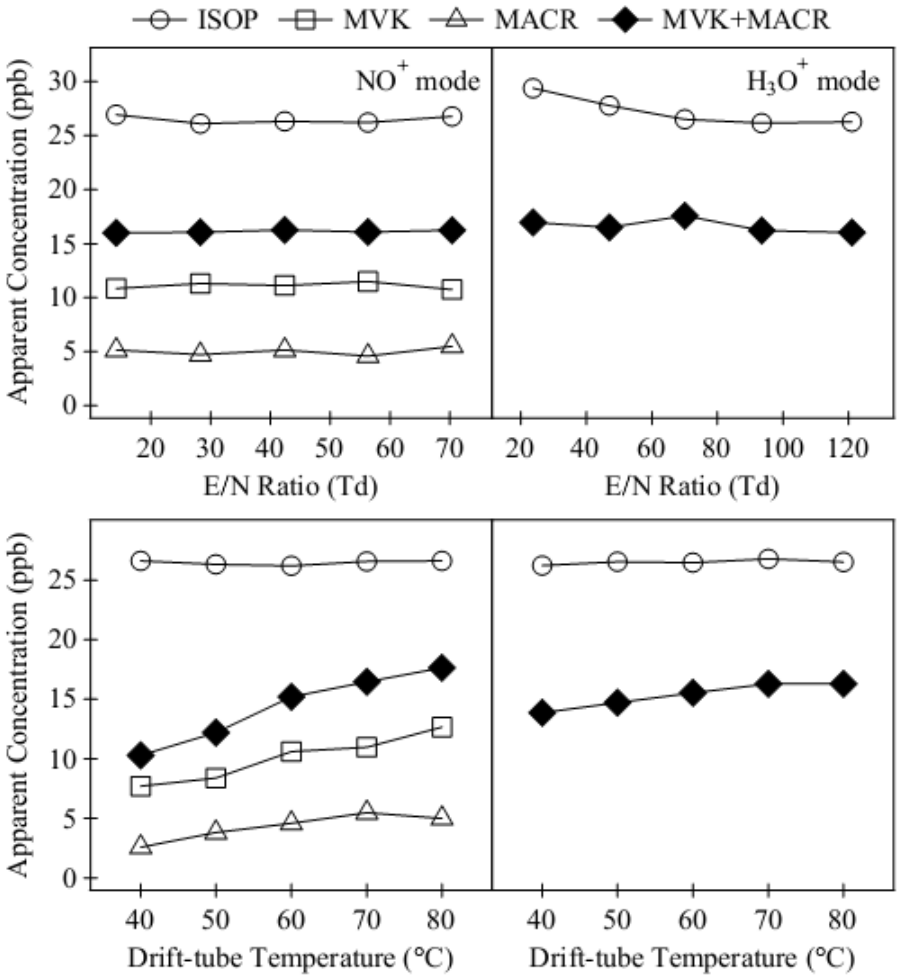

Figure A-2 Change in the apparent concentrations of isoprene, MVK, and MACR at steady state with the E/N ratios (top) and the drift-tube temperature (bottom) in both NO^+ (left) and H_3O^+ (right) mode. For the H_3O^+ mode, the combined concentration of MVK and MACR was calculated using the average sensitivity of MVK and MACR. The trap temperature was kept at +25 °C. For the experiments at various E/N ratios, the drift tube temperature was kept on 70 °C and the drift tube voltage was varied. For the experiments at various temperatures of the drift tube, the drift tube voltage was 300 V and 520 V for the NO^+ and H_3O^+ modes, respectively.

Appendix B: Effects of using a Particle Filter

This section provides evaluation of the effects of using a PFA particle filter upstream of SRI-TOF-MS on the gas-phase measurements for the experiments in Section 3 and 4.

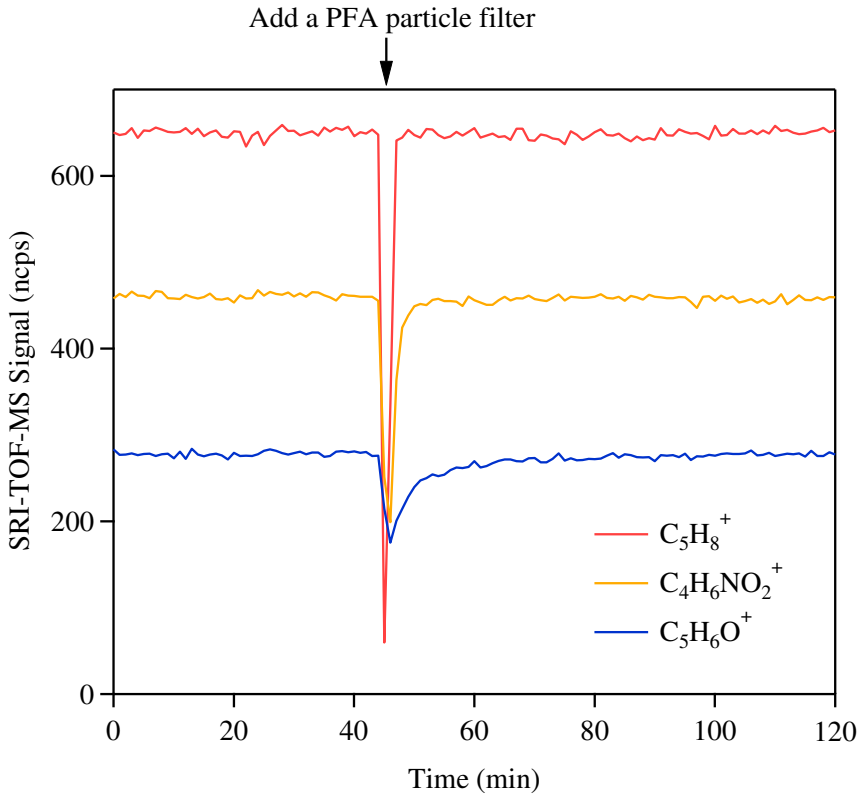

Figure B-1 Change in ion signals after adding a PFA filter between chamber and SRI-NO^+-TOF-MS. $C_5H_8^+$, $C_4H_6NO_2^+$, and $C_5H_6O^+$ are dominantly from isoprene, isoprene-derived hydroperoxide (ISOPOOH) isomers, and IEPOX isomers, respectively.

In control studies, the HEC outflow was sampled bypassing and through a clean Teflon particle filter into the SRI- NO^+-TOF-MS. As shown in Figure B-1, $C_5H_6O^+$ signal of HEC outflow recovered to the original level after adding the filter, although its recovery took a longer time than the signal recovery of ions from isoprene ($C_5H_8^+$) or isoprene-derived hydroperoxides ($C_4H_6NO_2^+$). Comparison of the detailed mass spectra bypassing and through the particle filter (after 2 hour equilibrium time) showed a negligible difference (not shown here). These observations indicate an insignificant effect

of the particle filter itself on the measured steady-state gas-phase signal of the oxidation products including IEPOX isomers.

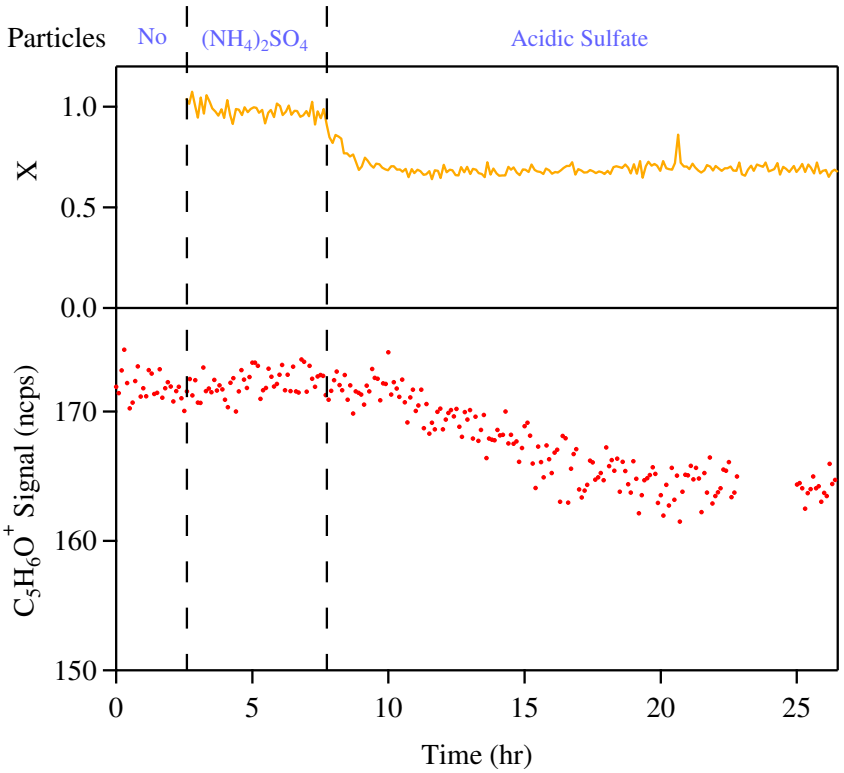

Figure B-2 Time series of extent of neutralization of particles and $C_5H_6O^+$ signal measured by SRI-TOF-MS (NO^+) during one part of the experiments. After injection of acidic sulfate particles, $C_5H_6O^+$ signal decreased and eventually leveled off. The absence of $C_5H_6O^+$ data at ~23-25 hour is due to calibration.

When sampling from Reactor #2, another possible effect of using particle filter is the uptake of the gas-phase species by the particles collected on the filter. Although we did not do a direct test for this possible effect, a separate experiment showed that the diameter growth of the particle population in Reactor #2 stopped when sulfate particle injection was shut off and the injection of the flow of isoprene oxidation products was kept on (Figure 3-3). The implication is that no further uptake of gas-phase species occurred to the particle population in Reactor #2 given a much longer exposure time. Therefore, when sampling the outflow of Reactor #2 through the particle filter, it is less

likely that particles collected on the filter can uptake additional organic material. In other words, the filter should have little effect on the measurement of the steady-state gas-phase signal of Reactor #2. The leveling off of IEPOX signals following the injection of acidic sulfate particles at certain X (Figure B-2) also supported insignificant uptake of IEPOX isomers by particles on the filter (i.e., if the particles collected on the filter could further uptake IEPOX, the measured IEPOX signal would decrease with time as particles continue accumulating on the filter).

Appendix C: Uncertainty Analysis

Contribution of $C_5H_6O^+$ to the total decrease of peak intensities

The uncertainties (2σ) for the contribution of $C_5H_6O^+$ ion to total decrease of ion signals in each individual experiment were estimated using a Monte Carlo method, in which the values of signal decrease of each ion were sampled from probability density functions of their individual values (i.e., their individual uncertainties based on measurements). The uncertainty for the contribution of $C_5H_6O^+$ ion to total ion signal loss in the complete set of experiments was estimated by bootstrapping method, in which the values were sampled from the Monte Carlo simulation of $C_5H_6O^+$ contribution in individual experiments. The results from the individual experiments and the complete set of experiments are shown in Table 4-1.

Contribution of IEPOX isomers to the total loss of gas-phase species

Two assumptions were used to translate the percent contribution of $C_5H_6O^+$ to the total decrease of peak intensities into the percent contribution of IEPOX isomers to total decreases of actual concentration. The first assumption was that a single calibration factor could be applied to all the ions to convert peak intensities to product concentrations within ±50% uncertainties. Consistent with the assumed uncertainty range, the measured sensitivities of trans- and cis-β-IEPOX are 78% and 63% of the sensitivity of MACR, respectively. The other assumption was that the oxidation products contributing to SOM production were all measurable by SRI-TOF-MS. This assumption is justified by considering the lower ionization energy for more oxygenated and carbonaceous compounds [Gross, 2004], which contribute to SOM production at higher likelihood compared with less oxygenated and carbonaceous compounds. Furthermore, no

significant wall loss of measurable species was observed in the second reactor in absence of particles, as demonstrated by the comparison of the gas mass spectra directly sampled from the HEC and through the second reactor (Figure 3-2).

As a check on the applicability of these assumptions for the present study, the concentration calculated for the sum of the measured oxidation products in the absence of particles were compared with the measured loss of isoprene on a carbon basis. Based on the measurements of initial and steady-state isoprene concentration in the HEC and the dilution ratio of the outflow from chamber to the second reactor, the reacted isoprene in the second reactor was 65 ± 6 ppb. Applying the calibration factor of MACR to all the carbonaceous product ions in the mass spectra except those arising from isoprene, the total concentration of the measurable oxidation products in the second reactor was 54 ppb. Similarly, the total concentration of oxidation products contributing to the C_3-C_5 product ions was 47 ppb. Some known C_1 and C_2 oxidation products, including formaldehyde and glyoxal, have significantly higher ionization energy than NO [Lias et al., 2011] and hence do not react with NO^+. The C_1-C_2 ions observed in the mass spectra were hence derived at least in part as fragment ions of C_3-C_5 products. Therefore, 47 ppb and 54 pbb represent lower and upper limits, respectively, of the equivalent-reacted isoprene. These values can explain 71-82% of the reacted isoprene. If the calibration factor of IEPOX isomers is applied instead, the measured gas-phase signal of oxygenated ions can explain 98-113% of the reacted isoprene.

The uncertainties (2σ) for the contribution of IEPOX to total loss of oxidation products were estimated in a similar manner as the estimate in peak intensities discussed above. For the estimate for individual experiments, a Monte Carlo method was used.

Assuming the same reaction rate coefficient with NO^+ for all the products, the concentration decrease of individual oxidation products was proportional to the decrease of peak intensities of corresponding product ions. An additional 50% uncertainty was added to the probability density functions of the product concentrations used in the Monte Carlo simulation to account for possible differences in the NO^+ reaction rate constant. For the estimate for the complete set of experiments, a bootstrapping method was used.

Bibliography

Ammann, C., C. Spirig, A. Neftel, M. Steinbacher, M. Komenda, and A. Schaub (2004), Application of PTR-MS for measurements of biogenic VOC in a deciduous forest, Int. J. Mass. Spectrom., 239(2-3), 87-101.

Archibald, A. T., M. C. Cooke, S. R. Utembe, D. E. Shallcross, R. G. Derwent, and M. E. Jenkin (2010), Impacts of mechanistic changes on HO_x formation and recycling in the oxidation of isoprene, Atmos. Chem. Phys., 10(17), 8097-8118.

Aschmann, S. M., and R. Atkinson (1994), Formation yields of methyl vinyl ketone and methacrolein from the gas-phase reaction of O_3 with isoprene, Environ. Sci. Technol., 28(8), 1539-1542.

Atkinson, R., and J. Arey (2003), Gas-phase tropospheric chemistry of biogenic volatile organic compounds: a review, Atmos. Environ., 37, S197-S219.

Atkinson, R., D. L. Baulch, R. A. Cox, J. N. Crowley, R. F. Hampson, R. G. Hynes, M. E. Jenkin, M. J. Rossi, and J. Troe (2006), Evaluated kinetic and photochemical data for atmospheric chemistry: Volume II - gas phase reactions of organic species, Atmos. Chem. Phys., 6(11), 3625-4055.

Baker, J., J. Arey, and R. Atkinson (2005), Formation and Reaction of Hydroxycarbonyls from the Reaction of OH Radicals with 1,3-Butadiene and Isoprene, Environ. Sci. Technol., 39(11), 4091-4099.

Bates, K. H., J. D. Crounse, J. M. St. Clair, N. B. Bennett, T. B. Nguyen, J. H. Seinfeld, B. M. Stoltz, and P. O. Wennberg (2014), Gas phase production and loss of isoprene epoxydiols, J. Phys. Chem. A, 118(7), 1237-1246.

Benkelberg, H. J., O. Boge, R. Seuwen, and P. Warneck (2000), Product distributions from the OH radical-induced oxidation of but-1-ene, methyl-substituted but-1-enes and isoprene in NO_x-free air, Phys. Chem. Chem. Phys., 2(18), 4029-4039.

Blake, R. S., P. S. Monks, and A. M. Ellis (2009), Proton-transfer reaction mass spectrometry, Chem. Rev., 109(3), 861-896.

Blake, R. S., K. P. Wyche, A. M. Ellis, and P. S. Monks (2006), Chemical ionization reaction time-of-flight mass spectrometry: Multi-reagent analysis for determination of trace gas composition, Int. J. Mass. Spectrom., 254(1-2), 85-93.

Budisulistiorini, S. H., et al. (2013), Real-time continuous characterization of secondary organic aerosol derived from Isoprene epoxydiols in downtown Atlanta, Georgia, using the Aerodyne aerosol chemical speciation monitor, Environ. Sci. Technol., 47(11), 5686-5694.

Bushick, R. D. (1971), The rearrangement of tertiary alicyclic hydroperoxides in acid, Tetrahedron Lett, 12(7), 579-582.

Butler, T. M., D. Taraborrelli, C. Brühl, H. Fischer, H. Harder, M. Martinez, J. Williams, M. G. Lawrence, and J. Lelieveld (2008), Improved simulation of isoprene oxidation chemistry with the ECHAM5/MESSy chemistry-climate model: lessons from the GABRIEL airborne field campaign, Atmos. Chem. Phys., 8(16), 4529-4546.

Carlton, A. G., C. Wiedinmyer, and J. H. Kroll (2009), A review of Secondary Organic Aerosol (SOA) formation from isoprene, Atmos. Chem. Phys., 9(14), 4987-5005.

Carter, W. P. L., D. R. Cocker Iii, D. R. Fitz, I. L. Malkina, K. Bumiller, C. G. Sauer, J. T. Pisano, C. Bufalino, and C. Song (2005), A new environmental chamber for evaluation of gas-phase chemical mechanisms and secondary aerosol formation, Atmos. Environ., 39(40), 7768-7788.

Chan, M. N., et al. (2010), Characterization and quantification of isoprene-derived epoxydiols in ambient aerosol in the southeastern United States, Environ. Sci. Technol., 44(12), 4590-4596.

Charlson, R. J. (1969), Atmospheric visibility related to aerosol mass concentration: review, Environ. Sci. Technol., 3(10), 913-918.

Chen, Q., Y. J. Liu, N. M. Donahue, J. E. Shilling, and S. T. Martin (2011), Particle-phase chemistry of secondary organic material: modeled compared to measured O:C and H:C elemental ratios provide constraints, Environ. Sci. Technol., 45(11), 4763-4770.

Chen, Q., et al. (2014), Fine-mode organic mass concentrations and sources in the Amazonian wet season (AMAZE-08), Atmos. Chem. Phys. Discuss., 14(11), 16151-16186.

Chen, X., D. Hulbert, and P. B. Shepson (1998), Measurement of the organic nitrate yield from OH reaction with isoprene, J. Geophys. Res., 103(D19), 25563-25568.

Claeys, M., et al. (2004), Formation of secondary organic aerosols through photooxidation of isoprene, Science, 303(5661), 1173-1176.

Cole-Filipiak, N. C., A. E. O'Connor, and M. J. Elrod (2010), Kinetics of the hydrolysis of atmospherically relevant isoprene-derived hydroxy epoxides, Environ. Sci. Technol., 44(17), 6718-6723.

Connelly, B. M., and M. A. Tolbert (2010), Reaction of Isoprene on Thin Sulfuric Acid Films: Kinetics, Uptake, and Product Analysis, Environ. Sci. Technol., 44(12), 4603-4608.

Cox, R. A., J. Munk, O. J. Nielsen, P. Pagsberg, and E. Ratajczak (1990), Ultraviolet absorption spectra and kinetics of acetonyl and acetonylperoxy radicals, Chem. Phys. Lett., 173(2–3), 206-210.

Crounse, J. D., F. Paulot, H. G. Kjaergaard, and P. O. Wennberg (2011), Peroxy radical isomerization in the oxidation of isoprene, Phys. Chem. Chem. Phys., 13(30), 13607-13613.

Czoschke, N. M., M. Jang, and R. M. Kamens (2003), Effect of acidic seed on biogenic secondary organic aerosol growth, Atmos. Environ., 37(30), 4287-4299.

da Silva, G., C. Graham, and Z. F. Wang (2010), Unimolecular beta-hydroxyperoxy radical decomposition with OH recycling in the photochemical oxidation of isoprene, Environ. Sci. Technol., 44(1), 250-256.

de Gouw, J., and C. Warneke (2007), Measurements of volatile organic compounds in the earths atmosphere using proton-transfer-reaction mass spectrometry, Mass. Spectrom. Rev., 26(2), 223-257.

DeCarlo, P. F., et al. (2006), Field-deployable, high-resolution, time-of-flight aerosol mass spectrometer, Anal. Chem., 78(24), 8281-8289.

Deno, N. C., W. E. Billups, K. E. Kramer, and R. R. Lastomirsky (1970), Rearrangement of aliphatic primary, secondary, and tertiary alkyl hydroperoxides in strong acid, The Journal of Organic Chemistry, 35(9), 3080-3082.

Di Carlo, P., et al. (2004), Missing OH Reactivity in a Forest: Evidence for Unknown Reactive Biogenic VOCs, Science, 304(5671), 722-725.

Dillon, T. J., and J. N. Crowley (2008), Direct detection of OH formation in the reactions of HO_2 with $CH_3C(O)O_2$ and other substituted peroxy radicals, Atmos. Chem. Phys., 8(16), 4877-4889.

Docherty, K. S., W. Wu, Y. B. Lim, and P. J. Ziemann (2005), Contributions of Organic Peroxides to Secondary Aerosol Formed from Reactions of Monoterpenes with O3, Environ. Sci. Technol., 39(11), 4049-4059.

Dommen, J., A. Metzger, J. Duplissy, M. Kalberer, M. R. Alfarra, A. Gascho, E. Weingartner, A. S. H. Prevot, B. Verheggen, and U. Baltensperger (2006), Laboratory observation of oligomers in the aerosol from isoprene/NOx photooxidation, Geophys. Res. Lett., 33(13), L13805.

Ebben, C. J., B. F. Strick, M. A. Upshur, H. M. Chase, J. L. Achtyl, R. J. Thomson, and F. M. Geiger (2014), Towards the identification of molecular constituents associated with the surfaces of isoprene-derived secondary organic aerosol (SOA) particles, Atmos. Chem. Phys., 14(5), 2303-2314.

Eddingsaas, N. C., D. G. VanderVelde, and P. O. Wennberg (2010), Kinetics and products of the acid-catalyzed ring-opening of atmospherically relevant butyl epoxy alcohols, J. Phys. Chem. A, 114(31), 8106-8113.

Edney, E. O., T. E. Kleindienst, M. Jaoui, M. Lewandowski, J. H. Offenberg, W. Wang, and M. Claeys (2005), Formation of 2-methyl tetrols and 2-methylglyceric acid in secondary organic aerosol from laboratory irradiated isoprene/NOX/SO2/air mixtures and their detection in ambient PM2.5 samples collected in the eastern United States, Atmos. Environ., 39(29), 5281-5289.

Enami, S., H. Mishra, M. R. Hoffmann, and A. J. Colussi (2012), Protonation and Oligomerization of Gaseous Isoprene on Mildly Acidic Surfaces: Implications for Atmospheric Chemistry, J. Phys. Chem. A, 116(24), 6027-6032.

Ervens, B., A. G. Carlton, B. J. Turpin, K. E. Altieri, S. M. Kreidenweis, and G. Feingold (2008), Secondary organic aerosol yields from cloud-processing of isoprene oxidation products, Geophys. Res. Lett., 35(2), L02816.

Francisco-Marquez, M., J. R. Alvarez-Idaboy, A. Galano, and A. Vivier-Bunge (2003), Theoretical study of the initial reaction between OH and isoprene in tropospheric conditions, Phys. Chem. Chem. Phys., 5(7), 1392-1399.

Froyd, K. D., S. M. Murphy, D. M. Murphy, J. A. de Gouw, N. C. Eddingsaas, and P. O. Wennberg (2010), Contribution of isoprene-derived organosulfates to free tropospheric aerosol mass, P. Natl. Acad. Sci. USA, 107(50), 21360-21365.

Galloway, M. M., A. J. Huisman, L. D. Yee, A. W. H. Chan, C. L. Loza, J. H. Seinfeld, and F. N. Keutsch (2011), Yields of oxidized volatile organic compounds during the OH radical initiated oxidation of isoprene, methyl vinyl ketone, and methacrolein under high-NO(x) conditions, Atmos. Chem. Phys., 11(21), 10779-10790.

Gaston, C. J., T. P. Riedel, Z. Zhang, A. Gold, J. D. Surratt, and J. A. Thornton (2014), Reactive uptake of an isoprene-derived epoxydiol to submicron aerosol particles, Environ. Sci. Technol., 48(19), 11178-11186.

Goldstein, A. H., and I. E. Galbally (2007), Known and Unexplored Organic Constituents in the Earth's Atmosphere, Environ. Sci. Technol., 41(5), 1514-1521.

Graus, M., M. Muller, and A. Hansel (2010), High resolution PTR-TOF: quantification and formula confirmation of VOC in real time, J. Am. Soc. Mass. Spectr., 21(6), 1037-1044.

Gross, J. H. (2004), Mass spectrometry: a textbook, 25-27 pp., Springer.

Guenther, A., T. Karl, P. Harley, C. Wiedinmyer, P. I. Palmer, and C. Geron (2006), Estimates of global terrestrial isoprene emissions using MEGAN (Model of Emissions of Gases and Aerosols from Nature), Atmos. Chem. Phys., 6(11), 3181-3210.

Guenther, A., et al. (1995), A Global-Model of Natural Volatile Organic-Compound Emissions, J. Geophys. Res., 100(D5), 8873-8892.

Guenther, A. B., X. Jiang, C. L. Heald, T. Sakulyanontvittaya, T. Duhl, L. K. Emmons, and X. Wang (2012), The Model of Emissions of Gases and Aerosols from Nature version 2.1 (MEGAN2.1): an extended and updated framework for modeling biogenic emissions, Geosci. Model Dev., 5(6), 1471-1492.

Hallquist, M., et al. (2009), The formation, properties and impact of secondary organic aerosol: current and emerging issues, Atmos. Chem. Phys., 9(14), 5155-5236.

Hamilton, J. F., A. C. Lewis, J. C. Reynolds, L. J. Carpenter, and A. Lubben (2006), Investigating the composition of organic aerosol resulting from cyclohexene ozonolysis: low molecular weight and heterogeneous reaction products, Atmos. Chem. Phys., 6(12), 4973-4984.

Hansel, A., and A. Wisthaler (2000), A method for real-time detection of PAN, PPN and MPAN in ambient air, Geophys. Res. Lett., 27(6), 895-898.

Hasson, A. S., G. S. Tyndall, and J. J. Orlando (2004), A product yield study of the reaction of HO_2 radicals with ethyl peroxy ($C_2H_5O_2$), acetyl peroxy ($CH_3C(O)O_2$), and acetonyl peroxy ($CH_3C(O)CH_2O_2$) radicals, J. Phys. Chem. A, 108(28), 5979-5989.

Hasson, A. S., K. T. Kuwata, M. C. Arroyo, and E. B. Petersen (2005), Theoretical studies of the reaction of hydroperoxy radicals (HO_2) with ethyl peroxy ($CH_3CH_2O_2$), acetyl peroxy ($CH_3C(O)O_2$), and acetonyl peroxy ($CH_3C(O)CH_2O_2$) radicals, J. Photoch. Photobio. A, 176(1–3), 218-230.

Heald, C. L., D. J. Jacob, R. J. Park, L. M. Russell, B. J. Huebert, J. H. Seinfeld, H. Liao, and R. J. Weber (2005), A large organic aerosol source in the free troposphere missing from current models, Geophys. Res. Lett., 32(18), L18809.

Heald, C. L., et al. (2008), Predicted change in global secondary organic aerosol concentrations in response to future climate, emissions, and land use change, J. Geophys. Res., 113(D5), D05211.

Henze, D. K., and J. H. Seinfeld (2006), Global secondary organic aerosol from isoprene oxidation, Geophys. Res. Lett., 33(9), L09812.

Hewitt, C. N., et al. (2010), Overview: oxidant and particle photochemical processes above a south-east Asian tropical rainforest (the OP3 project): introduction, rationale, location characteristics and tools, Atmos. Chem. Phys., 10(1), 169-199.

Hoyle, C. R., T. Berntsen, G. Myhre, and I. S. A. Isaksen (2007), Secondary organic aerosol in the global aerosol - chemical transport model Oslo CTM2, Atmos. Chem. Phys., 7(21), 5675-5694.

Iinuma, Y., O. Boge, A. Kahnt, and H. Herrmann (2009), Laboratory chamber studies on the formation of organosulfates from reactive uptake of monoterpene oxides, Phys. Chem. Chem. Phys., 11(36), 7985-7997.

Iinuma, Y., A. Kahnt, A. Mutzel, O. Böge, and H. Herrmann (2013), Ozone-Driven Secondary Organic Aerosol Production Chain, Environ. Sci. Technol., 47(8), 3639-3647.

Ion, A. C., R. Vermeylen, I. Kourtchev, J. Cafmeyer, X. Chi, A. Gelencsér, W. Maenhaut, and M. Claeys (2005), Polar organic compounds in rural PM2.5 aerosols from K-puszta, Hungary, during a 2003 summer field campaign: Sources and diel variations, Atmos. Chem. Phys., 5(7), 1805-1814.

Jacob, D. (1999), Introduction to atmospheric chemistry, 148-152 pp., Princeton University Press.

Jacob, D. J., and S. C. Wofsy (1988), Photochemistry of biogenic emissions over the Amazon forest, J. Geophys. Res., 93(D2), 1477-1486.

Jacobs, M. I., A. I. Darer, and M. J. Elrod (2013), Rate Constants and Products of the OH Reaction with Isoprene-Derived Epoxides, Environ. Sci. Technol.

Jang, M., and R. M. Kamens (2001), Atmospheric Secondary Aerosol Formation by Heterogeneous Reactions of Aldehydes in the Presence of a Sulfuric Acid Aerosol Catalyst, Environ. Sci. Technol., 35(24), 4758-4766.

Jang, M., G. Cao, and J. Paul (2008), Colorimetric Particle Acidity Analysis of Secondary Organic Aerosol Coating on Submicron Acidic Aerosols, Aerosol Sci Tech, 42(6), 409-420.

Jang, M., N. M. Czoschke, S. Lee, and R. M. Kamens (2002), Heterogeneous atmospheric aerosol production by acid-catalyzed particle-phase reactions, Science, 298(5594), 814-817.

Jenkin, M. E., S. M. Saunders, and M. J. Pilling (1997), The tropospheric degradation of volatile organic compounds: A protocol for mechanism development, Atmos. Environ., 31(1), 81-104.

Jenkin, M. E., A. A. Boyd, and R. Lesclaux (1998), Peroxy radical kinetics resulting from the OH-initiated oxidation of 1,3-butadiene, 2,3-dimethyl-1,3-butadiene and isoprene, J. Atmos. Chem., 29(3), 267-298.

Jenkin, M. E., M. D. Hurley, and T. J. Wallington (2007), Investigation of the radical product channel of the $CH_3C(O)O_2 + HO_2$ reaction in the gas phase, Phys. Chem. Chem. Phys., 9(24), 3149-3162.

Jenkin, M. E., M. D. Hurley, and T. J. Wallington (2008), Investigation of the radical product channel of the $CH_3C(O)CH_2O_2 + HO_2$ reaction in the gas phase, Phys. Chem. Chem. Phys., 10(29), 4274-4280.

Jordan, A., S. Haidacher, G. Hanel, E. Hartungen, L. Märk, H. Seehauser, R. Schottkowsky, P. Sulzer, and T. D. Märk (2009a), A high resolution and high sensitivity

proton-transfer-reaction time-of-flight mass spectrometer (PTR-TOF-MS), Int. J. Mass. Spectrom., 286(2-3), 122-128.

Jordan, A., S. Haidacher, G. Hanel, E. Hartungen, J. Herbig, L. Märk, R. Schottkowsky, H. Seehauser, P. Sulzer, and T. D. Märk (2009b), An online ultra-high sensitivity proton-transfer-reaction mass-spectrometer combined with switchable reagent ion capability (PTR+SRI-MS), Int. J. Mass. Spectrom., 286(1), 32-38.

Karl, M., H. P. Dorn, F. Holland, R. Koppmann, D. Poppe, L. Rupp, A. Schaub, and A. Wahner (2006), Product study of the reaction of OH radicals with isoprene in the atmosphere simulation chamber SAPHIR, J. Atmos. Chem., 55(2), 167-187.

Karl, T., A. Guenther, A. Turnipseed, G. Tyndall, P. Artaxo, and S. Martin (2009), Rapid formation of isoprene photo-oxidation products observed in Amazonia, Atmos. Chem. Phys., 9(20), 7753-7767.

Karl, T., A. Hansel, L. Cappellin, L. Kaser, I. Herdlinger-Blatt, and W. Jud (2012), Selective measurements of isoprene and 2-methyl-3-buten-2-ol based on NO^+ ionization mass spectrometry, Atmos. Chem. Phys., 12(24), 11877-11884.

Karl, T., P. K. Misztal, H. H. Jonsson, S. Shertz, A. H. Goldstein, and A. B. Guenther (2013), Airborne Flux Measurements of BVOCs above Californian Oak Forests: Experimental Investigation of Surface and Entrainment Fluxes, OH Densities, and Damköhler Numbers, Journal of the Atmospheric Sciences, 70(10), 3277-3287.

Karl, T., P. Harley, L. Emmons, B. Thornton, A. Guenther, C. Basu, A. Turnipseed, and K. Jardine (2010), Efficient Atmospheric Cleansing of Oxidized Organic Trace Gases by Vegetation, Science, 330(6005), 816-819.

Kesselmeier, J., and M. Staudt (1999), Biogenic Volatile Organic Compounds (VOC): An Overview on Emission, Physiology and Ecology, J. Atmos. Chem., 33(1), 23-88.

King, S. M., T. Rosenoern, J. E. Shilling, Q. Chen, and S. T. Martin (2009), Increased cloud activation potential of secondary organic aerosol for atmospheric mass loadings, Atmos. Chem. Phys., 9(9), 2959-2971.

King, S. M., T. Rosenoern, J. E. Shilling, Q. Chen, Z. Wang, G. Biskos, K. A. McKinney, U. Pöschl, and S. T. Martin (2010), Cloud droplet activation of mixed organic-sulfate particles produced by the photooxidation of isoprene, Atmos. Chem. Phys., 10(8), 3953-3964.

Kleindienst, T. E., E. O. Edney, M. Lewandowski, J. H. Offenberg, and M. Jaoui (2006), Secondary Organic Carbon and Aerosol Yields from the Irradiations of Isoprene and α-Pinene in the Presence of NOx and SO2, Environ. Sci. Technol., 40(12), 3807-3812.

Kleindienst, T. E., M. Jaoui, M. Lewandowski, J. H. Offenberg, C. W. Lewis, P. V. Bhave, and E. O. Edney (2007), Estimates of the contributions of biogenic and

anthropogenic hydrocarbons to secondary organic aerosol at a southeastern US location, Atmos. Environ., 41(37), 8288-8300.

Kroll, J. H., and J. H. Seinfeld (2008), Chemistry of secondary organic aerosol: Formation and evolution of low-volatility organics in the atmosphere, Atmos. Environ., 42(16), 3593-3624.

Kroll, J. H., N. L. Ng, S. M. Murphy, R. C. Flagan, and J. H. Seinfeld (2005), Secondary organic aerosol formation from isoprene photooxidation under high-NOx conditions, Geophys. Res. Lett., 32(18), L18808.

Kroll, J. H., N. L. Ng, S. M. Murphy, R. C. Flagan, and J. H. Seinfeld (2006), Secondary organic aerosol formation from isoprene photooxidation, Environ. Sci. Technol., 40(6), 1869-1877.

Kuhn, U., et al. (2007), Isoprene and monoterpene fluxes from Central Amazonian rainforest inferred from tower-based and airborne measurements, and implications on the atmospheric chemistry and the local carbon budget, Atmos. Chem. Phys., 7(11), 2855-2879.

Kuwata, M., Y. J. Liu, K. A. McKinney, and S. T. Martin (2014), Phase of inorganic sulfate can regulate the production of secondary organic material from isoprene photooxidation products, In preparison.

Lee, A., A. H. Goldstein, J. H. Kroll, N. L. Ng, V. Varutbangkul, R. C. Flagan, and J. H. Seinfeld (2006), Gas-phase products and secondary aerosol yields from the photooxidation of 16 different terpenes, J. Geophys. Res., 111(D17).

Lee, W., M. Baasandorj, P. S. Stevens, and R. A. Hites (2005), Monitoring OH-initiated oxidation kinetics of isoprene and its products using online mass spectrometry, Environ. Sci. Technol., 39(4), 1030-1036.

Lelieveld, J., et al. (2008), Atmospheric oxidation capacity sustained by a tropical forest, Nature, 452(7188), 737-740.

Lias, S. G., J. E. Bartmess, J. F. Liebman, J. L. Holmes, R. D. Levin, and W. G. Mallard (2011), Ion Energetics Data, in NIST Chemistry WebBook, NIST Standard Reference Database Number 69, edited by P. J. Linstrom and W. G. Mallard, National Institute of Standards and Technology, Gaithersburg MD.

Liggio, J., and S. M. Li (2008), Reversible and irreversible processing of biogenic olefins on acidic aerosols, Atmos. Chem. Phys., 8(7), 2039-2055.

Liggio, J., S.-M. Li, J. R. Brook, and C. Mihele (2007), Direct polymerization of isoprene and α-pinene on acidic aerosols, Geophys. Res. Lett., 34(5), L05814.

Lightfoot, P. D., R. A. Cox, J. N. Crowley, M. Destriau, G. D. Hayman, M. E. Jenkin, G. K. Moortgat, and F. Zabel (1992), Organic peroxy radicals: Kinetics, spectroscopy and tropospheric chemistry, Atmos. Environ. A-Gen., 26(10), 1805-1961.

Lim, Y. B., and P. J. Ziemann (2009), Kinetics of the heterogeneous conversion of 1,4-hydroxycarbonyls to cyclic hemiacetals and dihydrofurans on organic aerosol particles, Phys. Chem. Chem. Phys., 11(36), 8029-8039.

Limbeck, A., M. Kulmala, and H. Puxbaum (2003), Secondary organic aerosol formation in the atmosphere via heterogeneous reaction of gaseous isoprene on acidic particles, Geophys. Res. Lett., 30(19), 1996.

Lin, G., J. E. Penner, S. Sillman, D. Taraborrelli, and J. Lelieveld (2012), Global modeling of SOA formation from dicarbonyls, epoxides, organic nitrates and peroxides, Atmos. Chem. Phys., 12(10), 4743-4774.

Lin, Y. H., et al. (2011), Isoprene epoxydiols as precursors to secondary organic aerosol formation: acid-catalyzed reactive uptake studies with authentic compounds, Environ. Sci. Technol., 46(1), 250-258.

Lin, Y. H., et al. (2013), Epoxide as a precursor to secondary organic aerosol formation from isoprene photooxidation in the presence of nitrogen oxides, P. Natl. Acad. Sci. USA, 110(17), 6718-6723.

Lindinger, W., A. Hansel, and A. Jordan (1998), On-line monitoring of volatile organic compounds at pptv levels by means of proton-transfer-reaction mass spectrometry (PTR-MS) - Medical applications, food control and environmental research, Int. J. Mass. Spectrom., 173(3), 191-241.

Liu, Y. J., I. Herdlinger-Blatt, K. A. McKinney, and S. T. Martin (2013), Production of methyl vinyl ketone and methacrolein via the hydroperoxyl pathway of isoprene oxidation, Atmos. Chem. Phys., 13(11), 5715-5730.

McKinney, K. A., B. H. Lee, A. Vasta, T. V. Pho, and J. W. Munger (2011), Emissions of isoprenoids and oxygenated biogenic volatile organic compounds from a New England mixed forest, Atmos. Chem. Phys., 11(10), 4807-4831.

McMurry, P. H., and D. Grosjean (1985), Gas and aerosol wall losses in Teflon film smog chambers, Environ. Sci. Technol., 19(12), 1176-1182.

Mifflin, A. L., M. L. Smith, and S. T. Martin (2009), Morphology hypothesized to influence aerosol particle deliquescence, Phys. Chem. Chem. Phys., 11(43), 10095-10107.

Miyoshi, A., S. Hatakeyama, and N. Washida (1994), OH radical-initiated photooxidation of isoprene - an estimate of global CO production, J. Geophys. Res., 99(D9), 18779-18787.

Mochalski, P., K. Unterkofler, P. Španěl, D. Smith, and A. Amann (2014), Product ion distributions for the reactions of NO+ with some physiologically significant volatile organosulfur and organoselenium compounds obtained using a selective reagent ionization time-of-flight mass spectrometer, Rapid. Commun. Mass. Sp., 28(15), 1683-1690.

Muller, M., et al. (2010), First eddy covariance flux measurements by PTR-TOF, Atmos. Meas. Tech., 3(2), 387-395.

Navarro, M. A., S. Dusanter, R. A. Hites, and P. S. Stevens (2011), Radical dependence of the yields of methacrolein and methyl vinyl ketone from the OH-Initiated oxidation of isoprene under NO_x-free conditions, Environ. Sci. Technol., 45(3), 923-929.

Ng, N. L., J. H. Kroll, M. D. Keywood, R. Bahreini, V. Varutbangkul, R. C. Flagan, J. H. Seinfeld, A. Lee, and A. H. Goldstein (2006), Contribution of first- versus second-generation products to secondary organic aerosols formed in the oxidation of biogenic hydrocarbons, Environ. Sci. Technol., 40(7), 2283-2297.

Nguyen, T. B., M. M. Coggon, K. H. Bates, X. Zhang, R. H. Schwantes, K. A. Schilling, C. L. Loza, R. C. Flagan, P. O. Wennberg, and J. H. Seinfeld (2014a), Organic aerosol formation from the reactive uptake of isoprene epoxydiols (IEPOX) onto non-acidified inorganic seeds, Atmos. Chem. Phys., 14(7), 3497-3510.

Nguyen, T. B., et al. (2014b), Overview of the Focused Isoprene eXperiments at California Institute of Technology (FIXCIT): mechanistic chamber studies on the oxidation of biogenic compounds, Atmos. Chem. Phys. Discuss., 14(15), 21611-21658.

Pandis, S. N., S. E. Paulson, J. H. Seinfeld, and R. C. Flagan (1991), Aerosol formation in the photooxidation of isoprene and β-pinene, Atmos. Environ. A-Gen., 25(5–6), 997-1008.

Pankow, J. F., and W. E. Asher (2008), SIMPOL.1: a simple group contribution method for predicting vapor pressures and enthalpies of vaporization of multifunctional organic compounds, Atmos. Chem. Phys., 8(10), 2773-2796.

Paulot, F., J. D. Crounse, H. G. Kjaergaard, J. H. Kroll, J. H. Seinfeld, and P. O. Wennberg (2009a), Isoprene photooxidation: new insights into the production of acids and organic nitrates, Atmos. Chem. Phys., 9(4), 1479-1501.

Paulot, F., J. D. Crounse, H. G. Kjaergaard, A. Kurten, J. M. St Clair, J. H. Seinfeld, and P. O. Wennberg (2009b), Unexpected epoxide formation in the gas-phase photooxidation of isoprene, Science, 325(5941), 730-733.

Paulson, S. E., R. C. Flagan, and J. H. Seinfeld (1992), Atmospheric photooxidation of isoprene part I: The hydroxyl radical and ground state atomic oxygen reactions, Int. J. Chem. Kinet., 24(1), 79-101.

Peeters, J., and J.-F. Muller (2010), HO_x radical regeneration in isoprene oxidation via peroxy radical isomerisations. II: experimental evidence and global impact, Phys. Chem. Chem. Phys., 12(42), 14227-14235.

Peeters, J., T. L. Nguyen, and L. Vereecken (2009), HO_x radical regeneration in the oxidation of isoprene, Phys. Chem. Chem. Phys., 11(28), 5935-5939.

Peeters, J., J.-F. Müller, T. Stavrakou, and V. S. Nguyen (2014), Hydroxyl Radical Recycling in Isoprene Oxidation Driven by Hydrogen Bonding and Hydrogen Tunneling: The Upgraded LIM1 Mechanism, J. Phys. Chem. A.

Plewka, A., T. Gnauk, E. Brüggemann, and H. Herrmann (2006), Biogenic contributions to the chemical composition of airborne particles in a coniferous forest in Germany, Atmos. Environ., 40, Supplement 1(0), 103-115.

Pope III, C. A., and D. W. Dockery (2006), Health effects of fine particulate air pollution: lines that connect, J. Air & Waste Manage. Assoc., 56(6), 709-742.

Pye, H. O. T., et al. (2013), Epoxide pathways improve model predictions of isoprene markers and reveal key role of acidity in aerosol formation, Environ. Sci. Technol., 47(19), 11056-11064.

Rasmussen, R. A., and F. Went (1965), Volatile organic material of plant origin in the atmosphere, P. Natl. Acad. Sci. USA, 53(1), 215-220.

Rinne, H. J. I., A. B. Guenther, J. P. Greenberg, and P. C. Harley (2002), Isoprene and monoterpene fluxes measured above Amazonian rainforest and their dependence on light and temperature, Atmos. Environ., 36(14), 2421-2426.

Rivera-Rios, J. C., et al. (2014), Conversion of hydroperoxides to carbonyls in field and laboratory instrumentation: observational bias in diagnosing pristine versus anthropogenically-controlled atmospheric chemistry, Geophys. Res. Lett., 2014GL061919.

Robinson, N. H., et al. (2011), Evidence for a significant proportion of secondary organic aerosol from isoprene above a maritime tropical forest, Atmos. Chem. Phys., 11(3), 1039-1050.

Rohrer, F., B. Bohn, T. Brauers, D. Brüning, F. J. Johnen, A. Wahner, and J. Kleffmann (2005), Characterisation of the photolytic HONO-source in the atmosphere simulation chamber SAPHIR, Atmos. Chem. Phys., 5(8), 2189-2201.

Ruppert, L., and K. H. Becker (2000), A product study of the OH radical-initiated oxidation of isoprene: formation of C_5-unsaturated diols, Atmos. Environ., 34(10), 1529-1542.

Sanadze, G. A. (2004), Biogenic Isoprene (A Review), Russian Journal of Plant Physiology, 51(6), 729-741.

Saunders, S. M., M. E. Jenkin, R. G. Derwent, and M. J. Pilling (2003), Protocol for the development of the Master Chemical Mechanism, MCM v3 (Part A): tropospheric degradation of non-aromatic volatile organic compounds, Atmos. Chem. Phys., 3(1), 161-180.

Schlenker, J. C., and S. T. Martin (2005), Crystallization pathways of sulfate-nitrate-ammonium aerosol particles, J. Phys. Chem. A, 109(44), 9980-9985.

Shilling, J. E., et al. (2009), Loading-dependent elemental composition of α-pinene SOA particles, Atmos. Chem. Phys., 9(3), 771-782.

Silva, G. d., C. Graham, and Z.-F. Wang (2009), Unimolecular β-Hydroxyperoxy Radical Decomposition with OH Recycling in the Photochemical Oxidation of Isoprene, Environ Sci Technol, 44(1), 250-256.

Sindelarova, K., C. Granier, I. Bouarar, A. Guenther, S. Tilmes, T. Stavrakou, J. F. Müller, U. Kuhn, P. Stefani, and W. Knorr (2014), Global data set of biogenic VOC emissions calculated by the MEGAN model over the last 30 years, Atmos. Chem. Phys., 14(17), 9317-9341.

Slowik, J. G., et al. (2011), Photochemical processing of organic aerosol at nearby continental sites: contrast between urban plumes and regional aerosol, Atmos. Chem. Phys., 11(6), 2991-3006.

Smith, D., and P. Spanel (2005), Selected Ion Flow Tube Mass Spectrometry (SIFT-MS) for on-line trace gas analysis, Mass. Spectrom. Rev., 24(5), 661-700.

Španěl, P., Y. Ji, and D. Smith (1997), SIFT studies of the reactions of H_3O^+, NO^+ and O_2^+ with a series of aldehydes and ketones, Int. J. Mass. Spectrom., 165–166(0), 25-37.

Španěl, P., J. M. V. Doren, and D. Smith (2002), A selected ion flow tube study of the reactions of H_3O^+, NO^+, and O_2^+ with saturated and unsaturated aldehydes and subsequent hydration of the product ions, Int. J. Mass. Spectrom., 213(2–3), 163-176.

Sprengnether, M., K. L. Demerjian, N. M. Donahue, and J. G. Anderson (2002), Product analysis of the OH oxidation of isoprene and 1,3-butadiene in the presence of NO, J. Geophys. Res., 107(D15), 4268.

Stone, D., et al. (2011), Isoprene oxidation mechanisms: measurements and modelling of OH and HO_2 over a South-East Asian tropical rainforest during the OP3 field campaign, Atmos. Chem. Phys., 11(13), 6749-6771.

Sulbaek Andersen, M. P., M. D. Hurley, T. J. Wallington, J. C. Ball, J. W. Martin, D. A. Ellis, and S. A. Mabury (2003), Atmospheric chemistry of C_2F_5CHO: mechanism of the $C_2F_5C(O)O_2 + HO_2$ reaction, Chem. Phys. Lett., 381(1–2), 14-21.

Surratt, J. D., M. Lewandowski, J. H. Offenberg, M. Jaoui, T. E. Kleindienst, E. O. Edney, and J. H. Seinfeld (2007a), Effect of acidity on secondary organic aerosol formation from isoprene, Environ. Sci. Technol., 41(15), 5363-5369.

Surratt, J. D., A. W. H. Chan, N. C. Eddingsaas, M. N. Chan, C. L. Loza, A. J. Kwan, S. P. Hersey, R. C. Flagan, P. O. Wennberg, and J. H. Seinfeld (2010), Reactive intermediates revealed in secondary organic aerosol formation from isoprene, P. Natl. Acad. Sci. USA, 107(15), 6640-6645.

Surratt, J. D., et al. (2006), Chemical composition of secondary organic aerosol formed from the photooxidation of isoprene, J. Phys. Chem. A, 110(31), 9665-9690.

Surratt, J. D., et al. (2007b), Evidence for organosulfates in secondary organic aerosol, Environ. Sci. Technol., 41(2), 517-527.

Surratt, J. D., et al. (2008), Organosulfate Formation in Biogenic Secondary Organic Aerosol, J. Phys. Chem. A, 112(36), 8345-8378.

Taipale, R., T. M. Ruuskanen, J. Rinne, M. K. Kajos, H. Hakola, T. Pohja, and M. Kulmala (2008), Technical Note: Quantitative long-term measurements of VOC concentrations by PTR-MS - measurement, calibration, and volume mixing ratio calculation methods, Atmos. Chem. Phys., 8(22), 6681-6698.

Taraborrelli, D., M. G. Lawrence, J. N. Crowley, T. J. Dillon, S. Gromov, C. B. M. Grosz, L. Vereecken, and J. Lelieveld (2012), Hydroxyl radical buffered by isoprene oxidation over tropical forests, Nature Geosci., 5(3), 190-193.

Tobias, H. J., and P. J. Ziemann (2000), Thermal Desorption Mass Spectrometric Analysis of Organic Aerosol Formed from Reactions of 1-Tetradecene and O3 in the Presence of Alcohols and Carboxylic Acids, Environ. Sci. Technol., 34(11), 2105-2115.

Tuazon, E. C., and R. Atkinson (1990), A product study of the gas-phase reaction of isoprene with the OH radical in the presence of NO_x, Int. J. Chem. Kinet., 22(12), 1221-1236.

Turner, J. O. (1971), The acid-catalyzed decomposition of aliphatic hydroperoxides: reactions in the presence of alcohols, Tetrahedron Lett, 12(14), 887-890.

Wallington, T. J., P. Dagaut, and M. J. Kurylo (1992), UV absorption cross sections and reaction kinetics and mechanisms for peroxy radicals in the gas phase, Chem. Rev., 92(4), 667-710.

Wang, W., I. Kourtchev, B. Graham, J. Cafmeyer, W. Maenhaut, and M. Claeys (2005), Characterization of oxygenated derivatives of isoprene related to 2-methyltetrols in Amazonian aerosols using trimethylsilylation and gas chromatography/ion trap mass spectrometry, Rapid. Commun. Mass. Sp., 19(10), 1343-1351.

Wexler, A. S., and S. L. Clegg (2002), Atmospheric aerosol models for systems including the ions H^+, NH_4^+, Na^+, SO_4^{2-}, NO_3^-, Cl^-, Br^-, and H_2O, J. Geophys. Res., 107(D14), 4207.

Xie, Y., F. Paulot, W. P. L. Carter, C. G. Nolte, D. J. Luecken, W. T. Hutzell, P. O. Wennberg, R. C. Cohen, and R. W. Pinder (2013), Understanding the impact of recent advances in isoprene photooxidation on simulations of regional air quality, Atmos. Chem. Phys., 13(16), 8439-8455.

Yu, J., H. E. Jeffries, and R. M. Le Lacheur (1995), Identifying Airborne Carbonyl Compounds in Isoprene Atmospheric Photooxidation Products by Their PFBHA Oximes Using Gas Chromatography/Ion Trap Mass Spectrometry, Environ. Sci. Technol., 29(8), 1923-1932.

Zhang, Q., et al. (2007), Ubiquity and dominance of oxygenated species in organic aerosols in anthropogenically-influenced Northern Hemisphere midlatitudes, Geophys. Res. Lett., 34(13), L13801.

Zhang, Z., Y. H. Lin, H. Zhang, J. D. Surratt, L. M. Ball, and A. Gold (2012), Technical Note: Synthesis of isoprene atmospheric oxidation products: isomeric epoxydiols and the rearrangement products cis- and trans-3-methyl-3,4-dihydroxytetrahydrofuran, Atmos. Chem. Phys., 12(18), 8529-8535.

Zhao, J., and R. Zhang (2004), Proton transfer reaction rate constants between hydronium ion (H_3O^+) and volatile organic compounds, Atmos. Environ., 38(14), 2177-2185.

Zhao, J., R. Y. Zhang, E. C. Fortner, and S. W. North (2004), Quantification of hydroxycarbonyls from OH-isoprene reactions, J Am Chem Soc, 126(9), 2686-2687.

Ziemann, P. J., and R. Atkinson (2012), Kinetics, products, and mechanisms of secondary organic aerosol formation, Chem Soc Rev, 41(19), 6582-6605.